Recovery of Rare Earth Elements From Waste Materials: Leaching and Separation Using Supported Liquid Membranes

by

Andrew Paul Middleton

Department of Civil and Environmental Engineering
Duke University

Date:_____

Approved:

_____
Heileen Hsu-Kim, Supervisor

_____
Mark Wiesner

_____
Marc Deshusses

_____
Dan M. Park

Dissertation submitted in partial fulfillment of
the requirements for the degree of Doctor
of Philosophy in the Department of
Civil and Environmental Engineering in the Graduate School
of Duke University

2022

ABSTRACT

Recovery of Rare Earth Elements From Waste Materials: Leaching and Separation Using Supported Liquid Membranes

by

Andrew Paul Middleton

Department of Civil and Environmental Engineering
Duke University

Date:_____

Approved:

_____
Heileen Hsu-Kim, Supervisor

_____
Mark Wiesner

_____
Marc Deshusses

_____
Dan M. Park

An abstract of a dissertation submitted in partial
fulfillment of the requirements for the degree
of Doctor of Philosophy in the Department of
Civil and Environmental Engineering in the Graduate School of
Duke University

2022

Abstract

Rare earth elements (REEs; defined as the stable lanthanides, yttrium, and scandium) are ubiquitous in a wide range of modern technologies; however, their global market supply is dominated by a single source and has been subject to major disruptions in recent years. This has led to an interest in finding alternative, non-traditional sources of REEs. Potential non-traditional sources include secondary waste materials such as coal combustion residual (CCR), acid mine drainage (AMD), and electronic wastes (e-waste), among others.

While methods for processing and purification of REEs from traditional ores are reasonably well established, there are not well-established processing and purification methods for low-grade, non-traditional sources. This is in part because non-traditional sources have a complex and diverse chemical composition and relatively low REE concentrations. This work focused on understanding the factors controlling REE recovery in two steps of the recovery process: 1) acid leaching of REEs from solid wastes and 2) separation using a supported liquid membrane (SLM) process. The waste materials used in this research were CCR, coal processing refuse, and AMD. The overall aim of this work was to understand how the diverse chemistry of waste materials affects REE recovery during leaching and purification. Specifically, this research addressed the following aims:

1. Identify the factors that control REE solubility (e.g., pH and major element concentration) in acid leachates of coal fly ashes and coal residue.

2. Quantify the effects of various leachate characteristics such as major metal concentrations and feed pH on REE mass transfer in SLMs using synthetic feeds that mimic real feedstocks from low-grade waste materials.
3. Evaluate the effectiveness of SLMs as a method for selective separation of REEs from real AMD feeds from sites distinct water chemistries and identify feed characteristics that are predictive of SLM performance.

The aim of Chapter 2 of this research was to understand the connection between REE solubility, pH, and major elemental components of leachates for coal by-products. One of the early steps in recovering REEs from coal by-products is often acid leaching, which can result in low pH leachates with complex aqueous chemistry. To accomplish the aim of this chapter, we investigated the effects of solids concentration (i.e., pulp density) and pH adjustment on REE solubility in acid leachates of coal fly ashes from the Powder River Basin (PRB) and Appalachian Basin in the United States, and a coal processing refuse from the Southwestern U.S. For PRB ashes, the concentrations of soluble REEs generally increased with increasing pulp density; however, at pulp density values above 80-100 g/L, the soluble REE concentrations in the leachates were markedly lower. Similarly, the soluble concentrations of other major solutes (Fe, Al, Si) that leached from PRB fly ashes were also non-linear with pulp density. These major elements tended to reach maximum concentration values at 60-70 g/L pulp density. In contrast, for the Appalachian fly ashes and the coal by-product, soluble concentrations of REE and major elements in leachates increased linearly with pulp density. Chemical equilibria calculations of mineral saturation indices indicated that trends in soluble REE

concentrations could be explained by saturation conditions for Fe and Al-(hydr)oxides and possibility sulfate minerals, but not lanthanide hydroxides. Furthermore, pH adjustment of the acid leachates showed that REEs and many major solutes were removed from solution at pH values above 4.5, also consistent with Fe- and Al-(hydr)oxide precipitation. These results highlight the importance of understanding the chemical composition of leachates when designing REE recovery processes for low-grade geologic feedstocks and that precipitation of hydr(oxide) or sulfate minerals of major elements rather than discreet formation of REE mineral phases could be used for process optimization.

The aim of Chapter 3 of this work was to quantify the effects of three different competitive metals (Fe(III), Fe(II), and Al) and feed pH on the mass transfer and recovery of two rare earth elements (REE) (Nd and Er) using SLMs. SLMs are a promising alternative to solvent exchange processes that combine two different unit operations (extraction and stripping) into one. To our knowledge, there are no studies that have systematically assessed the effects of individual metals on REE mass transfer using SLMs with feeds that have metals concentrations relevant to low-grade waste materials. Previous work has suggested that competition by non-REE metals for metal binding sites at the membrane interface can decrease REE recovery when using CCR leachates. To accomplish the aim of this chapter, we used simulated feeds that are representative of low-grade feedstocks of REEs, such as coal fly ash and acid mine drainage (AMD). The simulated feeds consisted of either Nd or Er as the REE of interest and either Fe(III), Fe(II), or Al as the competitive metal. The feeds had relatively low REE concentrations

(0.01-100 µmol/L) compared to the competitive metals, Fe and Al (0.017-35 mmol/L), and had pH values from 1 to 3.5. The results showed that at sufficiently high concentrations of competitive metals REE mass transfer could be impeded. Further, the concentration at which REE mass transfer was inhibited was lowest for Fe(III) compared to Fe(II) and Al. The results also showed that feed pH is a major driver of REE transfer across the membrane, with feeds at higher pH having higher mass transfer. Additionally, we were able to show that the observed decreases in REE mass transfer were not due to unwanted loss mechanisms in the bulk feed (e.g., coprecipitation with mineral phases formed over the lifetime of the reactor) or due to mineral formation on the membrane surface blocking sorption sites at the feed-membrane interface. The results of this study will help to provide a framework for predicting how REE mass transfer will be affected when using real feeds with complex aqueous chemistries and multiple competitive metals.

In the fourth chapter of this research, we evaluated the recovery of REEs from a real potential feedstock, AMD, using SLMs. The major aims for this study were to: 1) assess the effectiveness of SLM-based REE separation from AMD samples representing a spectrum of aqueous compositions; 2) determine the effects of AMD storage and holding time on separation performance; and 3) assess the impact of AMD pre-treatment (e.g., filtration and pH adjustment) on REE recovery. The results showed that relative separation fluxes of REE by SLM correlated with AMD characteristics such as pH and major ions such as Fe and Ca. The purity of acid strippant product, expressed as REE dry weigh content, depended on the initial REE concentrations in the AMD. Additionally,

Fe(II) oxidation during the aging of AMD samples significantly decreased REE mass transfer by SLM separation. However, filtration of freshly collected AMD limited Fe(II) oxidation, enabling flexibility in feed stock storage time for separation of AMD. Pre-treatment of AMD samples by pH adjustment did not substantially improve separation performance. Overall, this study provides a framework for applying SLMs for REE recovery from AMD sources by establishing primary water quality parameters that influence separation flux and product purity. Such insights are needed to support a mechanistic understanding of critical metals separation by SLM for complex and nontraditional feedstocks such as AMD wastes.

In total, this research provides insight on key feed characteristics that control recovery of REEs from low-grade waste materials during two stages of the recovery process: acid leaching and separation using SLMs. The results from this research can be used to help engineer more efficient recovery processes that could help low-grade waste materials become economically viable sources of REEs.

Dedication

To my mom and dad.

Contents

List of Tables

List of Figures

Acknowledgements

I would first like to thank my advisor, Dr. Heileen Hsu-Kim, for her guidance and encouragement throughout the last five years. I am also grateful for my committee members Dr. Mark Wiesner, Dr. Marc Deshusses, and Dr. Dan Park for their support and advice. I would also like thank Dr. Yongqin Jiao at LLNL for the feedback and suggestions she provided during the early stages of this work. The final chapter this work would not have been possible without Dr. Ben Hedin helping plan and execute the AMD sampling trip in Pittsburgh.

I would also like to express my sincere gratitude to Dr. Nelson Rivera for his invaluable technical assistance and mentorship. I also could have not done this without the help and support of the other members of the Hsu-Kim lab. I am especially grateful to Faye, Talia, and Austin for their advice and encouragement throughout this journey.

I would also like to thank my cohort: Jake, Ethan, Anna, Paige, and Lucas. Your friendship and support have been incredibly meaningful, and I could not have made it through this process without all of you. I would also like to acknowledge all of the friends I have made and colleagues I have worked with in the CEE Department and at Duke.

Finally, I would like to thank my family, especially my mom, dad, and brother, for their unwavering belief in me.

1. Introduction

The rare earth elements (REE), defined here as the 14 stable lanthanides (La-Lu), yttrium, and scandium, are critically important in the energy, defense, and electronic industries, among others.[1, 2] Further, their unique chemistry makes them currently irreplaceable in products such as high strength permanent magnets, hard-disc drives, petroleum cracking catalysts, missile guidance systems, glass, and personal electronics, among others.[1-3] One of the biggest potential future growth sectors are in green industries, such as wind turbines and electric motors.[2] Traditional mining, extraction, and separation processes can all present major environmental and human health exposure issues. Additionally, most of the REE production and processing is currently done by a single party, which has created supply chain issues. There is therefore interest in finding alternative sources that help relieve strains in the supply chain and reduce the environmental impact of primary ore extraction.

Multiple waste materials have been proposed as alternative REE sources, such as e-waste, coal combustion residuals, acid mine drainage, and mining residuals, among others. All these materials have been shown to be enriched in REEs; however, they have widely variable chemistries and many of them have relatively low REE content.[4-7] This can make it difficult to predict REE recovery rates and to design efficient separation processes. Waste materials are also often spatially distributed in a way that can make it difficult to implement onsite industrial scale operations. In this work I explore how REE recovery varies based on the chemistry of two types of low-grade waste materials (acid

mine drainage and coal combustion residuals) at two steps in the recovery process: acid leaching and separation using supported liquid membranes.

Acid leaching is one of the primary steps in extraction and recovery of REEs from wastes. Likewise, supported liquid membranes are a promising separation process that have been proposed as an alternative to traditional processes for REE recovery from wastes. In this chapter specifically, I provide an overview of the REE recovery process, including the geochemical occurrence, mining, and separation of REE from complex aqueous feeds. I also present challenges that exist at each stage in the REE production process. Finally, I address how my work on REE recovery during acid leaching of coal combustion residuals and separation using SLMs will help address some of these issues.

1.1 Geochemical Occurrence of REEs

Despite their name, REEs are not particularly uncommon in terms of their crustal abundance relative to other valuable and precious metals. In total REEs have a crustal abundance of approximately 220 mg/kg, with cerium being the most abundant at 70 mg/kg and thallium being the least abundant at 0.2 mg/kg.[8] For comparison, copper, lead, and gold have crustal abundances of 45 mg/kg, 15 mg/kg, and 0.005 mg/kg, respectively.[8] REEs are broadly grouped into two categories: light REEs (LREE, La-Gd) and heavy REEs (HREE, Tb-Lu and Y), with HREEs being less abundant than LREEs; however, this definition does not correspond to the relative demand of individual elements. REEs have therefore also been categorized as critical (Y, Nd, Eu, Tb, Dy, Er, and Sc), uncritical (La, Pr, Sm, and Gd), and excessive (Ce, Ho, Yb, and Lu).[9] In this

work we focus on both recovery of total REEs and individual critical elements that represent both LREEs and HREEs (Sc, Nd, and Er).

1.2 Current Major Sources of REEs

Since 1996, REEs have mainly been mined from two sources: the Bayan Obo mine in northern China and ion adsorption clays in southern China.[10] In 2022, these two sources accounted for 60% of the global production, which is the lowest production percentage in at least the last decade.[3, 10] The Bayan Obo mine is the major producer of LREEs, while the HREEs are mostly mined from the ion adsorption clays. The major REE bearing phase in the Bayan Obo mine is the fluorocarbonate mineral bastnaesite ($(REE)CO_3F$).[11] The Bayan Obo mine is approximately 3000 feet deep, almost a mile wide, and produces 80,000-100,000 tons of REE per year.[12] The mine also produces over 8 million tons of waste rock annually, which can have high concentrations of toxic and radioactive elements.[13, 14] Weathering of the waste rock has led to contamination of soils and groundwater with high levels of toxic metals (e.g., Cr, Cd, Pb, and As) and fluoride which have caused negative impacts on human health and the environment in the areas near the mine.[15-20]

The ion adsorption clay resources refer to REE ions adsorbed to clay minerals such as kaolinite and halloysite and are mostly found within the top 20 meters of the soil spread evenly across a large surface area in southern China.[21, 22] The ion adsorption clays are mined either via strip mining or solution mining.[23] Strip mining involves removing the top layer of REE rich soil followed by heap leaching. Production of 1 ton of rare earth oxides (REOs) from the ion adsorption clays using strip mining and heap leaching

requires 300 sq. m of ground cover and produces 2000 tons of tailings and 1000 tons of wastewater.[24] In 2010, mining of the ion adsorption clays resulted in the destruction of 153 sq. km of forest, 302 abandoned mines, and 191 million tons of tailings, with estimated reclamation costs of $5.6 billion.[24] Solution mining involves pumping ammonium sulfate directly into the soil to mobilize the REEs (via ion exchange) and channeling the runoff into collection ponds.[22] Typical sizes of solution mining operations are 5000-10,000 square meters and injection wells are 2-3 meters deep, just above the REE rich strata.[25] This technique can result in discharges with very high concentrations of ammonia (up to 4000 mg/L) into nearby waterbodies, which can cause acute toxicity to aquatic life, severe deceases in dissolved oxygen, and eutrophication.[23, 25, 26]

1.3 Waste Materials as Sources of REEs

The reliance on limited sources for such critical elements has caused supply chain instability and large fluctuations in price.[27] This, in addition to the environmental risks associated with traditional mining processes, has caused increasing interest in finding alternative sources of REEs. Proposed alternatives include waste materials, such as coal combustion residuals (CCR), acid mine drainage (AMD), electronic waste, and mining residuals, among others.[4-7] In this work we focus on recovering REEs from CCR, coal processing residual, and AMD.

CCR is solid waste generated during the coal burning process. Recent surveys of CCR have shown that CCR can have REE contents that are 1.5 to 20 times above the average crustal abundance.[4, 5, 28, 29] REEs exist naturally in the coal seams and are concentrated during the combustion process.[30] In the U.S., there are three major coal

producing regions: the Appalachian Basin, Illinois Basin and the Powder River Basin. Coals from the Appalachian basin tend to produce CCR with the highest REE content and Powder River basin coals produce CCR with the lowest. In this work we will focus on CCR from the Appalachian and Powder River basins, and a coal processing residual from the southwestern U.S. CCR is also an attractive resource for REEs because of the large amounts generated annually (36 million tons of fly ash per year in the U.S. alone) , as well as the large reserves in legacy disposal sites that may be available due to renewed efforts to excavate or remediate these sites.[31]

AMD is generated from the oxidation and dissolution of sulfide minerals that have been exposed and perturbed during mining activities. AMD has also been shown to be enriched in REEs and it was estimated that AMD from the Appalachian region alone produces between 500-3400 metric tons of REE.[7, 32, 33] In this work, we will focus on AMD from the Appalachian region, specifically southwestern Pennsylvania. While enriched in REEs, these geologic wastes are still relatively low-grade compared to traditionally mined ores and the chemical compositions can vary greatly depending on the type of waste. These wastes are also distributed across large geographic areas, which increases the difficulty of efficiently scaling separation processes. By designing efficient leaching and separation techniques, we could take advantage of AMD and CCR as sources of REEs, which could potentially help ease supply chain risks and reduce the burden placed on primary extraction of REEs.

1.4 Primary Processing of REE Ores

Hydrometallurgical processing of REEs ores from the Bayan Obo mine consists of three major steps: physical separation (beneficiation), calcination, and leaching.[34] Physical separation processes include grinding, flotation, gravity separation, and magnetic separation.[34] The ores then undergo heated calcination with H_2SO_4 to breakdown the fluorocarbonate matrix.[34, 35] The solids are then leached using HCl to solubilize the REEs before they are precipitated using oxalic acid.[34, 35] This process use large amounts of acid and generate HF gas and carbon dioxide, which present environmental and occupational hazards.[34]

1.5 Acid Leaching of REEs from Coal Combustion Residuals and Byproducts

Acid leaching and alkaline sintering are also a common primary step in the extraction and recovery of REEs from CCR.[36-39] CCR has the advantage of not needing certain beneficiation steps, such as grinding, because it already exists as a fine powder. For American fly ashes, the elemental composition and REE leaching efficiency are specific to the region of coal origin.[4] While Appalachian CCR tends to have higher REE content, the REEs are more difficult to leach and a sintering step is required to achieve full recovery.[36, 37] In contrast, PRB CCR has lower REE content, but high recovery can be obtained using a one-step leaching.[36, 37] The differences in REE leachability are due to how the REEs are incorporated into the solid matrix.[40, 41] In this work, we focused on one-step acid leaching methods because they would be easier to implement industrially.

1.6 Solubility of REEs in Complex Aqueous Systems

Acid leachates of CCR are complex mixtures that have low concentrations of REEs, high concentrations of other metals (e.g., Ca, Al, Si, and Fe), and low pH. Highly complex, low pH leachates represent challenges for downstream separation processes.[42, 43] It is therefore important to understand how the pH and elemental composition of leachates affect REE solubility. This knowledge will help inform the design of leaching methods and for efficient separations.

While REE solubility in acid leachates of CCR is not well studied, previous work on REE solubility in acid leachates of other waste materials can provide insight into the controls on REE solubility. Previous studies have reported that REEs can be selectively precipitated from waste materials, due in part to the higher solubility of REEs compared to most major metals.[44, 45] However, REEs have also been shown to adsorb Fe-(hydr)oxides and alumino-silicate clay minerals in a process that was pH dependent.[22, 46-51] At pH 5-6 significant adsorption of REE to clay minerals has been observed, while below this pH range REEs remained soluble.[22, 48, 51] It has also been reported that in leachates of a coarse coal refuse REEs will readily sorb to aluminum and hydroxysulfates at pH greater than 3.5.[39] Saturation indices have also been able to be used to describe the solid phases formed during the staged precipitation of the coarse coal leachates.[39]

REEs can also sorb to mineral phases in natural waters. For instance, in groundwater with pH greater than 4, REEs were shown to sorb to oxides/clays and coprecipitated with carbonates and phosphates.[52] Precipitating Fe oxyhydroxides were effective scavengers of REEs in waters from a natural spring in the pH range of 3.6-6.2.[51]

In passive-remediation systems of acid mine drainage, both Al and Mn phases adsorbed REEs at pH values between 5.5-6.6.[7, 53] These works demonstrate the importance of understanding the effects of both pH and elemental composition on REE solubility in complex aqueous systems, such as acid leachates of coal byproducts.

In the second chapter of this dissertation, we investigate the role of the aqueous composition of leachates in controlling REE solubility during hydrometallurgical recovery of REEs. This chapter focuses on coal fly ash as an example alternative REE waste stream where acid leaching is one of the first steps in the REE recovery process. The hypothesis for this aim is that REE solubility will be controlled by formation of Fe, Al, and Si-hydroxide minerals which will act as sorption sites for REEs.

1.7 Introduction to SLMs

The most common industrial method for separating and purifying REEs from acid leachates is solvent extraction (SX). The SX process consists of two major steps: extraction and stripping. In the extraction step, an aqueous feed is mixed with an organic solvent that contains an oil-soluble extractant. Metal ions in the aqueous feed transfer to the oil phase by binding to the organic extractant. After separation of the oil phase from the aqueous feed, the REEs are stripped from the oil with an acidic stripping solution. This process is repeated over many cycles (often dozens) until the metals in the stripped liquor reach the desired purity. While SX is a robust and proven technology, it has several disadvantages such as high capital costs, large physical footprint, and high usage of organic solvents, which pose environmental and occupational hazards.

SLMs are a modification and promising alternative to SX because they have a smaller footprint, consume fewer chemicals, have modular designs, and can transfer metals against a concentration gradient.[54] In SLMs, the extraction and stripping steps are combined into one unit process. The specific mechanism by which metals in SLMs are transferred from the feed to the strippant can described by five major steps (Figure 1). 1) Aqueous metals in the bulk feed diffuse to the feed-membrane interface. 2) The aqueous metal reacts with the extractant at the interface to form an organic complex. For an acidic, counter-transport extractant, the type that is used in this work, H^+ ions are simultaneously released into the feed. 3) The metal complex diffuses across the membrane phase. 4) The metal is stripped from the organic phase by H^+ ions into the strippant phase. 5) The metal diffuses from the strippant-membrane interface to the bulk strippant. The uncomplexed extractant then diffuses back to feed-membrane interface, allowing the process to repeat. The separation is driven by concentration gradients that exist at each step of the separation.

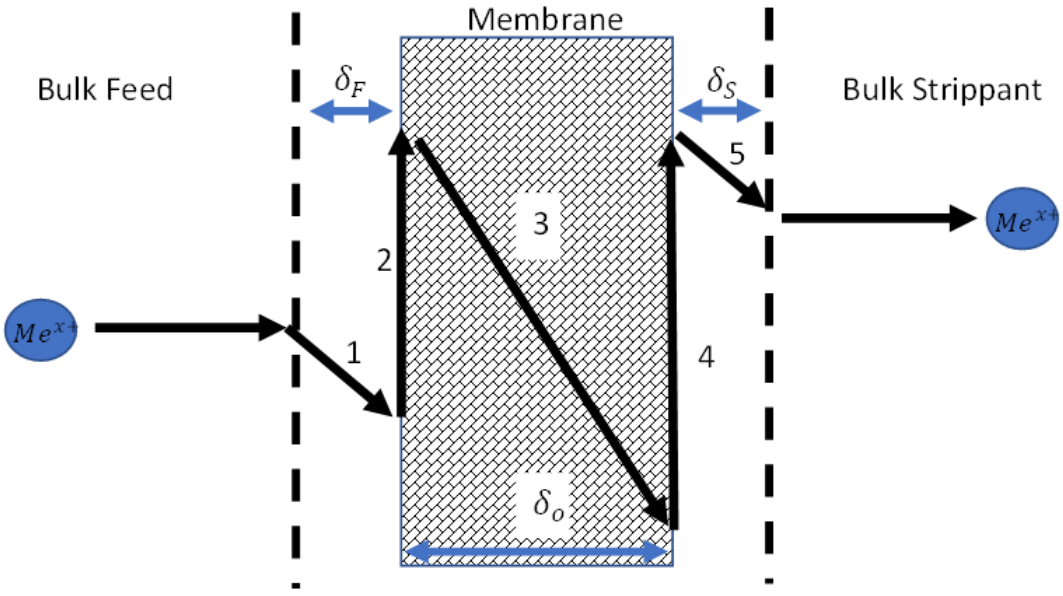

Figure 1: Schematic showing the individual transport steps for a metal ion, Me^{x+}, in an SLM. The arrows are a qualitative description of how the metal concentration changes during at each step.

Despite their advantages, SLMs are not common industrially, due in part to the limited lifetime of the liquid membrane phase.[55] The liquid membrane phase can degrade during operation, leading to short-circuiting of the membrane and bypassing of the separation mechanism. Another major limitation for industrial use of SLMs is the difficulty in accurately predicting performance for varied feedstocks. Because of the complexity of the process, an iterative approach for reactor optimization is often required. Transport of a metal from the feed to the strippant encompasses multiple mass transport steps and variables that can affect the process. These variables include the pH of the feed and strippant, concentrations of the metals in the feed, type of acids in the feed and strippant, type and concentration of the extractant, temperature, and mixing speed.[54, 56]

While there are multiple approaches to modelling SLMs, this work will evaluate mass transfer of metals across the membrane using the permeability coefficient, *P*. The *P* coefficient can be derived from the equation of the overall flux *J* of a metal across the membrane.[54]

$$J = -\frac{dC}{dt}\frac{V}{A} \quad (1)$$

Where *V* is the volume of the feed and *A* is the area of the interface, and *C* is the bulk concentration at time *t*. Dividing by *C* and integrating the above equation with respect to time allows us to define P as:

$$\ln\left(\frac{C}{C_0}\right) = -\frac{A}{V}Pt \quad (2)$$

The *P* coefficient is the flux of a metal across the membrane normalized the initial feed concentration and is therefore use for comparing across multiple different experiments. It is determined experimentally, by plotting ln(C/C_0) versus time. The P coefficient assumes that the flux into the membrane phase is the same as the flux out of the membrane and is only valid for metals at relatively low concentrations.[54]

1.8 Separation of Metals from Synthetic Feeds using SLMs

Potential feedstocks from waste materials are varied and complex, with concentrations of REEs and other metals varying by orders of magnitude.[6, 7, 57, 58] For example, in leachates of coal ash and acid mine drainage REEs are on the order of 0.0001-0.002 mmol/L.[6, 7, 57, 59] In contrast, leachates of e-waste have Nd concentrations as high as 120-230 mmol/L.[58] Fe concentrations also have similar levels of variability, with concentrations in coal ash leachates, acid mine drainage, and e-waste leachates of 1.5

mmol/L, 0.01-7 mmol/L, and 1100-1600 mmol/L, respectively.[6, 7, 57-59] While SLMs have been shown to be effective at separating and purifying multiple metals from a variety of synthetic and real feedstocks, there is little work on how the presence of metals at high concentrations in geologic waste materials (e.g., Ca, Fe, and Al) affects REE mass transfer in SLMs.[57, 58, 60-64] In this work, we therefore tested synthetic feeds with relatively simple compositions and systematically evaluated one composition variable (e.g., Nd, Fe concentrations, pH) to quantify its individual effects.

This section discusses the major mechanisms that control mass transfer of metals in relatively simple synthetic feeds of one to three elements. While there is a large amount of data on metals separation using SLMs, it can be difficult to compare results because of the differences in experimental designs of individual experiments and the differences in approach to modelling. Still, there are some useful insights that can be gained from the literature when trying to understand REE behavior in feeds of leachates of solid waste materials.

REEs have a high affinity for and very fast reactions with organophosphorus extractants, such as di-2-ethylhexyl phosphoric acid (DEHPA), the extractant used in this work.[65-68] Additionally, equilibrium constants and distribution coefficients for the DEHPA-REE reaction are higher for HREEs than LREEs and the values can vary by up to five orders of magnitude from the lightest REE to the heaviest.[69-71] This is important because relative differences in equilibrium constants for the DEHPA-REE reaction are likely a major factor affecting separation of individual REEs from a mixture in SLMs.[72]

Reactions of other relevant metals (e.g. Fe, Al, Ca) with DEHPA are relatively slow compared to REEs. Reported activation energies for the reaction of DEHPA with Fe(III) and Al(III) are 40.3 kJ/mol and 79.4-82.4 kJ/mol, respectively.[65, 73-75] The kinetics of the reaction of DEHPA with Group I and II elements are considered to be relatively slow, and the affinities with DEHPA have been shown to increase with decreasing ionic radius ($Mg^{2+} > Ca^{2+} > Sr^{2+} > Ba^{2+} > Na^{+}$).[76, 77] Equilibrium binding constants for metals like Ca, Fe, and Al with DEHPA are either not available or not comparable to studies using REEs, making it to directly compare affinities; however, it is well established that the non-REE metals can have strong affinities for DEHPA that can vary by large amounts.[76, 78] These results suggest that at high enough concentrations, non-REE metals could interfere with REE mass transfer by consuming large amounts of DEHPA.

Previous work has shown that high degrees of separation can be achieved when separating REEs from simple mixtures with Fe.[65, 66, 79, 80] However, a baseline for maximum possible mass transfer was not provided for most of the studies separating REEs from Fe, so it is difficult to explicitly state how the presence of Fe affected REE separation. One study was able to show that mass transfer of Gd in an equimolar Fe/Gd feed was lower than in a single element Gd feed.[65] While this result demonstrates that Fe can affect REE mass transfer, an equimolar Fe/Gd feed is not representative of low-quality feedstocks that are of interest in this work. The pH gradient across the membrane has also been identified as a major driver of mass transfer for SLM units that use DEHPA as the extractant. This factor is important because the pH of candidate feedstocks such as AMD and CCR leachates can vary from 1 to circumneutral.[6, 57, 81, 82] The pH gradient

across the membrane is a major driver of REE mass transfer because DEHPA is a cation exchange extractant that exchanges a stoichiometric amount of H^+ ions for every mole of metal ion transported across the membrane (e.g., 3 mol H^+ for 1 mol of Nd^{3+}). To our knowledge, there is no work that systematically evaluates the effect of non-REE metal concentrations and pH on REE mass transfer using synthetic feeds that are representative of low-grade feedstocks.

Chapter 3 of this work explores the ways in which mass transfer of REEs is affected by the feed concentration of competitive metals at varying [REE]:[Competitor] concentration ratios using simple feeds of one competitor and one REE. This will provide important information on the effects of specific metals on REE mass transfer that will ultimately be used to understand REE mass transfer in more complex feeds. The hypothesis for this aim is that REE mass transfer will be greater at high [REE]:[Competitor] molar ratios and lower at lower molar ratios due to increased competition for metal binding sites at the liquid membrane interface.

1.9 Recovery of REEs from Leachates of Waste Materials using SLMs

Recently, SLMs have been shown to efficiently separate and purify REEs from complex mixtures, such as coal ash leachates, e-waste leachates, and nuclear wastes.[57, 58, 61, 62, 83, 84] For examples, in e-waste leachates, Nd mass transfer was shown to be high despite the presence of Al, Ni, Zn, and Fe in the feed.[58] Additionally, Fe was the only non-REE metal that was significantly separated.[58] The extraction of non-REE metals was concluded to be low because of their weak affinity for the extractant (tetraoctyl diglycolamide, TODGA) compared to REEs. Changes in REE feed concentrations were

therefore surmised to have a larger impact on the extraction rate of REEs than changes in the concentration of non-REE metals. Other work using SLMs to separate REEs from a CCR leachate showed competition for limited metal binding sites at the feed-membrane interface was the major factor limiting REE mass transfer.[57] The results of studies using real leachates indicate REE mass transfer could be inhibited when a competitive metal with a sufficiently high affinity for the extractant is present at sufficiently high concentrations. The effect of competitive metals outcompeting REEs for metal binding sites at the feed-membrane interface is significant for feedstocks where REE concentrations are much lower than other metals (e.g., CCR and AMD).

While the literature has multiple examples of SLMs that were able to successfully and selectively separate REEs from real leachates with a complex chemistry, they were not able to fully comment on how the composition of the feed affected REE mass transfer. There is a gap in the literature in understanding the full impact that differences in feed chemistry could have on REE recovery, especially in complex feeds with multiple competitive metals. Therefore, in this work we investigate the potential application of SLMs as a method to selectively separate REEs from real AMD feedstocks, which to the best of our knowledge has not been tested.

Chapter 4 of this work focuses on determining the effectiveness of SLMs as a method for selectively separating REEs from real AMD from southwestern Pennsylvania. It also tries to identify key feed characteristics that affect SLM performance. This work will help to provide a framework for predicting REE mass transfer when using real low-grade feeds based on the aqueous chemistry of the feed. The main hypotheses are 1) that

mass transfer of REEs would be lower for feed with higher concentrations of major competitive cations due to higher competition for metal binding sites at the membrane interface and 2) feeds with higher pH would have higher REE mass transfer due to a higher pH gradient across the membrane.

2. Major Element Composition Controls Rare Earth Element Solubility During Leaching of Coal Fly Ash and Coal By-Products

Published in 2020 in the International Journal of Coal Geology (Middleton et al. 2020; https://doi.org/10.1016/j.coal.2020.103532).

2.1 Introduction

Rare earth elements (REE), defined here as the 14 stable elements of the lanthanide series plus yttrium and scandium, are essential materials for a wide variety of applications that includes modern electronics, military applications, catalysts, and green industries for manufacturing wind turbines.[85, 86] In many of their applications REEs are not easily replaceable and demand is only expected to continue increasing.[87] Currently more than 90% of the global REE supply market is based in China, and recent instabilities in REE prices have motivated efforts to diversify the REE supply market [88, 89], particularly for the critical elements such as Nd, Eu, Tb, Dy, Y, and Er .[90]

Coal mining wastes and combustion residuals have received much attention in recent years as a potential alternative resource for REEs. The REE contents in certain types of coal refuse and coal combustion residues (CCR) can be elevated 1.5 to 20 times above average crustal abundance, depending on the geologic origin of the coal. [4, 5, 28, 29]CCR may be an attractive resource for REEs because of the large amounts of CCR generated annually (36 million tons of fly ash per year in the U.S. alone) [31], as well as the large reserves in legacy disposal sites that may be available due to renewed efforts to excavate or remediate these sites .

Acid leaching is typically the primary step in the extraction and recovery of REEs from coal refuse and CCR.[36-39] In order to maximize recovery of REEs from these leachates, it is important to understand the connection between REE solubility, pH, and major elemental components of the leachate (Ca, Al, Si, and Fe) because leachate complexity and acid content can have major effects on subsequent REE purification processes.[42, 43] Some studies have proposed using the enhanced solubility of REEs relative to major elements at higher pHs for REE purification of several different feedstocks [44, 45]; however this approach has not been fully investigated in relatively dilute geological feedstocks such as coal wastes or coal fly ash.

Recent work on geochemical behaviors of REEs in the surface and subsurface environment provides clues to understanding REE solubilization from coal related materials. For instance, in groundwater, REEs can be sorbed to oxides/clays or coprecipitated with carbonates and phosphates and REE concentrations tend to decrease at pH values greater than 4.[52] Similar observations have been reported for heap leaching of a coarse coal refuse, in which solubilization of REE was substantially decreased at pH greater than 3.5, reportedly due to REE sorption to aluminum and iron hydroxysulfates.[39] Additionally, sorption to an aluminum sulfate mineral, basaluminite, was found to be a major sink of soluble REE ions in a passive-remediation system of acid mine drainage at pH greater than 5.5.[53] These studies show the importance of understanding the tandem effects of pH and aqueous composition of major elements on REE concentrations in complex aqueous systems, such as the acid leachates of coal byproducts.

This study investigated the effects of leachate pH and major element composition on REE solubility and extraction potential from CCR and a coal processing refuse residual. We accomplished these objectives by analyzing the aqueous elemental composition of acidic leachates of selected fly ash and coal refuse samples as well as the elemental and mineralogical characteristics of residual and precipitated solids that remain or are generated during the leaching process. Chemical equilibrium and mineral saturation calculations were performed to evaluate how the experimental results could apply more broadly to REE extraction and recovery efforts from unconventional geological feedstocks beyond coal byproducts. Results show that the chemical composition of leachates can provide insights on REE solubility and purity in leachates, information that is essential for evaluating efficacy of REE separation processes in downstream separation processes.

2.2 Experimental Methods

2.2.1 Feedstocks

This study involved fly ash samples from seven different pulverized coal combustion boilers in the U.S. (Table 1). Most of these samples were characterized from our previous work [4] (Table 1) and were generated from the coals of two major coal producing regions of the U.S. - the Powder River Basin (PRB) and Central Appalachian Basin (APP). Sample PRB-FA1.2 was obtained from the same power station but different year as sample PRB-FA1, which was studied in our previous work.[36, 37, 40] We also tested a coal processing residual (N003) from the Southwestern U.S., a coal source that has yet to be extensively characterized and studied for REE extractability. Leaching studies were

replicated for a subset of the samples: PRB-FA1.2 (n=3), PRB-FA2 (n=2), APP-FA1 (n=2-9), APP-FA3 (n=2).

Table 1: Fly ash and coal waste samples selected for this study and their elemental compositions. The asterisk * denotes data that were originally reported in a previous study [4]. Sample ID codes for the fly ash samples are the same as those in other studies [4, 36, 37]. Total REE refers to the sum of Sc, Y, and the lanthanides.

Sample ID	Type	Feed Coal Basin	Collection year	Si (% as SiO_2)	Al (% as Al_2O_3)	Fe (% as Fe_2O_3)	Ca (% as CaO)	Mg (% as MgO)	Total REE (mg/kg)
APP-FA1	fly ash storage silo	Central Appalachian	2014	50.8	30.3	10.2	1.5	0.97	735
APP-FA3	fly ash	Central Appalachian	2014	54.2*	28.4*	7.6*	4.01*	1.07*	708
PRB-FA1	fly ash	Powder River	2015	38.3*	22.5*	5.21*	22.9*	4.21*	399*
PRB-FA1.2	fly ash	Powder River	2017	34.0	22.2	6.1	23.2	4.9	422
PRB-FA2	fly ash	Powder River	2013	39.2*	20.7*	5.98*	22.4*	5.08*	462
PRB-FA3	fly ash	Powder River	2013	29.5*	16.6*	4.8*	31.1*	6.98*	289
PRB-FA4	fly ash	Powder River	2015	30.1*	15.3*	4.4*	33.6*	7.79*	262
N003	coal refuse residue	Southwestern U.S.	2019	27.5	14.1	1.4	0.5	0.6	176

Trace element content of the fly ash samples were determined at Duke University by Na_2O_2 alkaline sintering followed by acid dissolution, as described previously.[4, 91-93] Analysis of major and trace element concentrations in these digestates was accomplished by inductively coupled plasmas mass spectrometry (ICP-MS), as described below. The content of major elements (Si, Al, Ca, Fe, Mg, etc.) of the fly ash feedstocks were determined by solid state X-ray fluorescence spectroscopy, also described below. Elemental content in the coal refuse sample N003 was determined by ALS Limited using lithium borate fusion, followed by acid digestion and analysis by ICP-MS for trace elements and ICP-atomic emission spectroscopy for major elements.

2.2.2 Materials for leaching experiments

All reagents were prepared using doubly deionized water (>18MΩ-cm, Millipore Milli-Q). Leaching solutions comprised 1 M HCl, prepared by diluting trace metal grade concentrated HCl (Fisher Scientific) in water. A solution of 10 M NaOH (BDH Chemicals) was used for pH adjustments. All acid leaching experiments were performed in 50-mL polypropylene tubes (VWR International) on a temperature-regulated hotblock (Environmental Express). Trace metal grade nitric acid (Fisher Scientific) was used for the sintering method and for dilution of samples for ICP-MS analysis.

2.2.3 REE Leaching Procedure

The REE leaching method (schematic in Supporting Information Figure A1) was adapted from a procedure described by King et al. and had resulted in relatively high recovery of REEs (>95%) for fly ashes from PRB coal sources.[37] Variable masses of ash (0.4 g to 8 g) were leached at 85˚C for four hours in 40 mL of 1 M HCl. The sample mass concentrations in the leachate solutions (herein referred as pulp density) were between 10 and 250 g/L. Following leaching, the samples were cooled and then centrifuged at 3000 rfc for 10 minutes. The supernatant was decanted to new tubes. The leachate solutions were reserved for major and trace element analysis by ICP-MS while the solids were freeze-dried and rinsed with doubly deionized water for 30-60 minutes for elemental and mineralogical analyses.

For these leachates, 40-mL aliquots received dropwise additions of a 10 M NaOH stock solution until a desired endpoint pH value was achieved (as monitored by a combination pH electrode). Each aliquot was adjusted to a different pH value in order to

achieve multiple intervals up to pH 6. The samples were then held for 4-12 hours after the NaOH addition, and then centrifuged at 3000 rfc for 10 minutes. The supernatant was decanted and preserved in 2% HNO_3 for ICP-MS analysis. Solids that formed after the pH adjustment were freeze-dried after centrifugation and rinsed with doubly deionized water for 30-60 minutes for elemental and mineralogical analysis.

2.2.4 Chemical Analyses

Metals concentrations in aqueous samples were determined by ICP-MS (7900, Agilent Technologies). All samples were preserved in 2% v/v HNO_3 before analysis and were typically diluted 100-fold with a 2% HNO_3 diluent prior to injection into the instrument. The REEs and most other metals were analyzed in helium gas reaction mode to reduce polyatomic interferences. Aqueous Si, Ca, and Se concentrations were analyzed in hydrogen gas reaction mode. Instrument calibration was performed at the start of the sample batch and verified by an aqueous standard reference material (High Purity Standards (CRM-TMDW-A), traceable to NIST SRM 3100 series). Internal standards of indium and rhodium were co-injected for all samples to correct for shifts in signal intensity during the batch run. Bismuth was also used as an internal standard for high mass elements for some batch runs.

Elemental composition of the coal refuse, N003, was analyzed separately by Australian Laboratory Services (ALS Limited) and the analytic methods are described in brief below. The lanthanides and Y were quantified using a lithium borate fusion prior to acid dissolution and ICP-MS analysis. The same fusion was then analyzed using ICP-

AES to determine major elemental composition. Sc was analyzed for using a four acid digest followed by ICP-AES.

Elemental composition of residual and precipitated solids was analyzed by X-ray fluorescence spectroscopy (XRF) using a Rigaku Supermini200 Benchtop Sequential Wave-Dispersive XRF Spectrometer (50 kV, 200 W Pd-anode, Rigaku, Tokyo, Japan). Previously freeze-dried samples were mixed with a binding agent (Spectroblend, Chemplex) at a ratio of 8.57:1 and pellet-pressed under vacuum at 12 tons of force prior to analysis. XRF analyses were performed under vacuum. A LiF crystal was used to quantify heavy elements ($Z>20$) while a PET crystal was used for lighter elements ($Z<20$). A semi-quantitative EZ scan analysis routine was used with the results verified with a coal fly ash SRM 1633c.

Mineralogical composition was evaluated by synchrotron X-ray diffraction (XRD), performed at the Stanford Synchrotron Radiation Lightsource on beamline 11-3. Freeze-dried samples were homogenized and then mounted on clear, X-ray amorphous tape for transmission measurements. Samples were collected at a beam energy of 12.7 keV with a two-dimensional Rayonix MX 225 CCD area detector. Raw data files were processed and converted into 2-theta patterns using the Nika package in Igor.[94] Patterns were then analyzed using the Panalytical X'Pert HighScore software and compared to crystal patterns from the ICDD database.[95]

2.2.5 Thermodynamic Modelling

Chemical equilibrium calculations for soluble phase speciation of major metals and REE was performed using VisualMinteq (ver 3.1).[96] The purpose of the calculations

was to evaluate the possibility of mineral hydroxide precipitation of REEs and major metals in the leachates. The inputs for the model calculations were values for pH and Al(III), Si(IV), Fe(III), Mg(II), K(I), Ca(II), and La(III) concentrations measured in the leachates. These metals were selected because of their dominant concentration relative to other analytes of ICP-MS. To simplify the model, La was the only REE included, and it was assumed that all other REEs would behave similarly to La. Total Cl^- concentration was another input parameter and entered as 1 mol/L (the molarity of the original acid leaching solution). XRD analyses suggested the presence of sulfate minerals in some residual solids after leaching. Dissolved sulfate concentrations were not measured in the leachates and not available for equilibrium calculations. Thus, the calculations were performed with two different assumed total SO_4^{2-} concentrations, 1.5 mM and 15 mM. These values are based previous coal fly ash leaching studies performed with deionized water or river water.[97, 98]

Calculations were performed using single leachates for samples PRB-FA1.2, APP-FA1, and N003 (i.e., not on the average composition of multiple leachates). From the aqueous phase speciation calculations, we examined the model output of saturation index, *SI*, for selected mineral hydroxide phases, where *SI* is defined as:

$$SI = log \frac{(ion\ activitiy\ product)}{K_{sp}}$$

For a given mineral phase with known solubility product K_{sp}, *SI* values greater than 0 suggest conditions of oversaturation for the respective mineral phase.

2.3 Results and Discussion

2.3.1 REE solubility as a function of pulp density

To understand how the major ion concentrations in the leachates affect extraction and solubilization of REEs during acid leaching, we first examined the importance of pulp density, i.e., the mass of solids relative to acid leachate volume. The results (Figure 2) showed that solubilized REE concentrations generally increased with pulp density; however, key differences were observed between the PRB fly ashes and the other materials (APP ashes and Navajo coal refuse). For the PRB ashes, the concentrations of REEs increased nearly proportionally with increasing pulp density until a pulp density of approximately 70-100 g/L. Above this threshold, soluble REE concentrations were substantially lower compared to the leachates at lower pulp densities. Maximum aqueous concentrations of Sc were observed at a pulp density of 40-50 g/L, which is lower than the pulp density at which maximum soluble concentrations were observed for the lanthanides and Y. Trends for the APP ashes and Navajo coal refuse leachates were markedly different: aqueous REE concentrations increased linearly with increasing pulp density for the range of pulp densities tested. Higher pulp densities were not tested due to the potential of gel formation. The trends in aqueous concentration of Sc in APP ashes and Navajo coal refuse were similar to other REEs.

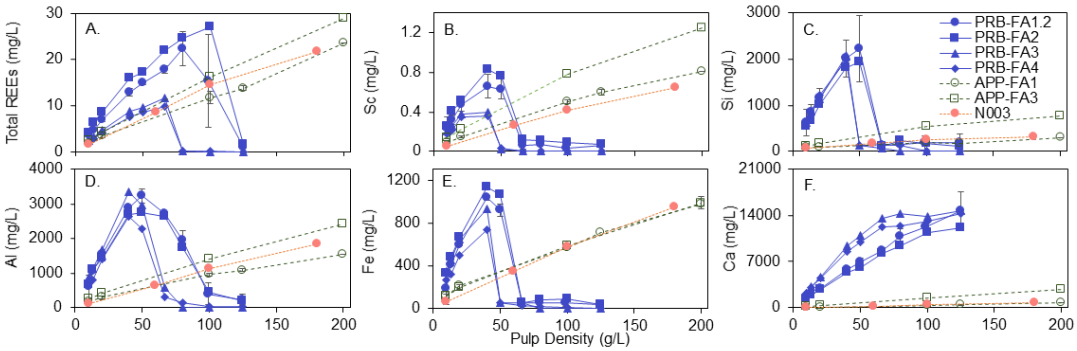

Figure 2: Effect of leaching pulp density on aqueous concentrations of (A) total REEs, (B) Sc, (C) Si, (D) Al, (E) Fe, and (F) Ca for four PRB ashes (blue), two APP ashes (green), and a Navajo coal (orange). Data points and error bars represent the average and standard deviation of replicate leachates for PRB-FA1.2 (n=3), PRB-FA2 (n=2), and APP-FA1 (n=2-9), APP-FA3 (n=2). Data points for all other samples represent single leachates.

2.3.2 Effect of pulp density on major ion solubilization

The acid leachates comprised not only of soluble REEs, but also a large variety of other solutes that affect the final leachate pH and major ion composition. The solute composition can help explain the observed trends of extractable REEs versus pulp density in the leachates as wells as differences in these trends between feedstocks. For instance, for Navajo coal refuse and APP ash, the final pH of the leachates was less than 1 at all pulp densities, while for PRB leachates the pH increased from less than 1 to 5 for pulp densities between 10 and 100 g/L (Supporting Information Figure A2).

Major soluble metals in the leachates included Fe, Si, and Al, and their concentrations also varied non-linearly with pulp density for the PRB fly ashes (Figure 1C-E), similar to the trend observed for REEs (Figure 2A). The maximum concentrations of soluble Al, Si, and Fe were observed at pulp densities of approximately 40-60 g/L. Note that this pulp density is lower than pulp density threshold for the maximum soluble

REE concentrations (70-100 g/L, Figure 2A). This result suggests that for PRB fly ashes, the pulp density can serve as an adjustable leaching parameter in an REE recovery process as a means to optimize aqueous REE concentrations while minimizing potentially interfering metals. For example, the REE purity in the leachate at 80-100 g/L pulp density was double compared to pulp densities below 60 g/L for PRB-FA1.2 (Figure A3). In contrast to the PRB fly ashes, the aqueous concentrations of Fe, Al, and Si for leachates of the Navajo coal refuse and APP fly ashes increased linearly with pulp density, similar to the REE behavior in these feedstocks.

Calcium (Ca) was another major metal element in the leachates, and the concentration of soluble Ca increased linearly with pulp density for all feedstocks tested (Figure 2F). Other group I and II elements (e.g., Na, K, Mg) were similar to Ca in this respect. Some of these ions (e.g., Ca, Fe, Al cations) are competing ions with the REEs in some purification processes.[57, 99] Thus, linearly increasing concentrations of these major ions could make high pulp density leachates of APP ashes and Navajo coal refuse less operationally feasible than low pulp density leachates despite higher aqueous REE concentrations.

2.3.3 REE recovery during leaching

Despite significant differences in total REE content in the feedstocks (Table 1), the aqueous concentration of total REEs was similar for all starting materials, especially at low pulp densities (Figure 2A). The percentage recovery for total REEs for PRB ashes was 80-90%, approximately 80% for the Navajo coal refuse, and 20-40% for APP ashes at pulp densities lower that 40 g/L (Figure 3). The % recoveries remained constant across

all pulp densities for the APP ashes and Navajo coal refuse, while % recoveries for the PRB ashes decreased significantly for leaching conditions above the previously described pulp density threshold (70-100 g/L). These results are generally consistent with previous work showing that acid leaching alone is insufficient for high recovery of REEs from APP ashes.[4, 36, 37] In these types of fly ashes, the REE are likely to be encapsulated in the aluminosilicate glassy particles that are not readily dissolved in most low-temperature acids.[100, 101]

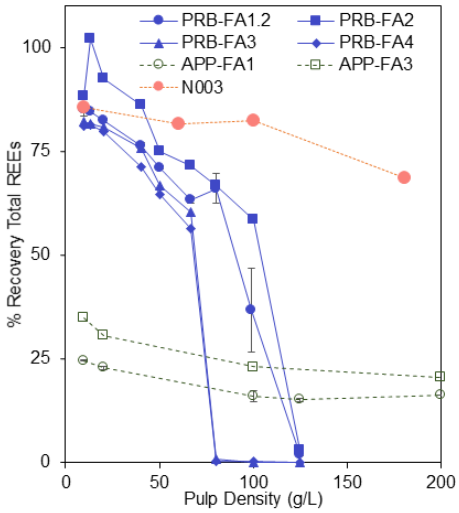

Figure 3: Percent recoveries of total REEs for four PRB ashes (blue), two APP ashes (green), and a Navajo coal (orange) after leaching at various pulp densities.

2.3.4 Characteristics of the solid residues after leaching

After the leaching and centrifugation process, two types of solids remained: undissolved ash/refuse residue and a secondary precipitate formed only at high pulp densities for PRB ashes. The leaching process resulted in minor changes in the major mineralogical composition of the feedstock samples. For example, the raw PRB-FA1.2 ash comprised primarily of quartz, mullite, periclase, anhydrite, and sodium calcium

silicate (Figure 4). After leaching, the quartz and mullite peaks were still observable at all pulp densities, while the other major phases of periclase, anhydrite, and sodium calcium silicate were absent. This result indicates that Ca and Mg phases are readily dissolvable.

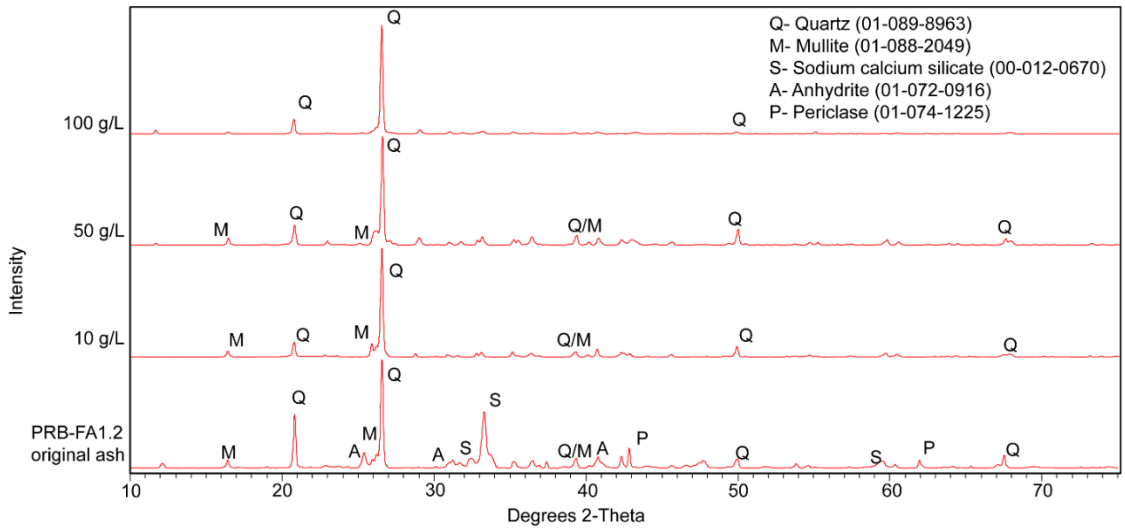

Figure 4: X-ray diffraction patterns showing the identified mineralogical composition of PRB-FA1.2 ("original ash") and residuals remaining after acid leaching (1 M HCl) at pulp densities of 10, 50, and 100 g/L in 1 M HCl.

Although the formation of new mineral phases in the leachate was not observed via XRD, the residuals, particularly at the high pulp density (>50 g/L), appeared visually different in color and texture from the feedstock, suggesting the presence of x-ray amorphous precipitating secondary phases (Figure A6). In general, the mineral phases were mainly unchanged at all pulp densities, although the quartz and mullite peaks were less prominent. This change in peak intensity does not necessarily indicate change in concentration, as newly formed amorphous phases could absorb X-rays and contribute to the overall reduction of diffracted X-ray flux. XRD patterns for other PRB-FA2 and PRB-FA3 show the formation of barite at low pulp densities and gypsum at high pulp

densities (Figures A7 and A8). These samples were not immediately freeze-dried after centrifugation, so these phases likely formed slowly in the aging wet solid. Such precipitates could provide available surface area for REE ion sorption, a process known to occur for other sulfate mineral phases.[39, 53]

Elemental analysis of the solids provided a more direct observation of the characteristics of the secondary precipitates than the XRD analysis. XRF analysis of PRB-FA1 showed that the major elemental components (>2% as oxides) in the raw ash were Na, Mg, Al, Si, Ca, and Fe (Figure 5). After leaching, there was a large relative decrease in the Ca content of the residual solids compared to the raw ash. At low pulp densities, we observed a decrease in Fe and Al contents in the residual solids compared to the raw ash; however, at high pulp densities, the relative Al and Fe content in the residual solids was comparable to the raw ash. These results indicate that the solids precipitating at high pulp densities are x-ray amorphous Fe and Al phases.

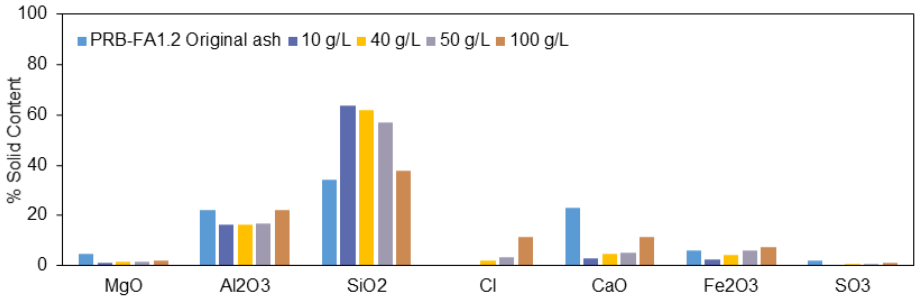

Figure 5: Major elements composition, as determined by XRF, of PRB-FA1.2 and residuals after leaching at various pulp densities.

2.3.5 Saturation States of Metal Hydroxides in the Leachates

The saturation indices (*SI*), which describe whether a given mineral is over- or under-saturated in an aqueous system, were calculated to understand the thermodynamic

potential for mineral hydroxide phase formation in the leachates and how these phases may affect aqueous REE concentrations. *SI* values for $La(OH)_3$ were negative for the leachates of all feedstock materials at all pulp densities (Figure 6A). These results suggest that the formation of discrete REE minerals was not thermodynamically favorable under all conditions tested.

The *SI* values for ferrihydrite and gibbsite appeared to be consistent with observed trends in soluble Fe and Al concentrations (Figure 6B-C). More specifically, the maximum soluble Fe and Al concentrations were observed at the pulp density and leachate conditions corresponding to *SI* values below zero for ferrihydrite and gibbsite. Note that the *SI* values for other Fe- and Al-(hydr)oxide minerals (Fe minerals: ferrihydrite (aged), hematite, lepidocrocite, maghemite; Al minerals: $(Al)OH_3$ (am), $Al(OH)_3$ (Soil), Al_2O_3(s), boehmite, diaspore) and alumino-silicate minerals (halloysite, imogolite, and kaolinite) followed the same trend as ferrihydrite and gibbsite *SI* values versus pulp density. These *SI* calculations indicate that the REEs were not precipitating as pure REE minerals in the leachates, but instead were sorbing to precipitating minerals of major elements such as X-ray amorphous Fe- and Al-hydroxides formed under certain leaching conditions (i.e. high pulp density).

Sorption of REEs to Fe-(hydr)oxides and alumino-silicate clay minerals is well documented and has been shown to be a pH dependent process.[22, 46-51] At low pH values, mineral surfaces tend to be protonated and have positive surface charge that inhibits sorption of positively charged ionic and hydrated REE species; however, at higher pH values, deprotonation of mineral surfaces hydroxyl groups results in negative surface

charge or available sorption sites for trivalent REE cations. As previously noted, leachate pH increased with increasing pulp density for the PRB fly ashes (Figure A2). Previous work showed that REE sorption to clay minerals increases at pH greater than 5, while at pH lower than 3 the clay minerals begin to solubilize.[22] Additionally, several studies showed that REEs remain in solution in the presence of Fe solids at pH values less than 4.5-5, but are removed from solution at pH 5-6.[48, 51] For PRB ashes, pH values of leachates were less than 5 at pulp density less than 100 g/L and pH was greater than 5 above this pulp density threshold. The observed difference for Sc relative to the other REEs may be due to Sc hydrolysis occurring at a lower pH than other REEs.[102] Alternatively, the loss of Sc at a lower pulp density could be due sorption to or coprecipitation with Fe minerals, as Sc has been shown to be readily associated with goethite particles and with Fe-(hydr)oxide minerals in bauxite and bauxite residue.[103-105]

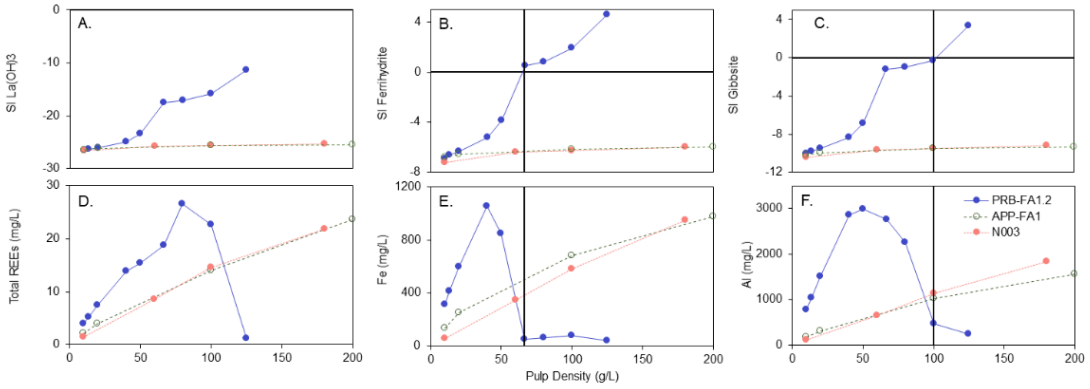

Figure 6: (A-C) Saturation Index (*SI*) values for three mineral phases: (A) $La(OH)_3$, (B) ferrihydrite, and (C) gibbsite. Positive values indicate that the mineral phase is oversaturated and will precipitate (D-F). Calculations were performed using the measured pH and aqueous concentrations of major ions including (D) La, (E) Fe, and (F) Al for leachates of PRB-FA1.2 (blue), APP-FA1 (green) and N003 (orange).

As previously discussed, barite and gypsum were both observed via XRD analyses, suggesting sulfate minerals could also influence soluble REE levels. Unfortunately, measured dissolved SO_4^{2-} in leachates were not available for *SI* calculations. Nevertheless, we performed the calculations assuming SO_4^{2-}concentrations of 1.5 mM and 15 mM, as observed in previous leaching studies.[97, 98] The results for the PRB-FA1 leachates indicated that barite was supersaturated at all pulp densities and both SO_4^{2-} concentrations while gypsum was only oversaturated with the observed Ba and Ca concentrations in leachates generated at high pulp densities (above than 100 g/L) at 15 mM SO_4^{2-} (Figure A10). For APP-FA1 and N003, barite formation was predicted at all pulp densities and both SO_4^{2-} concentrations, while gypsum formation was not predicted at any pulp density for either SO_4^{2-} concentration (Figure A10). For Al and Fe bearing sulfate minerals (Al- $Al_4(OH)_{10}SO_4$, $AlOHSO_4$, alunite; Fe- K-Jarosite and H-Jarosite), conditions for oversaturation roughly coincided with the pulp densities at which aqueous Fe and Al concentrations decreased significantly (Figure A10), especially at 15 mM SO_4^{2-}. Note that these previously reported SO_4^{2-}concentrations were measured in leachates of neutral pH, and leachable anions typically decrease with decreasing pH. Regardless, the results suggest that sulfate mineral particles, formed after leaching, could also act as sorbents for REE ions.

2.3.6 Aqueous metals concentrations after adjustment of leachate pH

The pH of leachates is a major control variable for metal solubility and also is essential for the performance of REE purification processes (e.g., solvent extraction, ion exchange (bio)sorption). Thus, we examined the effects of pH adjustments on REE

solubility for leachates generated at two pulp densities (10 g/L and 100 g/L) (Figure 7A and Figure A11A).

For the experiments performed at 10 g/L pulp density, we tested leachates with measured initial total REE concentrations of approximately 4 mg/L for the three PRB ashes tested, 2 mg/L for the APP ash, and 1.6 mg/L for the Navajo coal refuse. Prior to adjustment, the pH of the leachates was less than 1 for all sample types. In the adjustment of these leachates to higher pH values, REE concentrations were constant for target pH value of 4 or lower, regardless of the starting material (Figure 7). Decreases in REE concentrations were observed for target pH values above 4. In all leachates, adjustment to pH values greater than 6 resulted in more than 90% of the total REEs removed from solution.

Trends for Sc in the pH adjustments was different than those observed for the other REEs. At pH values 3 to 4, the Sc concentration decreased substantially in leachates of the PRB ashes (Figure 7A). The trend for Sc is similar to that of Fe, which, as noted earlier, may be due to sorption or coprecipitation with Fe-(hydr)oxide phases.[103-105] However, we note that the Sc concentrations were relatively low in these leachates and the ICP-MS signal for ^{45}Sc may be reflecting inefficient removal of polyatomic interferences (e.g., $^{28}Si^{16}O^{1}H$). With the high price of Sc, economic assessment of REE recovery processes is often driven by efficient recovery of this element.[4, 106] Nevertheless, we recommend caution in relying only on the Sc data from this study, given the uncertainties of the measurements of Sc in our leachate samples.

For most other major solutes (e.g., Fe, Al, Si), significant removal from the aqueous phase was observed at pH 4 or greater for all feedstocks (Figure 7C-F). For the PRB fly ash leachates, pH adjustments to endpoints of 2.5 to 4 resulted in variable aqueous concentrations of Fe and Si (Figure 7C and E). In contrast to most other major solutes, the aqueous concentrations of Group 1 and 2 elements (e.g., Na, Ca, Mg, K) were not affected by the pH adjustments. In general, removal of the REEs and major elements from solution occurred at similar pH thresholds. These results further support the suggestion that REE solubility is controlled by sorption to the precipitating hydroxides of Fe, Al, Si, and other major metals, similar to the sorption that occurred at high pulp densities for PRB ashes.

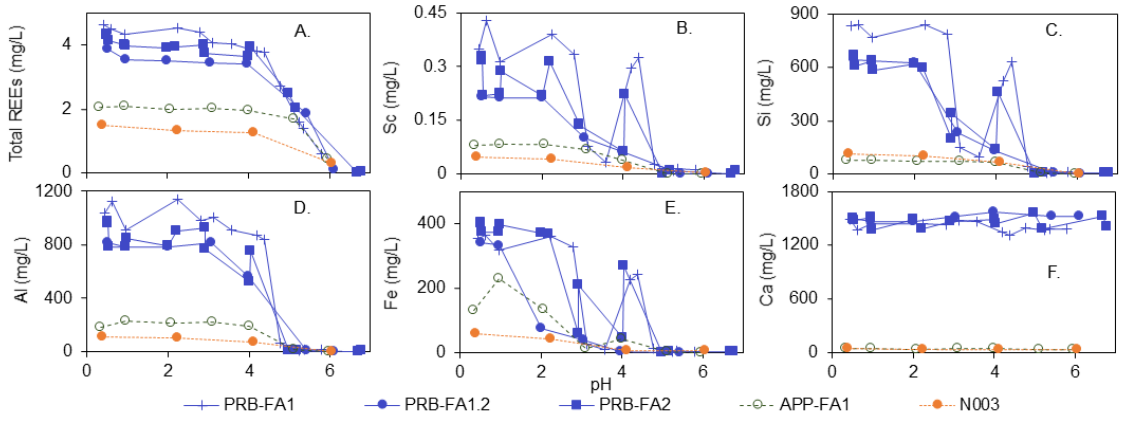

Figure 7: Aqueous concentrations of (A) total REEs, (B) Sc, (C) Si, (D) Al, (E) Fe, and (F) Si after adjusting the pH of leachates generated from three PRB ashes (blue), one APP ash (green), and a Navajo coal refuse (orange) after leaching at a pulp density of 10 g/L.

For the pH adjustments of leachates generated at 100 g/L pulp density, the trends for aqueous REE concentrations were similar to the trends observed with leachates of a lower pulp density (10 g/L) (Figure A11A), though REE concentrations were

approximately 5 times greater for 100 g/L than 10 g/L leachates. For the leachates produced at 100 g/L for PRB ashes, the initial pH value prior to adjustment was approximately 3.8, while for the APP ashes and Navajo coal refuse the pH was less than 1. Nevertheless, similar pH thresholds were observed for soluble REE concentration - approximately pH 4.8 for PRB leachates and pH 4.2 for APP ash and Navajo coal refuse leachates. These values are the same pH threshold at which other major solute metals also decreased. Since the concentrations of Fe, Si, and Al were lower at pulp densities of 100 g/L than 10 g/L, pH adjustment has more potential applicability because the pH adjustment at 100 g/L would be used to make the leachates more amenable to downstream purification processes and not as its own purification step.

XRD mineralogical analysis of the solids precipitated during pH adjustment showed that they were largely x-ray amorphous (Figures A12-16). The patterns of multiple samples suggested the presence of halite, which might have formed during the drying of the samples. Barite was also observed, but only in samples that were not freeze-dried immediately.

2.4 Conclusions

In this study, we showed that in acid leachates of coal by-products, including fly ash and coal refuse, the pulp density of the leaching step could be tuned for selective precipitation of major interfering solutes (e.g., Fe, Al, and Si) for some fly ashes. We also showed that that direct precipitation of REE-hydroxides is not a viable purification/recovery mechanism for complex and relatively REE-dilute feedstocks such as coal fly ash and coal wastes. Nevertheless, the observed trends in aqueous REE

concentrations at various pulp densities can be explained by understanding the aqueous chemistry of other major solutes. In this respect, thermodynamic analysis of leachates at different pulp densities showed that formation of amorphous Al- and Fe-(hydr)oxide and alumino-silicate phases can be predicted, while formation of pure REE-hydroxide phases is not thermodynamically favorable. Similarly, the results of subsequent pH adjustment of the acid leachates show a loss of aqueous REEs at a pH lower than values that would be expected based on thermodynamics [45]; instead, REEs precipitate concurrently with major solutes, such as Fe, Al, and Si. These results underscore the importance of understanding the overall aqueous chemistry of leachates when designing leaching and purification processes.

3. Separation of Rare Earth Elements from Low-Grade Feedstocks by Supported Liquid Membranes: Impacts of Soluble Iron, Aluminum, and pH

3.1 Introduction

The global demand for rare earth elements (REE) is increasing due to their necessity in a variety of modern technologies.[1, 2, 107] As such, waste materials enriched in REE, such as coal ash, acid mine drainage, red mud, and electronic waste (e-waste), are receiving much attention as potential alternative REE resources.[4-7, 108] Recovery of REEs from waste materials could also have the added benefit of reducing the production demands on mines, which are known to have significant negative environmental impacts.[15, 17, 18, 20]

Despite the positive aspects of waste valorization, recovery of REEs from geological and combustion wastes remains difficult because the feedstocks have relatively low REE content compared to traditional ores.[32] Moreover, the composition of solid waste materials is heterogenous with multiple modes of REE incorporation.[40] Therefore, leachates of these solids residuals are highly complex and variable, resulting in challenges for predicting the performance of separation processes. For example, leachates of coal ash and acid mine drainage have REE concentrations on the order of 0.0001-0.002 mmol/L.[6, 7, 57, 59] In contrast, leachates of e-waste have Nd concentrations as high as 120-230 mmol/L.[58] Concentrations of other metal ions in these leachates also have similar variability, with reported iron (Fe) concentrations in coal ash leachates, acid mine drainage, and e-waste leachates of 1.5 mmol/L, 0.01-7 mmol/L, and 1100-1600

mmol/L, respectively.[6, 7, 57-59] The concentrations of other elements, including Al, Ca, Na, and Si, relative to the desired REE metals can also vary by multiple orders of magnitude depending on the waste.[6] Therefore, the development of separation processes for these secondary REE resources must be able to accommodate variability in the aqueous composition of feedstocks.

Supported liquid membranes (SLM) are a potential method for separating REEs from secondary feedstocks and other complex mixtures.[57, 58, 60-62] SLMs entail a hydrophobic membrane embedded with an organic extraction solution that facilitates transfer of REEs from the aqueous feedstock to a strippant solution on the opposite side of the membrane. This approach is advantageous compared to the more industrially common solvent extraction process because SLMs consume fewer chemicals, can transfer metals against a concentration gradient [54], and can be configured for a modular process design that is advantageous for geographically distributed feedstocks. Numerous studies have demonstrated the efficacy of SLMs for metals separations in a variety of synthetic feedstocks and real leachates; however, these studies generally focus on process configuration optimization (e.g., mixing speeds, extractant choice, type of solvent, etc.) or not been relevant to complex low-grade feedstocks.[60, 63, 64, 83] No studies, to our best knowledge, have systematically studied the impact of feed composition on REE recovery, particularly at concentrations relevant for leachates of waste materials.

Previous work using SLMs to selectively separate REEs from e-waste leachates concluded that REE flux across the membrane depended more strongly on REE concentrations than concentrations of other metals in the feed (e.g., Fe, Al, Ni, and Zn).[58]

A different observation was made in the application of SLMs for coal ash leachates, in which competition for limited chelator sites at the feed-membrane interface was a rate-limiting step for REE mass transfer.[57] This metal competition effect is especially relevant for cases when metal affinities for the extractant and their concentrations in the feed vary by orders of magnitude. One potential implication of these studies using e-waste and coal ash leachates is that the [REE]:[Competitor] concentration ratio will control mass transfer.[57, 58] Other works have also shown that precipitating mineral phases of major metals such as Fe and Al can adsorb REEs in bulk solution [39], which could potentially foul membrane surfaces.[109]

The overall aim of this work was to quantify the effects of various leachate characteristics such as major metal ions (Fe and Al) and the feed pH on mass transfer of REEs in SLMs. Here, we systematically tested the relevance of these characteristics by studying SLM separations of ionic forms of neodymium (Nd) or erbium (Er) in synthetic feed solutions that were based on the composition of leachates of potential waste feedstocks including acid mine drainage and coal fly ash.[6, 57] We focused on Nd and Er because both are considered critical REEs and are representative of a light REE (Nd) and a heavy REE (Er).[9] We tested feeds that had relatively low Nd or Er concentrations (0.01-100 µmol/L) compared to competitor metals Fe or Al (0.017-17 mmol/L) and tested feed pH values from 1 to 3.5. We hypothesized that with REE mass transfer would be greater at higher [REE]:[Fe] and [REE]:[Al] molar ratios and lower at lower molar ratios because of competitions for metal binding sites in the liquid membrane.[57]

3.2 Methods

3.2.1 Materials

All solutions were prepared with doubly deionized water (>18 MΩ-cm, Millipore Milli-Q). Trace metal grade HNO_3 (Fisher Scientific) was used to adjust the pH of all feed and strippant solutions, and for diluting samples for elemental analysis. Aqueous standards of Er and Nd (1000 µg/mL) (Inorganic Ventures) were used for synthetic test solutions. Synthetic test solutions with Fe(III), Fe(II), or Al were made by dissolving Fe(III) nitrate nonahydrate (99+%, Acros Organics), Fe(II) chloride tetrahydrate (Fischer Chemical), or Al nitrate nonahydrate (98%, Alfa Aesar) in solution with HNO_3. The Fe(II) chloride tetrahydrate was stored in an anaerobic chamber (Coy Labs) when not in use.

3.2.2 Supported Liquid Membrae (SLM) Reactor Design

SLM separations were performed in a flat sheet membrane configuration that involved placement of the membrane at the interface connecting two 250-mL glass vessels in a H-cell reactor, as described previously [57]. The membrane (47 cm diameter, 0.22 µm nominal pore size, PVDF, Durapore) was prepared by an overnight soak in a volumetric mixture of 10% bis(2-ethylhexyl) phosphate (DEHPA, 97%, Aldrich) and 90% kerosene (purum, Sigma-Aldrich). A synthetic feed solution was placed in one side of the H-cell reactor, and a 5 mol/L HNO_3 acid strippant solution was placed on the other side. All H-cell reactors, other glassware, and reused plasticware were acid washed with 10% HCl (ACS Grade, VWR) and rinsed with deionized water between each use. SLM separations were performed with continuous mixing in each reactor vessel for 24 hours,

during which aliquots (0.1 to 1 mL) from both the feed and strippant were collected at 5 or 6 time points. Aliquots were then acidified in 2% HNO_3 and analyzed for metal concentration by inductively coupled plasma mass spectrometry (ICP-MS). A portion of SLM experiments were performed in triplicate to establish reproducibility. Additionally, the feed pH values were measured at the beginning and end of the 24-hour separation period.

3.2.3 Composition of synthetic feedstocks

The composition of test mixtures for the SLM experiments were based on prior observations of real leachates derived from coal ash and AMD wastes (Table B1).[6, 7, 36, 57, 59] Feed compositions consisted of 0.01 to 100 μmol/L dissolved Nd(III) and either Fe(II), Fe(III), or Al at concentrations of 0.18-18 mmol/L, 0.018-18 mmol/L, or 0.018-35 mmol/L, respectively. This composition resulted in [Nd]:[Fe] and [Nd]:[Al] molar concentration ratios from 1:1.7 to $1:3.5\times10^6$. A subset of experiments entailed mixtures of Er and Fe(III) and mixtures with Er alone, prepared at similar concentrations as the Nd solutions. The initial pH was 1 for most feed solutions, and for a subset of experiments, a range of pH values from 1 to 3.5 was tested.

Based on the composition of these feed solutions, saturation indices for Fe-oxide and Al-oxide minerals were calculated by chemical equilibrium speciation modeling with VisualMINTEQ (v3.1).[96] The saturation index values were used to determine feed stock conditions in which colloidal Fe- and Al-oxide formation was possible during the experiment.

3.2.4 Unreacted Feed Controls

In the solutions with Fe(III), the loss of soluble Nd and Er in the feed chamber was possible through adsorption to or coprecipitation with colloidal Fe(III) that might form during the separation time. Therefore, we performed control experiments in which freshly prepared synthetic feed solutions with Fe(III) and Nd were portioned into multiple 50-mL polypropylene tubes (Environmental Express) and mixed end over end for 24 hours. Over multiple time points in the mixing period, the contents of a tube were centrifuged at 175,000 rcf for 2 h 45 min. The top 5 mL of supernatant was then filtered through either a 20 or 200 nm Anodisc syringe filter (Anotop inorganic membrane filter, Whatman). Aliquots of the solution prior to centrifugation and after centrifugation/filtration were preserved in 2% HNO_3 for analysis of Nd and Fe concentrations by ICP-MS.

3.2.5 Quantification of Metals in the Liquid Membrane Phase

Membranes from a subset of experiments were taken from reactors after 24 hours and leached to determine the mass of metals present in the liquid membrane phase. The membranes were soaked at room temperature in a mixture of 8 mL HNO_3 and 2 mL H_2O_2 for one hour then leached using a microwave digestor (MARS 6, CEM Corporation) in acid clean digestion vessels (MARSXpress, CEM Corporation). The microwave digestor protocol was 1030 to 1800 W, 200 ºC and 800 psi for 15 min, with a ramp time of 20 min. Aliquots of digestates were preserved in 2% HNO_3 for ICP-MS analysis. Method blanks which entailed unsoaked membranes and membranes that were soaked in DEHPA and kerosene, but not used for SLMs experiments, were also leached using the same

protocol. The amount of organic phase in each membrane was estimated by taking the difference in weight between soaked and unsoaked membranes. Since a known volume of kerosene and DEHPA were used in the soaking solution, the masses of each component were calculated by multiplying by the densities. The mass of DEHPA in a soaked membrane is then the mass fraction of DEHPA in the soaking solution multiplied by the total mass of organics in the soaked membrane.

3.2.6 Elemental Analysis

Aqueous concentrations of all metals were analyzed using ICP-MS (7900, Agilent Technologies) operated in helium gas reaction mode. All samples were preserved in 2% v/v HNO_3 before analysis. Instrument calibrations was performed at the start of the sample batch run and verified by an aqueous standard reference material (High Purity Standards (CRM-TMDW-A), traceable to NIST SRM 3100 series). All samples were spiked with internal standards of Rh, In, and Bi to correct for shifts in signal intensity during the analysis.

3.2.7 Imaging of spent membranes

Scanning electron microscopy (SEM) (ThermoFisher Scientific) analysis of membranes after a separation experiment was performed to assess changes in surface morphology and elemental composition of the membrane. Spent membranes from a subset of the Nd/Fe(III) experiments were blot dried immediately after use and then air dried and stored for analysis. Samples were not coated in conductive material prior to analysis. SEM images, collected at 2 kV, 25 pA current, and a detector distance of 10 mm, were obtained for both the feed and strippant sides of each membrane. Energy

dispersive x-ray spectrometry (EDS) (Oxford Instruments) using a voltage and current of 20 kV and 0.8 nA, respectively, was also performed to obtain the elemental composition of the membrane surfaces.

3.2.8 Permeability Coefficients

Rates of Nd and Er transfer across the membrane was compared between experiments by calculating from the experiment data permeability coefficients *P*, a measure of metal flux normalized to the initial feed concentration. The derivation of this coefficient [110] is based on the overall flux of the metal *J* (in mol m^{-2} h^{-1}) across the membrane:

$$J = -\frac{dC}{dt}\frac{V}{A} \qquad (1)$$

where *C* is the concentration of the metal in the feed (mol L^{-1}) that changes with separation time *t*, *V* is the volume of the feed (L), and *A* is the surface area of the membrane at the feed-membrane interface (m^2). By dividing eq. 1 by C and integrating with respect to time, we obtain the following equation:

$$\ln\left(\frac{C}{C_0}\right) = -\frac{A}{V}Pt \qquad (2)$$

where C_0 is the initial concentration of the metal in the feed (mol L^{-1}). With eq. 2, the permeability coefficient *P* (in units $Lm^{-2}h^{-1}$) was obtained from the slope of a linear regression of experimental data plotted as $\ln(C/C_0)$ versus time (Figure B3). The *P* coefficient, as derived, is an overall mass transfer coefficient that was used to compare Nd and Er separation efficacy as a function of feed solution composition.

3.3 Results and Discussion

For all Nd and Er separation experiments, which varied the pH, Fe or Al concentration in synthetic feed solutions, the concentration of Nd and Er was observed to decrease in the feed side of the membrane and increase in the strippant acid chamber over the 24 h experiment (Figures B1 and B2). The linear regressions of Nd and Er data plotted as $\ln(C/C_0)$ versus time (Figure B3) resulted in R^2 values that were generally >0.94. Exceptions were experiments where Nd mass transfer was very low (i.e., greater than approximately 95% of the original Nd remained in the feedstock chamber) and Nd concentrations changed very little over the 24 h timeframe. For the linear regressions corresponding to Fe and Al data plotted at $\ln(C/C_0)$ vs. time, the R^2 values were lower and more varied (0.1-1) compared to respective regressions of Nd and Er data (>0.94) even for feeds where relatively high concentrations of Fe and Al were recovered in the strippant. The lack of log-linearity in the Fe and Al data was expected because the derivation of *P* coefficients is based on assumption of relatively low concentrations.[54]

3.3.1 Mass Transfer Rates for Solutions Containing only Nd or Er

The experiments involving single component feedstock solutions with only Nd or Er (no other metals) were used to establish maximum rates of mass transfer and *P* coefficients in our SLM experimental configuration. The *P* coefficients were within the range of 6.8 to 11.5 $Lm^{-2}h^{-1}$ for Nd and 10.5 to 16.5 $Lm^{-2}h^{-1}$ for Er (Figure 8). For Nd-only solutions, the *P* coefficient value increased with increasing initial pH of the feedstock (Figure 8). The trend was expected because the DEHPA in the liquid membrane acts as a cation exchanger (3 mol H^+ per mol of Nd^{3+}). Thus, a larger H^+

gradient between the feed chamber and the strippant acid chamber increases overall Nd^{3+} transfer rates. Because of this cation exchange process, we also observed a pH decrease in the feed chamber from pH values 2.8 and 3.6 in two freshly prepared feed solutions to final pH 1.4 after 24 h experiment with both solutions. We note, however, that this change in pH was too large based on the moles of Nd^{3+} transferred. This observation suggests that there might have been some leakage of the strippant across the reactor to the feed chamber was occurring.

For multiple experimental solutions prepared with initial pH 1, the *P* coefficients did not appear to depend on the initial Nd or Er concentration in the feed solution (Figure 8). All experiments contained relatively low concentrations of Nd or Er. From this result, we posit that that mass transfer rates in these single-component feed solutions were not limited by availability of the carrier agent (i.e., the DEHPA in the oil phase). Rather, the range of *P* values for each metal ion likely was due to experimental variability, such as mixing and fluid transport at the membrane interface.

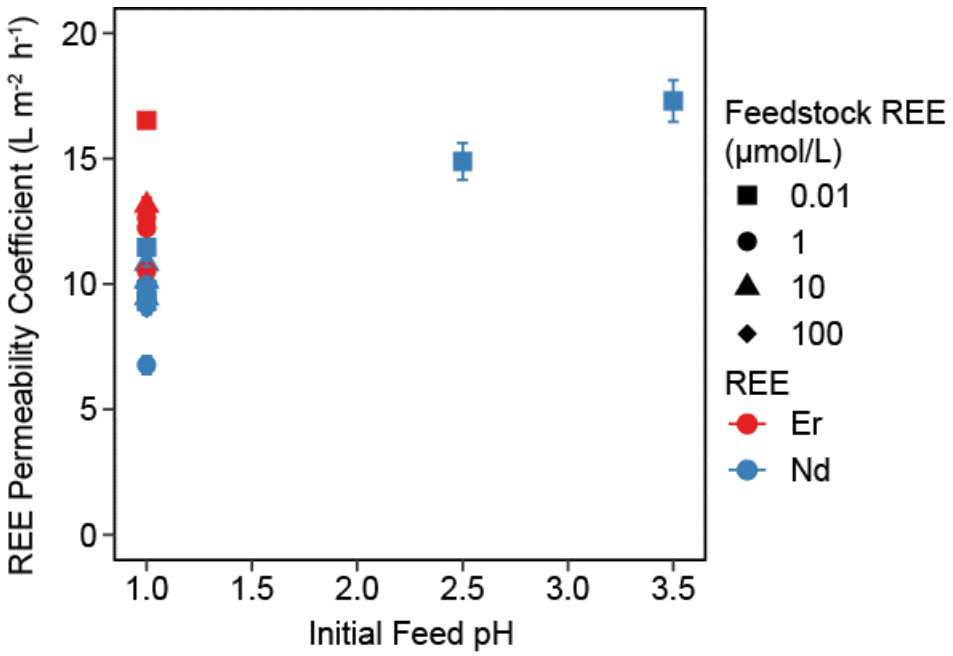

Figure 8: Permeability coefficients, *P*, for Nd (blue) and Er (red) for single-component aqueous feedstocks containing Nd or Er at 0.01, 1, 10 or 100 µmol/L and a range of initial pH values. Error bars correspond to the standard error of the regression slope value for calculating *P*.

In addition, the *P* coefficients for Er were higher than for Nd (10.5 to 16.5 and 6.8 to 11.5 $Lm^{-2}h^{-1}$, respectively) (Figure 8). This outcome aligns with the results of a previous study which demonstrated that Er has a higher affinity for DEHPA than Nd.[71] Thus, the relative affinity of the rare earth ion for the carrier ligand (i.e., DEHPA) is a factor for mass transfer rates across the supported liquid membrane.

3.3.2 Impact of Ferric Fe(III) on Nd and Er Mass Transfer

For the two-component feed solutions with Fe(III), we expected that large relative amounts of Fe(III) would decrease rates of Nd and Er mass transfer due to competition for the DEHPA carrier in the liquid membrane, as posited in previous work.[57] However, the results indicate that Nd and Er mass transfer was not a direct function of the

[Nd]:[Fe(III)] and [Er]:Fe[(III)] molar ratios (Figure 9A, C). For example, at a [Nd]:[Fe(III)] ratio of 1:1700, *P* coefficients for Nd ranged from 0-12.4 $Lm^{-2}h^{-1}$. Experiments performed with solutions comprising other [Nd]:[Fe(III)] ratios showed a similar range of values. The experiments with Er/Fe(III) mixtures also yielded *P* coefficients for Er that do not vary as a direct function of the [REE]:[Fe(III)] , with *P* coefficients ranging from 3.2-12.7 $Lm^{-2}h^{-1}$ at an [Er]:[Fe(III)] ratio of 1:1700.

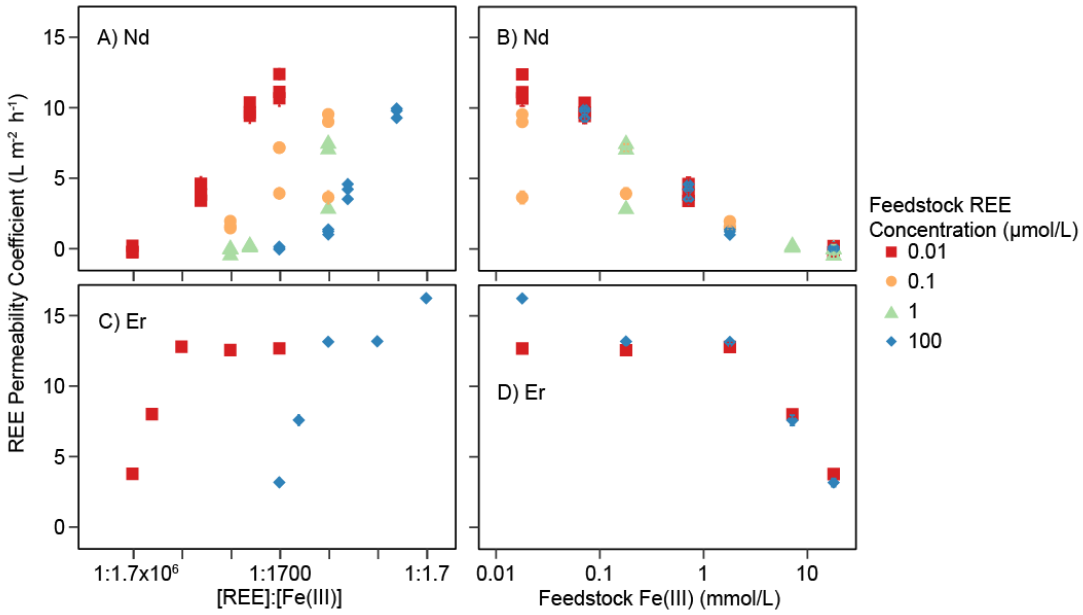

Figure 9: Permeability coefficients, *P*, for supported liquid membrane separations of: (A, B) Nd ; and (C,D) Er in pH 1 synthetic feed solutions with dissolved ferric Fe(III). *P* values are plotted as a function of [REE]:[Fe(III)] molar ratio (panels A and C) and as a function of the initial Fe(III) concentration in the feedstock (panels B and D). The initial Nd and Er feed concentrations were 0.01-100 µmol/L.

The results of these experiments instead showed that the feed Fe(III) concentration rather than [REE]:[Fe] ratio controlled REE mass transfer (Figure 9B, D). The *P* coefficients for Nd and Er generally decreased with increasing concentration of

Fe(III) in the feed solution, regardless of the [REE]:[Fe] molar ratio. For the Nd/Fe(III) mixtures, this decreasing trend of *P* coefficients values occurred over the entire range of Fe(III) concentration values tested (from 0.1 to 10 mmol/L). At the highest Fe(III) level, no transfer of Nd was observed across the membrane. For Er, *P* coefficients were constant with Fe(III) concentrations between 0.01 and 1 mmol/L and decreased with Fe(III) levels above this threshold. This result suggests that Fe(III) can also impact Er mass transfer rates; however, compared to the Nd/Fe(III) mixtures, at least a 10-fold increase in Fe(III) concentration is required to observe changes in *P* coefficients for Er. Such differences between the Er/Fe(III) and Nd/Fe(III) two-component mixtures is likely due to the higher affinity of Er for DEHPA as compared to Nd.

The trends in recovery percentage of Nd and Er in the acid strippant are similar to the observed trends for the *P* coefficients (Figure B5). For feed solutions with the lowest Fe(III) concentration (0.017 μmol/L), Nd recovery in the strippant was 31-90% of the initial amount in the feed solution. The % recovery decreased with increasing Fe(III) concentrations in the feedstock, with less than 1% Nd recovered at the highest Fe(III) concentration (17.8 mmol/L). The % recoveries for Er in the strippant chamber were generally between 69-80% for Fe(III) concentrations <1.78 mmol/L. At Fe(III) concentrations of 17.8 mmol/L, Er recovery was 26-34%.

P coefficients for Fe(III) and recovery of Fe(III) in the strippant were generally much lower than for REEs (Figures B6-7). This is because Fe(III) has a lower affinity for DEHPA than REEs. The highest *P* coefficient for Fe(III) was 1.5 $Lm^{-2}h^{-1}$ and the highest recovery in the stippant was 15.4%, both of which were for feeds with initial Fe(III)

concentrations of 0.0178 mmol/L. We noted that small changes in Fe(III) concentration in the feedstock chamber were observed during the separation time frame. Thus, the relative uncertainty of the *P* coefficients is greater for the Fe(III) than for Nd and Er. Regardless, we did observe an increase in the final Fe(III) concentration in the strippant chamber with increasing feed concentrations (Figure B8). All of the observed trends for Fe(III) were independent of the initial Nd and Er concentrations in the feed.

3.3.3 Impact of Ferrous Fe(II) on Nd Mass Transfer

In the two-component mixtures containing ferrous Fe(II), the *P* coefficients for Nd were also observed to decrease as a function of the feed Fe(II) concentrations, regardless of the [Nd]:[Fe(II)] ratio (Figure 10). At Fe(II) concentrations between 0.1 and 10 mmol/L, the *P* coefficients for Nd ranged from 7.4 to 9.1 $Lm^{-2}h^{-1}$, slightly lower than the *P* coefficients for single component feeds with Nd. Significant decreases of *P* coefficients were observed for Fe(II) concentrations at >10 mmol/L, a threshold that is approximately 100 times greater than the amount of Fe(III) needed to impact Nd mass transfer. The % recovery of Nd was also observed to decrease from ~50% at Fe(II) < 10 mmol/L to less than 25% for Fe(II) > 20 mmol/L (Figure B9).

These separation experiments were performed under ambient atmospheric conditions where dissolved O_2 could oxidize Fe(II) to Fe(III). Assuming pseudo-first order kinetics with a rate constant of $10^{-3.5}$ day^{-1} at constant atmospheric O_2 levels [111, 112], we estimate that only 0.03% or 0.056 mmol/L of the Fe(II) in the most concentrated feed (178 mmol/L Fe(II)) would have oxidized to Fe(III) after 24 hours at pH 1. This amount of Fe(III) did not alter Nd mass transfer rates in the Ne/Fe(III) experiments shown in

Figure 9B. This result suggests that Fe^{2+} ions, and not oxidized forms, were influencing Nd mass transfer in the Nd/Fe(II) experiments..

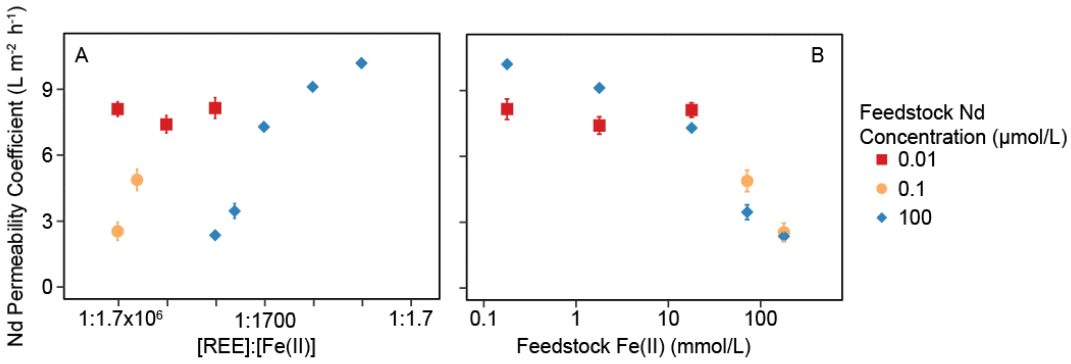

Figure 10: Impact of ferrous Fe(II) on *P* coefficients of Nd mass transfer. Experimental feed solutions contained 0.01, 0.1 or 10 µmol/L Nd (denoted by symbol) and Fe(II) concentrations ranging from 0.17-170 mmol/L at initial pH 1. Error bars correspond to the standard error of the regression slope value for calculating *P*.

Effects of Al(III) and Initial Feed pH on Nd Mass Transfer

In two-component feed solutions with Nd and Al(III), the *P* coefficients for Nd increased with increasing initial feed pH values (Figure 11A). The relative concentration of Al(III) also impacted Nd permeability, but only if the feed pH value was 3 or greater. More specifically, at pH 1 the *P* coefficient values for Nd were similar (7.9 to 10.4 $Lm^{-2}h^{-1}$) for a wide range of Al(III) concentrations (0.0175 to 35 mmol/L). In contrast at initial pH 3.5, *P* coefficients values were 23.2 and 15.9 $Lm^{-2}h^{-1}$, for Al(III) concentrations of 0.0175 and 35 mmol/L, respectively. The recovery percentages of Nd in the strippant acid were 55-67% for pH 1 feeds and higher if the pH was higher (~76% recovered for pH 3.5).

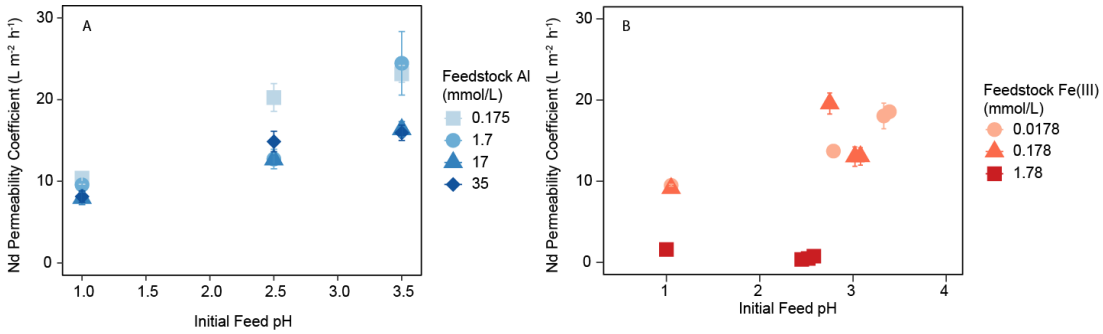

Figure 11: Impact of initial pH on permeability coefficients, *P*, for two component feed solutions with: (A) Nd/Al(III); and (B) Nd/Fe(III). The initial feed Nd concentration was 0.01 µmol/L for Nd/Al(III) mixtures and 1 µmol/L for Nd/Fe(III) mixtures. Error bars represent the standard error of the regression slope value for calculating *P*.

In the two-component Nd/Fe(III) systems, the initial pH of the feed solution had a similar impact on Nd mass transfer as in the Nd/Al(III) systems. The *P* coefficients for Nd increased with increasing initial feed pH for feeds with 0.0178 and 0.178 mmol/L Fe(III) (Figure 11B). At these Fe(III) concentrations, the maximum observed *P* coefficient values at pH 3 were ~19 $Lm^{-2}h^{-1}$, which is close to the *P* values in the one-component feed solutions containing only Nd (Figure 8). At the highest Fe(III) concentration tested (1.78 mmol/L), the *P* coefficient for Nd did not change with increasing feed pH (Figure 11B). Final recovery of Nd in the strippant chamber was consistent with trends observed for *P* coefficients (Figure B11).

While increasing feed pH correlated with an increase in the transfer rate of Nd across the membrane and an increase in Nd recovery, the competitive metals in the feeds (i.e., Al or Fe(III)) were also transported across the membrane at higher rates with increasing pH (Figures B10-11). These results suggest that the feedstock characteristics that can increase the flux of Nd and other REEs, will also impact the flux of impurities

(e.g., Fe and Al). Thus, modification of the feedstock prior to separation should consider these trade-offs that will ultimately influence product purity.

3.3.4 Mechanisms of Fe Interference on Nd and Er Mass Transfer

Overall, the separation experiments demonstrated that the presence of Fe(III), and to a certain extent Al and Fe(II), influenced the *P* coefficients for Nd and Er. This impact was directly related to the concentration of Fe(III), and not the Nd:Fe and Er:Fe molar ratios. Note that *P* values in Figures 9, 10, and 11 are based on the loss of Nd and Er in the feed chamber, which could represent adsorption of these metal ions to the reactor system in addition to transfer across the membrane. However, mass balances of total Nd and Er in solution in the reactor chambers indicate that such artefacts were not a factor. The summation of Nd and Er concentrations in feed and strippant solutions after 24 h was 95% (±11% standard deviation) of the initial Nd or Er in the feed solution for all component experiments. Additionally, less than 0.001% of the initial Er was directly quantified in the membrane phase after a 24h experiment for the membranes analyzed. This result indicates that Nd and Er ions were not accumulating to a substantial degree in the membrane or adsorbing to the internal wall of the reactor chambers.

The formation of colloidal particles was also a concern, particularly for experiments with Fe(III). At pH 1, hematite is supersaturated for total Fe(III) concentrations exceeding 1.4 mmol/L, based on equilibrium speciation calculations performed with VisualMINTEQ. Thus, it was possible that the decrease of Nd permeability with Fe(III) concentration (Figure 9B) could be due to adsorption of Nd ions to freshly formed particles of Fe-oxides. However, in control experiments of feed

solutions that were held for 24 h (i.e., no SLM separation), we did not observe change of Nd concentration in filtrates of this solution (Figure B12). These results demonstrate that the formation of particle phases was not occurring in the feed solutions.

Colloidal Fe particles might also be accumulating at the membrane interface rather than remaining suspended in solution. For example, previous works have shown that fouling by Fe-hydroxides on the membrane surface and third phase formation can cause a decrease in flux of metals across an SLM.[109, 113] In our experiments, however experiments, we did not observe new particles in SEM images of the membrane surface (both leachate and strippant sides) after the separation process (Figure B13). For membranes taken from Nd/Fe(III) separation experiments with 1.7 mmol/L Fe(III) (and substantially suppressed Nd mass transfer according to Figure 9B), EDS spectra indicated that Fe content was 0.23% on the leachate side and 0.19% on the strippant side of the membrane (Figures B14-15), values that are greater than unused membrane controls in which Fe was not detected by SEM-EDS imaging. The Fe EDS signal in these spent membranes was evenly distributed across the membrane surface (Figures B14-15), and we did not observe any large Fe-containing hotspots occluding pore spaces. These results indicate that the decrease in mass transfer of Nd at high Fe(III) concentrations was not occurring because of fouling of the membrane surface by Fe-oxide phases. The mechanisms of Fe interference for Nd and Er mass transfer remains to be firmly established.

3.4 Insights for REE Recovery from Low-Grade Feedstocks by SLM Separations

In this study we showed that Fe and Al, and the pH of feedstocks have a major impact of the mass transfer of REE ions during SLM separations. With sufficiently high concentrations of these competing metals, particularly for Fe(III), Nd and Er transfer across the membrane was generally impeded. This impact on REE mass transfer rates appeared to require a critical concentration of the competitor metal and did not depend on the molar ratios of REE to competitor metals (Figures 9A, 9C, and 10A). This threshold critical concentration was lowest for Fe(III) in comparison to Fe(II) and Al as competitor metals (Figures 9-11). Further analysis of the spent membranes and feed solution after the separations suggest that the competitor metals did not induce losses of Nd and Er in the bulk feed phase or cause occlusion of pore spaces at the membrane interface by newly formed mineral phases.

These results support the original hypothesis of the study that Fe and Al interfere with REE mass transfer by SLM due to competition for the carrier ligand (e.g., DEHPA) in the liquid membrane. This hypothesis was informed by our prior work with coal ash leachates [57] in which faster rates of separation for heavy REE compared to light REE could be explained by differences in relative binding affinities of the REE for the DEHPA. Coal ash leachates and other low-grade feedstocks (e.g., acid mine drainage, red mud leachates) comprise many other metals that could also be expected to influence the efficacy of SLMs for REE separations.

Given the framework of metal competition for DEHPA in the liquid membrane, we also hypothesized that REE mass transfer rates would increase with increasing ratios of REE to competitor ions in binary mixtures. However, we did not observe this effect (Figures 9A and 9C). This lack of dependence on the [REE]:[Fe] molar ratio might be explained by estimates of DEHPA speciation in the liquid membrane: we estimate from the mass difference of dry and wetted membrane that the liquid membrane contained 4 mmol of DEHPA. Our measurements of Er and Fe(III) in the membrane after separations of two-component mixtures (Er/Fe(III)) showed that the moles of metals in the membrane were less than half of the estimated amount of DEHPA. Thus, the protonated forms of DEHPA were the dominant form of the ligand in the solvent. These estimates of DEHPA speciation explain why the pH gradient between the stripping and feed solutions, rather than the [Nd]:[Fe] and [Nd]:[Al] molar ratios, had a substantial impact on Nd mass transfer rates. In effect, the competition with protons needed consideration in these two-component mixtures. For real feedstock solutions that contain multiple metal ions that can bind DEHPA (e.g., Fe, Al, Ca, Mg, other divalent metals, and REEs), multi-cation competition effect might still be a factor as indicated by REE selectivity in SLM separations of coal ash leachates.[57]

While we recognize that the two-component feed solutions are idealized simulations of real feedstocks, we were able to quantify impacts of matrix constituents, specifically for Fe(III), Fe(II), Al, and pH on REE mass transfer. In this respect, the results of this study can be used to inform decisions about how to design SLMs for different types of feeds. For instance, Fe(III) causes a decrease in REE mass transfer at

much lower feed concentrations than either Al or Fe(II). Therefore, Fe(III) concentration, not total Fe, should be considered when evaluating candidate low-grade feed stocks for SLM separation. Additionally, monitoring of oxidation could be necessary for separations with feed stocks of high Fe(II) concentrations (such as freshly emerged acidic seepage from mine tailings). The results here also suggest that acid mine drainage feed stocks that are dominated by high concentrations of Al rather than Fe could be immediately amenable to SLM separations without any pretreatment, especially at low pH.

This work also demonstrates how the affinity of individual REEs for the carrier chelator in the solvent can impact REE mass transfer. DEHPA has a higher affinity for heavy REEs compared to light REEs, which resulted in higher mass transfer of Er compared to Nd. This result suggests that knowledge of the relative affinities of the solvent carrier for metal ions is an important part of the design process in the application of SLM for mixtures of REEs in waste leachates. Future work should focus on a variety of leachates from REE waste resources to fully understand the impacts of matrix impurities on separation efficiency. This work with simulated feeds provides a framework for determining how feedstock complexity can influence REE mass transfer.

4. An Evaluation of the Effects of Feed Chemistry on the Separation of Rare Earth Elements from Acid Mine Drainage Using Supported Liquid Membranes

4.1 Introduction

Rare earth elements (REE) are critical materials for a large number of modern industries.[107] Due to the unstable global supply markets and increasing demand, there is growing interest in using waste materials as sources of REEs.[2, 27, 89] Proposed waste materials include acid mine drainage (AMD), e-waste, and coal fly ash, all of which have been shown to be enriched in REEs.[4-7] Using waste materials as sources of REE also has the added benefit of potentially reducing the environmental burden associated with mining of primary ores.[15, 17, 18, 20] Challenges remain though because many of these waste sources have low REE content and are spatially distributed, making it difficult to recovery REEs in a selective and economically viable manner. In this paper we evaluate the effectiveness of using supported liquid membranes (SLM) as a method for selectively separating REEs from AMD feedstocks.

AMD is generated from oxidative leaching and dissolution of sulfide minerals from waste rock piles and exposed rock formations generated during mining activities. Water that continuously leach from these mined areas are often enriched in soluble minerals and metals such as the REE.[6, 7, 53] For example, hundreds of abandoned coal mines in the northern Appalachia Region of the United States, collectively release 500-3400 metric tons of REE annually.[7, 32, 33] While the total loading of REE into watersheds is large, the concentrations of REE can be relatively low, and as much as 5 orders of

magnitude lower in concentration than other metals such as Fe, Al, Ca, and Mn.[6] As such, the development of separation processes for dilute feed stocks such as AMD require an understanding of the impact of these impurities and other water quality variables REE recovery processes.

Separations by SLMs are a modification of solvent extraction where the extraction and stripping processes have been combined into one unit operation. In SLM separations the feedstock and product solutions are separated by a hydrophobic membrane that has been impregnated with an organic phase that consists of an organic solvent and an extractant molecule. The liquid membrane facilitates the transfer of metals from the feed to the product. The advantages of SLMs compared to solvent extraction are that SLMs use fewer chemicals and can transport metals against a concentration gradient.[54] SLM units also have a modular configuration that enables flexibility in process design, a feature that is especially relevant for geographically distributed REE resources such as AMD. SLMs have been shown to selectively and efficiently separate REEs from a variety of synthetic mixtures and leachates of waste materials such e-waste and coal ash.[57, 58, 60] Previous work using SLMs to separate REEs from coal ash showed that a major rate limiting step for REE mass transfer competition for limited binding sites at the feed-membrane interface by non-REE metals (e.g., Fe, Al, and Ca). The pH gradient across the membrane has also been identified as a major driver of mass transfer for SLM units that utilize DEHPA as the extractant.[81, 82] We are therefore interested in investigating how pH and high concentrations of potentially competitive metal cations affect REE separation AMD using SLMs.

The primary objective this paper was to determine the effectiveness of SLMs as a method for selective separation of REEs from AMD. To the best of our knowledge, SLMs have not previously been tested for recovery of REEs from AMD. We compared separation flux and efficiencies for water collected a seven AMD sites that span a range of aqueous composition that is expected for candidate REE resources. We also sought to understand how aging and storage of the AMD samples prior to separation would affect SLM performance. Finally, we evaluated the effectiveness of feed stock modifications (filtration and pH adjustment) as means to increase SLM performance. Separation performance was evaluated using permeability coefficients *P* (i.e., metal flux normalized to initial feedstock concentration), dry weight purity of the product after 24 h separation, and REE production rates from SLM separations based on the drainage flow rates at the AMD sites. The main hypothesis was that mass transfer of REEs would be controlled by two major water quality factors: 1) higher concentrations of competitive metal cations in AMD will decrease REE mass transfer by competing for metal chelation sites at the membrane interface and 2) AMD samples with higher initial pH will have higher REE mass transfer because metal cation transport across the membrane is partially driven by the H^+ gradient between the feed stock and product solutions.

4.2 Methods

4.2.1 Sample Collection and Storage

AMD was collected on May 25, 2022, from seven abandoned coal mine sites near the metropolitan region of Pittsburgh, Pennsylvania, USA (Figure 12). Drainage water samples were collected at the influent of AMD treatment systems at each site by filling

multiple 2-liter polypropylene bottles. At the time of sampling, smaller aliquots were immediately apportioned to (50-mL polypropylene tubes, VWR International). One set of aliquots was filtered with a 0.2 μm polysulfone syringe filter (Acrodisc) for analysis of filter-passing metals concentrations and major anions. Another 50 mL sample was acidified with 0.1 mL concentrated HNO_3 (Fisher Scientific) for analysis of total metals. A third 50 mL sample was taken that was not acidified or filtered. Flow rates for five of the seven sites were measured of the treatment system by manually timing the fill rate of a 5-gallon container. Conductivity and pH of the AMD were measured *in situ* with a YSI multiparameter probe. All collected samples were placed on ice while transported to laboratories at Duke University and stored at 4 ºC until further processing.

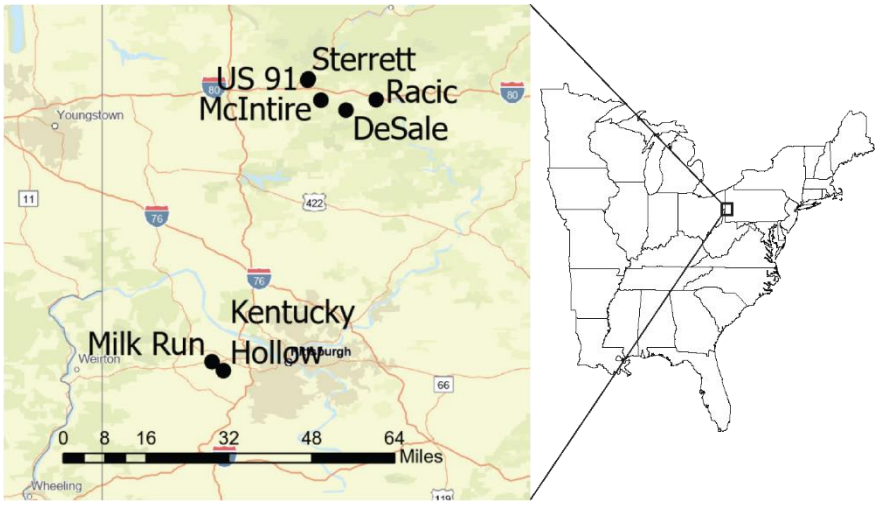

Figure 12: Locations of AMD sample collection sites.

4.2.2 Sample Preparation for SLM Separation Experiments

Upon arrival at Duke University laboratories (within 40 h after collection), the AMD samples were processed for SLM separation experiments. Approximately half of the sample volume for each site was passed through a vacuum filtration apparatus fitted

with a polyethersulfone membrane filter (0.2 μm nominal pore size). The other half was stored in unfiltered form. SLM separation experiments were performed according to the following sample sets: 1) 'Freshly collected', unfiltered AMD samples processed by SLM separations within 21 days of the sampling event; 2) 'Aged' unfiltered AMD samples that were held at 4 ºC for 11-12 weeks prior to SLM separations; 3) Filtered AMD samples separated by SLM 5-7 weeks after the collection date; and 4) Filtered AMD samples for which the pH was adjusted before separation. This 4th experiment sought to explore pre-treatment by pH adjustment as a means for improving REE separation flux and recovery. On the day of the SLM separation experiment, the pH of the sample was adjusted to lower or higher values (pH 2 and 4) relative to the original sample pH. The adjustment was performed by dropwise addition of concentrated trace metal grade HCl (Fisher Scientific) or 10 mol/L NaOH until the desired pH was reached.

4.2.3 SLM Reactor Design

The SLM separations were performed with a flat sheet membrane reactor that comprised a two cell (250-mL each) H-reactor, as described previously.[57] In the preparation of the reactor, a 47-cm diameter PVDF membrane (0.22 μm nominal pore size, Durapore) was soaked overnight in a mixture of 10% v/v bis(2-ethylhexyl) phosphate (DEHPA, 97%, Aldrich) and 90% kerosene (purum, Sigma-Aldrich). The membrane was then placed at the interface of the two 250-mL glass vessels in the H-cell reactor. The AMD sample was placed in the feed side of the reactor while a 5 mol/L HNO_3 stripping solution was placed in the product side. The reactor was continuously mixed for 24 h, during which 0.5 to 1 mL aliquots of both feed and product sides were

collected and preserved for metals analysis. All H-cell reactors and reused plasticware were acid washed with 10% HCl (ACS Grade, VWR) and rinse with doubly deionized water (>18 MΩ-cm, Millipore Milli-Q) between each use.

4.2.4 Chemical Analyses

Aqueous concentrations of all metals were quantified by inductively coupled plasma mass spectrometry (ICP-MS) (Agilent Technologies 7900). All samples were preserved and diluted in 2% HNO_3 prior to analysis. Si, Ca, and Se concentrations were analyzed in hydrogen gas reaction mode. All other metals (38 total, including the REEs) were analyzed in helium gas reaction mode to reduce polyatomic interferences. Instrument calibrations was performed at the start of the sample batch run and verified by an aqueous standard reference material (High Purity Standards (CRM-TMDW-A), traceable to NIST SRM 3100 series). Internal standards of Rh, In, and Bi were amended to all samples prior to introduction into the ICP-MS instrument, and their respective spectral signals were used to correct for shifts in signal intensity during the batch run.

Fe(II) concentrations were determined using a variation of the 1,10-phenanthroline method.[114] The method entailed adding 1 mL of sample to 0.5 mL acetate buffer and 0.5 mL of 1, 10-phenanthroline (0.1% w/v, Ricca Chemical Company). An additional 1:10 dilution with doubly deionized water was also performed for two sites (McIntire and DeSale) to reduce the concentration to a measurable range. The absorbance at 510 nm was measured by UV-vis spectrophotometry (BMG Labtech). Calibrations were performed with standards prepared from Fe(II) chloride tetrahydrate (Fischer

Chemical), which was stored in an anaerobic chamber (Coy Labs). Fe(III) concentrations were calculated as the difference between the total Fe and Fe(II) concentrations. .

In samples filtered at the time of collection, anions sulfate, chloride, nitrate, and bromide were quantified by ion chromatography (Dionex ICS-2000) with a KOH eluent generator and an IonPac AS-18 analytical column, as outlined by EPA method 300.0(A).[115]

4.2.5 SLM Performance Metrics

Rates of REE transfer across the membrane are reported in the form of permeability coefficient *P*. based on time-dependent concentration *C* of metal ion in the feed side of the SLM reactor. The calculation for *P* for a metal ion is based on the overall flux *J* (in units g $m^{-2}h^{-1}$) of the metal across the membrane[54]

$$J = -\frac{dC}{dt}\frac{V}{A} \qquad (1)$$

where the concentration *C* of the metal in the feed reactor (mol L^{-1}) changes with separation time *t*, *V* is the volume of the feed solution (L), and *A* is the surface area of the membrane at the feed-membrane interface (m^2). The *P* coefficient can then be derived by dividing eq. 1 by *C* and integrating with respect to time to obtain the following:

$$\ln\left(\frac{C}{C_0}\right) = -\frac{A}{V}Pt \qquad (2)$$

where C_0 is the initial concentration of the metal in the feed (mol L^{-1}). We calculated the *P* coefficient from the regression slope of the experimental data plotted as $\ln(C/C_0)$ versus time (Figure C1).

We also assessed SLM performance by calculating individual REE contents in the product expressed as a dry weight percentage and REE production rates. The product

purity was calculated by assuming that upon drying of the strippant solution, the metal ions would form metal oxide salts. The concentration of individual REE was calculated as the mass of the single element (in oxide form) divided by the total mass of all metals in their oxide form. The REE production rates were calculated by multiplying the flowrate by the concentration in the product at 24 hours.

4.3 Results and Discussion

4.3.1 Aqueous composition of AMD samples

The major metal and anion concentrations, pH, and flow rates of each site sampled are summarized in Table 2. The total REE concentrations span just over one order of magnitude (from 0.12 to 1.5 mg/L). The three most abundant REEs were Y, Ce, and Nd, which composed over 50% of the total REE concentration (Table C1). The major anions were Cl^- and SO_4^{2} for all sites. Table 2 shows concentration of major competitive cations, which we define as cations that can compete with REEs for binding sites at the feed-membrane interface and have at least 1% of the total metal concentration (in mg/L) for at least one site. Based on the concentration of total competitive cations, concentration of Fe, and pH, we divided the sites into three groups: 1. high total competitive cations, high Fe, and low pH (McIntire and DeSale); 2. average total competitive cations and pH (Racic, Kentucky Hollow, US 91, Milk Run, and US 91); 3. low pH and low total metals (Sterrett). For each of set of experiments performed (as described in Section 4.2.2), we used at least one site from each of the groups.

Table 2: Composition of acid mine drainage (AMD) water samples collected at former coal mine sites in western Pennsylvania (USA). Samples were collected at

the influent of on-site AMD treatment systems. Total REE refers to the sum of Sc, Y, and the lanthanides.

AMD Site Name	pH	Fe	Al	Mn	Ca	Mg	Na	Si	K	Cl^-	SO_4^{2-}	Total REE	Flow Rate
		mg/L	mg/L	mg/L	mg/L	mg/L	mg/L	mg/L	mg/L	mg/L	mg/L	mg/L	L/min
McIntire	2.98	105	60	38	115	92	29	21	5.4	57	1629	1.5	143
DeSale	3.08	49	14	64	180	136	8.8	9.7	5	21	1864	0.78	--
Racic	3.19	1.1	7.1	12	59	41	1.6	11	3.5	76	913	0.17	--
Kentucky Hollow	3.24	2.7	13	6.5	152	42	38	14	2.2	124	848	0.24	582
US 91	3.27	1.5	27	6.6	105	34	7.5	16	2.0	19	831	0.38	64
Milk Run	3.30	1.1	13	1.1	118	43	128	12	2.38	3.51	698	0.12	1220
Sterrett	3.52	0.9	25	1.83	115	54	53	10	1.7	2	556	0.23	378

4.3.2 SLM Separation of REEs from Fresh Unfiltered Feeds

The results of the SLMs for fresh feeds showed differences between the seven different sites for the measure *P* coefficients of the REE during SLM separation. For example, *P* coefficients of Nd were generally highest for the Group 3 site (Sterrett) (18.9 to 23.4 $Lm^{-2}h^{-1}$) and lowest for the Group 1 sites (McIntire and DeSale) (10.7 to 13.5 $Lm^{-2}h^{-1}$). Furthermore, the *P* coefficients of the REE were positively correlated with the initial feed pH (Figure 13). The reason for this trend is that the DEHPA in the membrane is a cation exchange extractant that in which 3 mol H^+ exchanges for 1 mol of Nd^{3+} across the membrane. As a result of this cation ion exchange process, we observed a decrease in pH over the 24 h separation periods to pH values 1.06 to 1.43. An exception occurred for a replicate separation of the US 91 sample, for which the final pH was 0.33. This large pH change indicates leakage of the acid strippant solution. As a result, the data from this replicate was not used for comparisons. The data also showed that the R^2 values for the linear regressions of REE data plotted as $\ln(C/C_0)$ versus time were generally >0.95 (Figure C1).

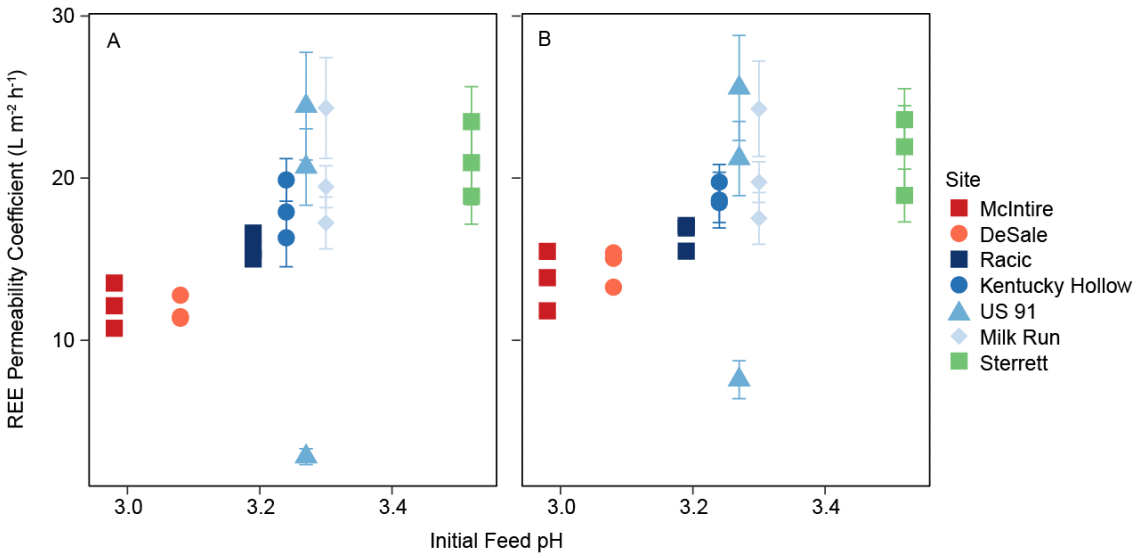

Figure 13: (A, B) *P* coefficients for (A) Nd and (B) Er as a function of initial feed pH for each of the AMD sites tested. The error bars represent the standard error associated with the slope of the linear regression of the ln(C/C_0) versus time data used to calculate the *P* coefficient.

P coefficients for Nd also correlated with the concentrations of total competitive cation concentrations and concentrations of individual competitive cations (Figure 14). Feeds with higher total concentrations of competitive cations generally had lower Nd *P* coefficients. This trend was also observed for all REEs. This is likely because in feeds with higher total competitive cation concentrations there is more competition for chelation sites at the feed-membrane interface, which has been shown to limit REE mass transfer.[57] Individual competitive cations such as, Ca, Fe, and Mn, also correlated with the observed decrease in Nd *P* coefficients. The limited sample size prevented us from disentangling the effects of individual competitive cations and feed pH on REE mass transfer. Still, the results demonstrate that both pH and major competitive cation concentrations in the feed could be strong indicators of REE mass transfer, and this conclusion is supported by both the data and a mechanistic understanding of SLMs.

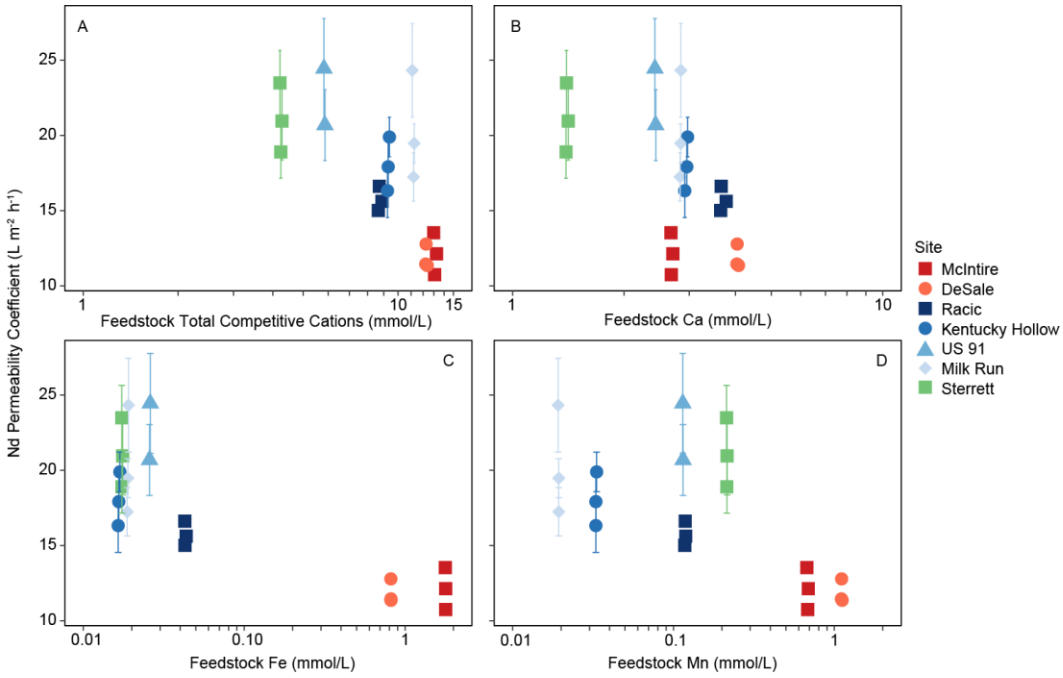

Figure 14: (A, B, C, D) Nd *P* coefficients as a function of feedstock concentration (mmol/L) of (A) total competitive cations, (B) Ca, (C) Fe, and (D) Mn. The total metal concentration was calculated as the sum of the concentrations (mmol/L) of all metals detected in the feedstocks. The error bars represent the standard error associated with the slope of the linear regression of the ln(C/C_0) versus time data used to calculate the *P* coefficient.

The results also showed a trend of *P* coefficients increasing with the heavier REEs on the lanthanide series. This effect was especially apparent when comparing La and Lu (Figure C2). For example, in the AMD sample from the Group 1 sites (McIntire and DeSale), the *P* coefficient for Lu 11.9-15.7 $Lm^{-2}h^{-1}$, approximately two times greater than the *P* coefficients for La. The difference between heavy and light REE was less drastic for the Group 2 and 3 sites. For example, the *P* coefficient for Lu was only ~15% greater than the *P* coefficient for La for the Group 3 site (Sterrett). Heavy REE ions tend to have stronger affinities for the extractant DEHPA compared to the light REE.[71]

Therefore, these results highlight the capability for SLM separations to select for the heavy REE, which tend to be the critical elements (e.g. Er, Y).

In contrast to *P* coefficients, Nd_2O_3 weight % in the product was more strongly correlated with the initial REE concentrations ($R^2 = 0.89$) (Figure 15) than the initial feed pH ($R^2 = 0.56$) (Figure C3). Sites with higher Nd concentrations had higher Nd_2O_3 weight % in the product. We observed a similar trend for all REEs. The reason for this trend is that feeds with higher initial REE concentrations will have a higher amount of REEs transferred across the membrane. The *P* coefficient is normalized to initial concentrations, so it does not provide information on the absolute mass of a metal transferred. As a result, despite have the lowest REE *P* coefficients, the Group 1 sites had the highest Nd_2O_3 dry weight % in the product.

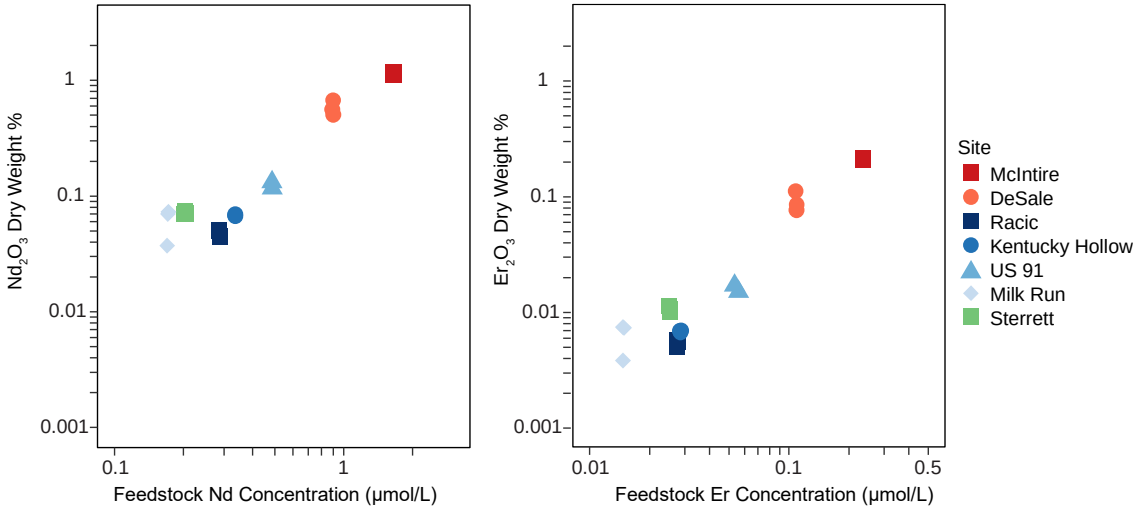

Figure 15: (A, B) Dry weight % of (A) Nd_2O_3 and (B) Er_2O_3 in the product as a function of the initial feed concentration of (A) Nd and (B) Er using fresh unfiltered feeds.

The results also showed that dry weight percent of total REE_2O_3 in the product was 5-25 times more concentrated in the product than in the feed (Figure 16). On

average, Group 1 sites (McIntire and Desale) had the highest increase in purity from the feed to the product and the Group 3 site (Sterrett) had the lowest increase.

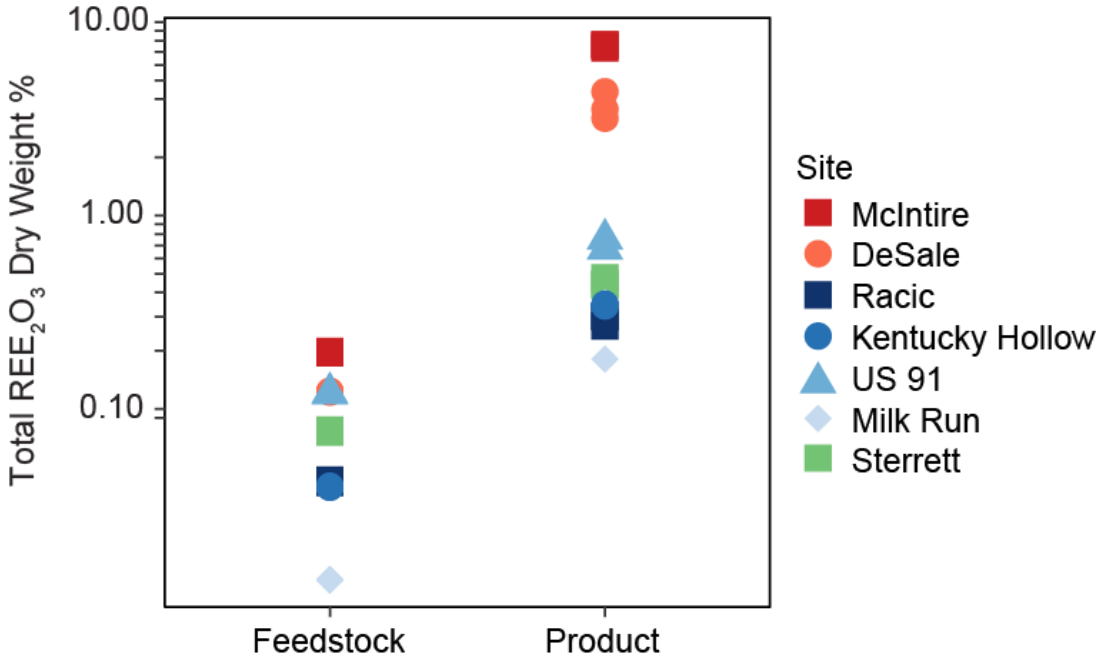

Figure 16: Total REE_2O_3 dry weight % in the feedstock and product for unfiltered fresh feeds.

Calculation of production rates showed that the Milk Run (Group 2) site had the highest daily production rate of Nd (32-35 g/day) and US 91 (Group 2) had the lowest (4.3-4.4 g/day) (Figure C4). These results show that neither the site with the highest REE *P* coefficients (Sterrett, Group 3), nor the site with the highest REE product purity (McIntire, Group 1) had the highest production rate. The reason for this result is that the Milk Run had a flow rate more than double that of the next highest flow rate (Kentucky Hollow, Group 2) and more than an order of magnitude higher than the site with the highest product purity (McIntire, Group 3). The production rates for the other REEs all followed the same trend.

4.3.3 Transport of Major Competitive Cations using Fresh Unfiltered Feeds

Fe and Ca were the two major competitive cations transported across the membrane at the highest rates (Figure C5). Similar to the results for REEs, Fe and Ca *P* coefficients generally increased with increasing feed pH. This result shows that the pH gradient across the membrane is a major driver of mass transfer for all metals, not just REEs. The data also showed that the R^2 values for the linear regressions of major competitive cation data plotted as $\ln(C/C_0)$ versus time were generally lower compared to the REEs. This result is expected as the *P* coefficient is only valid for relatively low concentrations.[54] Additionally, the final dry weight % of the product for group 1 sites was dominated by Fe_2O_3 (78-82%) (Figure C6). In contrast, Group 2 and 3 sites were dominated only by CaO (55-81%) (Figure C6). No other metal oxide accounted for >15% of the product dry weight for any of the sites. These results indicate that Fe and Ca are the major competitors of concern when separating REEs from AMD using SLMs.

4.3.4 SLM Separation of Aged, Unfiltered AMD

During the aging process, the Group 1 sites (McIntire and DeSale), which had the highest total Fe concentrations, visibly turned a reddish-orange color. The Fe(II) concentrations in the aged McIntire and DeSale feeds were lower by 0.7 mmol/L and 0.62 mmol/L compared to the fresh feeds, respectively. Additionally, the pH decreased by 0.12-0.14 pH units for the Group 1 sites (McIntire and DeSale). For Group 2 and 3 sites tested (Milk Run and Sterrett), the measured Fe(II) concentrations were slightly higher in the aged feeds compared to the fresh feeds and the pH of the aged and fresh feeds differed by less than 0.03 pH units. Additionally, for all sites the total REE

concentration differed by less than 3% between the aged and fresh feeds, indicating that REEs were not adsorbed by precipitating Fe hydroxide phases observed forming in the McIntire and DeSale feeds. Also, the concentrations of major elements (Na, Mg, Al, Ca, Mn, and Fe) in the aged and fresh feeds generally differed by less than 10% for all sites. Overall, the data showed that the only major differences between the aged and fresh feeds were the change Fe(II) concentration and the associated decrease in pH.

In the separation experiments with the aged unfiltered AMD, the Group 1 sites had lower Nd *P* coefficients compared the separation experiments using fresh feeds. In contrast, for the Group 2 and 3 sites, there was no difference in the Nd *P* coefficients between the fresh and aged feeds (Figure 17). We attribute the difference in Nd *P* coefficients between the aged and fresh feeds for Group 1 sites to the higher Fe(III) concentrations in the aged feeds compared to the fresh feeds. The pH in the aged Group 1 feeds was also lower than the fresh feeds, which could explain why the aged Group 1 feeds had lower Nd *P* coefficients compared to the fresh feeds. However, because the decrease in pH and increase in Fe(III) are directly linked, it is difficult to distinguish their individual effects. The results also showed that heavy REEs were slightly less affected by the aging process compared light REEs (Figure C7).

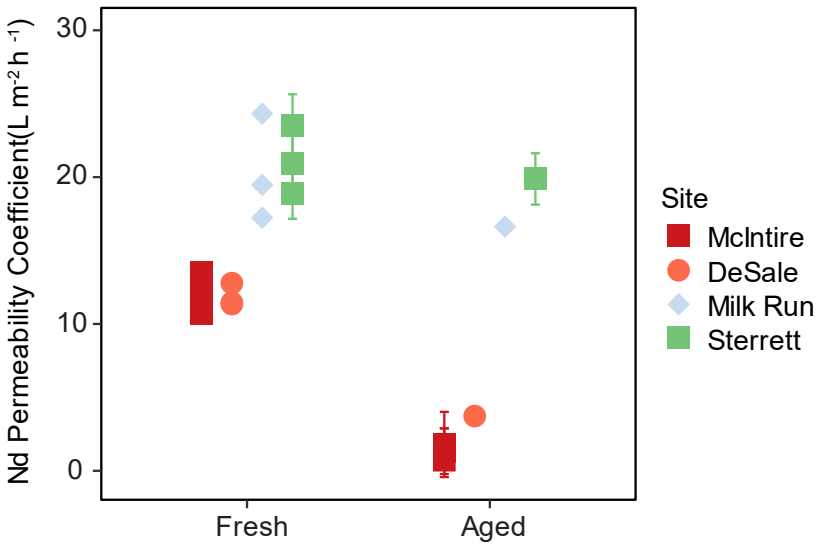

Figure 17: Comparison of Nd *P* coefficients for fresh versus aged feeds for four sites (McIntire, DeSale, Milk Run and Sterrett). The error bars represent the standard error associated with the slope of the linear regression of the ln(C/C_0) versus time data used to calculate the *P* coefficient.

The data also showed that for the Group 1 sites Fe transport across the membrane was higher for the aged feeds compared to the fresh feeds. Relative to the fresh feeds the Fe *P* coefficients for the Group 1 sites were 109-120% higher. Also, for the Group 1 sites, the Fe_2O_3 dry weight % in the product was higher in the aged feeds than in the fresh feeds. The increase in Fe dry weight % in the product was offset by a decrease in Ca dry weight %. For the Group 2 and 3 sites, the Fe *P* coefficient and dry weight % in the product for the aged feeds were largely unchanged compared to the fresh feeds. Additionally, for the Group 1 feeds, the total molar amount of Fe transported across the membrane was 47-146% higher for the aged feeds compared to the fresh feeds; however, the total molar amount of all metals transported across the membrane was lower in the aged feeds than the fresh feeds. Fe in the aged feeds was therefore transferred instead of and not addition to Ca. Overall, our results suggest that the aged Group 1 feeds had high

transport of Fe compared to the fresh feeds because Fe(III) is a stronger competitor for chelation sites at the feed-membrane interface than Fe(II).

4.3.5 SLM-based Separation of Filtered AMD samples

We also investigated the impact of filtering feeds through a 0.2 μm PES filter within 40 hours of sample collection. We anticipated that filtering would remove particles that could foul the membrane surface and decrease mass transfer. The results showed that REE *P* coefficients were very similar for the filtered feeds and fresh feeds (Figure C8). It should also be noted that the separations were done on the filtered feeds approximately 5-6 weeks after filtration and that the samples remained stable over that time period (i.e., no significant Fe(II) oxidation or change in pH). The filtration of AMD is known to stabilize ferrous Fe(II) by removing Fe oxidizing bacteria and other particles that catalyze oxidation at acidic pH.[116]

4.3.6 pH Adjustment AMD prior to SLM Separation

Since pH was identified as a strong influencer of REE mass transfer, we also evaluated the impact of adjusting pH as a means of improving SLM performance. The results generally showed that decreasing the feed pH led to a slight decrease in Nd *P* coefficients, an increase in product dry weight %, and a slight decrease in Nd production rate compared to the unadjusted feed (Figure 18). Though the effects were not dramatic, these results generally agree with the observations in previous section. By decreasing the feed pH, we decreased the pH gradient across the membrane, which is a driver of mass transfer and the cause of the decrease in Nd *P* coefficients and production rate. However, decreasing the pH also caused a decrease in mass transfer of all metals, which caused the

relative increase Nd_2O_3 dry weight % and decrease in dry weight % of competitive cations in the product because REEs have a higher affinity for DEHPA than the competitors.

In contrast, adjustment the pH to 4 did not change P coefficients for Nd, dry weight % in the product, or production rates (Figure 18). One reason why increasing the pH did not have a large impact on REE separation is the way that the feeds were prepared. We adjusted the pH to approximately 4 and then immediately began the separation. This feed was not at equilibrium and the pH naturally decreased over 24 hours. For example, when using the McIntire feed (Group 1), the pH was adjusted up to 4.18 and after 24 hours an aliquot of the feed that was not exposed to the membrane was at 3.89. This natural decrease in pH over time may have prevented us from observing the full extent of the attempted pH adjustment. Overall, the results showed that adjusting the feed pH either up or down is not an effective solution to improve SLM performance.

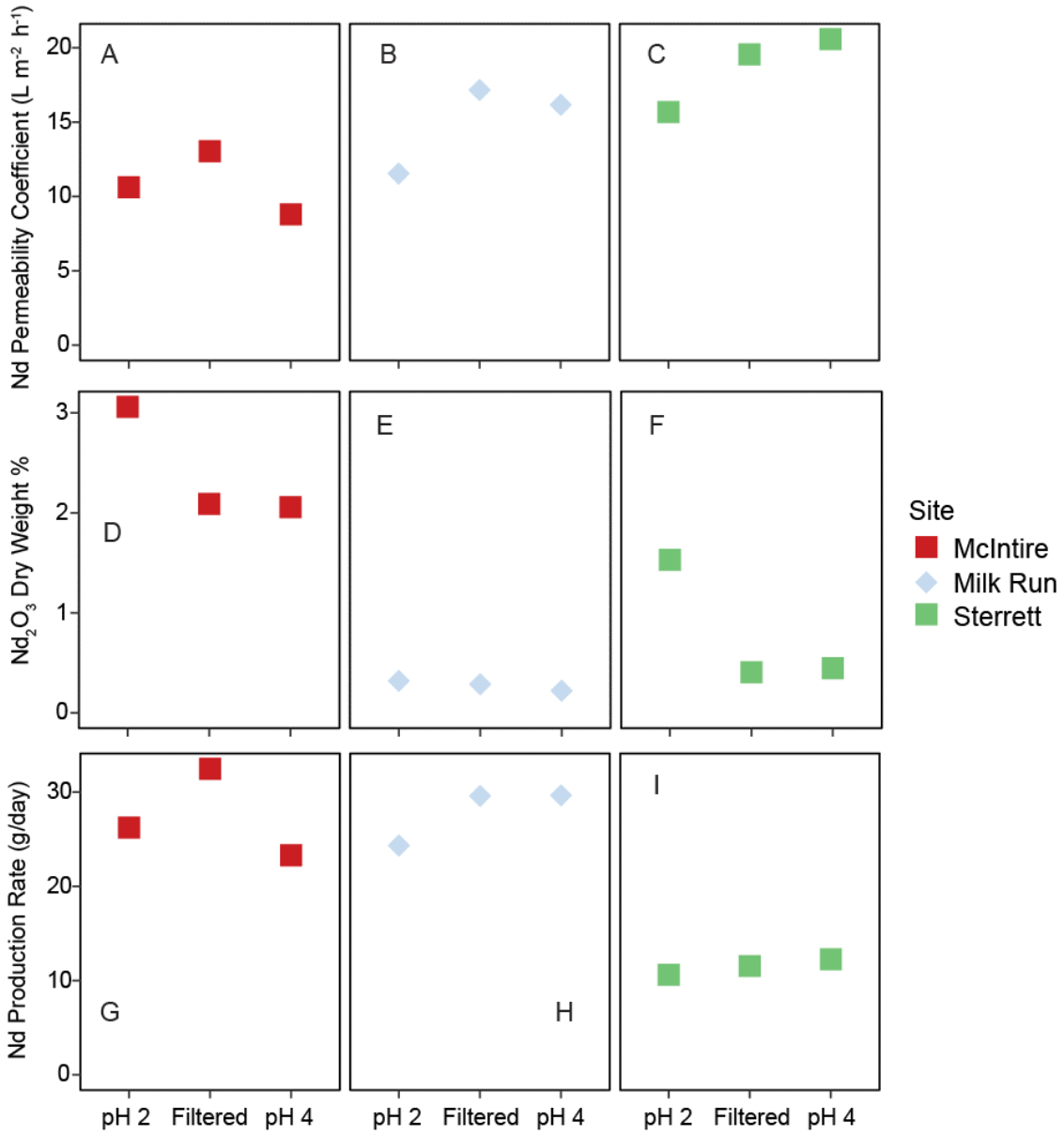

Figure 18: Effect of pH adjustment on (A-C) *P* coefficient for Nd, (D-F) Nd_2O_3 dry weight % in the product, and (G-I) the daily production rate for Nd (g/day).

4.4 Conclusions

In this study, we showed that REEs can be efficiently and selectively separated from AMD sites with varied chemistries. We also identified key characteristics that could

be used to predict REE mass transfer rates, dry weight % in the product, and production rates; however, these performance metrics were not always driven by the same process variable. For instance, we showed that REE mass transfer rates correlated strongly with feed pH and that REE dry weight % in the product correlated strongly with the initial REE concentration in the feed. The basis for these correlations can be understood from a mechanistic description of separation by SLM. Feeds with higher pH will have a higher pH gradient across the membrane, which is a strong driver of mass transfer. Our results also suggest the REE *P* coefficients are negatively correlated with concentrations of major elements (Ca, Fe, Mg, etc.). This result suggest that these metals are competing with REEs for limited chelation sites at the feed-membrane interface and decreasing REE mass transfer rates. This result also demonstrates the difficulty in disentangling the effects of multiple variables when using complex feeds such as AMD

In contrast to other performance metrics, REE production rate is strongly influenced by flow rate and hard to predict based on other metrics. For example, the site with the highest production rate (Milk Run, Group 2) had one of the lowest REE product purities and average REE *P* coefficients compared to the other sites. The site with the highest product purity (McIntire) had the second highest production rate and the site the highest REE *P* coefficients (Sterrett) had one of the lowest production rates. These results highlight difficulty in designing separation systems for AMD and underscore the importance of not relying on a singular performance metric to assess overall SLM performance.

The results also provide some insights that can help when making process design decisions related to SLMs. For instance, the results showed that Fe(III) is a stronger competitor than Fe(II), and therefore Fe(II) oxidation should be closely monitored if storing feeds long term prior to separation; however, immediate filtration of AMD upon collection can reduce Fe(II) oxidation and increase the hold time. Finally, the data showed that adjustment of the pH either up or down immediately prior to separation has marginal effect on SLM performance and is not an effective engineering solution to increase REE mass transfer. Overall, the results of this study help to provide a framework for predicting REE recovery from AMD feeds and further work should build on this by using feedstocks from other AMD sites and types of waste materials.

5. Conclusions

5.1 Summary

In this work, we sought to determine the major factors that drive recovery of REEs from real and synthetic low-grade waste materials the during the acid leaching process and separation using SLMs. REEs are critical materials for many modern industries and their demand is expected to continue to increase. Due to potential supply chain risks and the environmental risks associated with current mining operations, there is interest in recovering REEs from waste materials, such as e-waste, coal by product, and acid mine drainage. However, the low REE content and variable composition of waste materials can make it difficult to design efficient separation processes. The overall objective of this work was to understand how the chemistry of feedstocks of waste materials affects recovery of REEs during acid leaching and separation using supported liquid membranes. To achieve this overall objective, this research addressed the following three aims:

1. Identify the factors that control REE solubility (e.g., pH and major element concentration) in acid leachates of coal fly ashes and coal residue.
2. Quantify the effects of various leachate characteristics such as major metal concentrations and feed pH on REE mass transfer in SLMs using synthetic feeds that mimic real feedstocks from low-grade waste materials.
3. Evaluate the effectiveness of SLMs as a method for selective separation of REEs from real AMD feeds from sites distinct water chemistries and identify feed characteristics that are predictive of SLM performance.

To fulfill these objectives, we used real leachates of CCR (Chapter 2), synthetic feedstocks that mimicked low-grade waste materials (Chapter 3), and real AMD feedstocks (Chapter 4).

In Chapter 2 of this work, we were able to show that major elements control REE solubility in acid leachates of CCR and coal refuse. We were specifically able to show that PRB fly ashes form secondary Fe-(hydr)oxides and alumino-silicate minerals that can adsorb REEs when leached at high pulp density. The implication of this result is that pulp density can also be tuned for PBR ashes to selectively precipitate non-REE major metals (e.g., Fe, Al, and Si), but not for the Appalachian ashes or coal refuse tested. We can further use thermodynamic calculations (e.g., saturation index) to show under what conditions formation of Fe-(hydr)oxide and alumino-silicate mineral phases is favorable. In this work, we were able to use thermodynamic calculations to show that precipitation of pure REE hydroxides was not favorable in any condition, but that formation of Fe-(hydr)oxide and alumino-silicate minerals were oversaturated for PRB leachates at high pulp density. This result shows that the change in REE solubility we saw for high pulp density PRB leachates was due to adsorption to Fe-(hydr)oxides and alumino-silicate minerals. We also showed that simple pH adjustment of acid leachates of coal byproducts is not an efficient way to purify REEs. This was also because REEs were adsorbed and co-precipitated with oversaturated mineral phases of major elements (e.g., Fe and Al). The results of this chapter can help the design of new leaching methods by providing information about how the overall aqueous chemistry of acid leachates affects REE solubility and recovery.

In Chapter 3, we sought to understand how differences in aqueous chemistry affect mass transfer of REEs when using SLMs. To do this, we evaluated the specific effects that competitive metals (Fe(II), Fe(III), and Al) and feed pH have on REE mass transfer rates in SLMs when using synthetic feeds that mimic low-grade feedstocks. We showed that at high enough concentrations, competitive metals can significantly inhibit REE mass transfer, with Fe(III) impeding REE mass transfer at the lowest concentration. The concentration at which Fe(III) began to cause a decrease in REE mass transfer was at least two orders of magnitude lower than either Fe(II) and Al. The results also showed that the [REE]:[Competitor] molar ratio did not affect REE mass transfer, which is contrary to one of our original hypotheses. The observed decrease in mass transfer at high competitor concentrations was due to high consumption of the extracting agent, and not due loss in the bulk feed or fouling at the membrane interface. Our results also highlighted the importance pH of feed by showing that REE mass transfer was higher in feeds with higher pH. Finally, our work demonstrated the impact of REE affinity for the extracting agent by showing that Er mass transfer rates were higher than Nd. This trend was observed because DEHPA has a higher affinity for HREEs compared to LREEs. While this work used simple feeds that lack the complexity of real feedstocks, it still provides insight into the mechanisms controlling REE mass transfer in SLMs when using low-grade feedstocks. These results can provide a framework for predicting what types of feedstocks would be best suited for separation of REEs using SLMs.

In Chapter 4, we built upon the results of Chapter 3 by using real low-grade feedstocks, seven different types of AMD, to understand how REE mass transfer in

SLMs is affected when using more complex feedstocks. The overall aim of this chapter was to find feed characteristics that were predictive of SLM performance and evaluate the effectiveness of feed modifications (filtration and pH adjustment) as methods for improving REE mass transfer. The AMD was collected from seven abandoned coal mine sites in southwestern Pennsylvania that had a range of aqueous chemistries. The results showed that for fresh feeds there were clear differences between SLM performance among the different sites and that performance could be correlated with several different feed variables. For example, REE mass transfer correlated strongly with feed pH, and REE product purity correlated strongly with the REE feed concentration. Feeds with higher pH had higher REE mass transfer rates, which can be explained by the higher pH gradient driving mass transfer across the membrane. The observed trend in REE product purity occurred because feeds with higher REE concentrations had higher total REE flux across the membrane.

The results also showed that feeds with higher concentrations of major competitive cations (e.g., Fe, Mg, and Ca) had lower REE *P* coefficients. This suggests that competition for metal binding sites at the membrane surface may limit REE mass transfer; however, we could not separate the effects of metals concentrations and pH because of the limited sample size. We also calculated daily production rates for each site assuming a continuous separation process. Our results showed that the Milk Run site had the highest production rate, despite not having the highest *P* coefficient or product purity. This is because it had the highest flow rate of all the sites.

The results of Chapter 4 also showed that Fe(II) oxidation rates can have a major impact on REE mass transfer rates, which has implications for how long AMD can be stored prior to separation. Feeds with high Fe(II) oxidation rates had lower REE *P* coefficients after aging compared to the fresh feeds, while feeds with no Fe(II) oxidation had no change in REE *P* coefficients after aging. This suggests that Fe(III) is a much stronger competitor than Fe(II) and shows that Fe(II) oxidation should be monitored for industrial applications of SLMs; however, we were able to demonstrate that filtering is an effective way to increase AMD shelf life because it will remove Fe-oxidizing bacteria and solid phases that can catalyze Fe oxidation. Finally, we showed that adjusting the feed pH immediately prior to separation is not an effective method to increase SLM performance. Overall, the results of Chapter 4 demonstrate that specific feed variables, such as feed pH and major element composition, can be used to predict SLM performance when using complex feedstocks. These results can be used to help make informed decisions about which types of AMD are most suitable for REE recovery when using SLMs.

The results of Chapters 3 and 4 also showed that simplified feeds are effective at predicting feed components that can influence REE mass transfer (Figure 19). For example, the maximum Nd *P* coefficients observed when using real AMD were similar to the maximum *P* coefficients observed in the simplified feeds (Figure 19A). This would suggest that the complexity of the real AMD feeds has relatively little impact on REE mass transfer rates. The results of the simplified feeds also showed the importance of Fe oxidation state on REE mass transfer rates, a result that was directly observed in the

results of the fresh versus aged experiments using real AMD (Figure 19B). We also observed that the pH of AMD feeds correlates with Nd *P* coefficients in a manner that would be expected based on the results of the synthetic feeds (Figure 19A). These results further support our claim that the results of Chapter 3 using simplified synthetic solutions can be built upon to provide a framework for predicting SLM performance of real complex feedstocks.

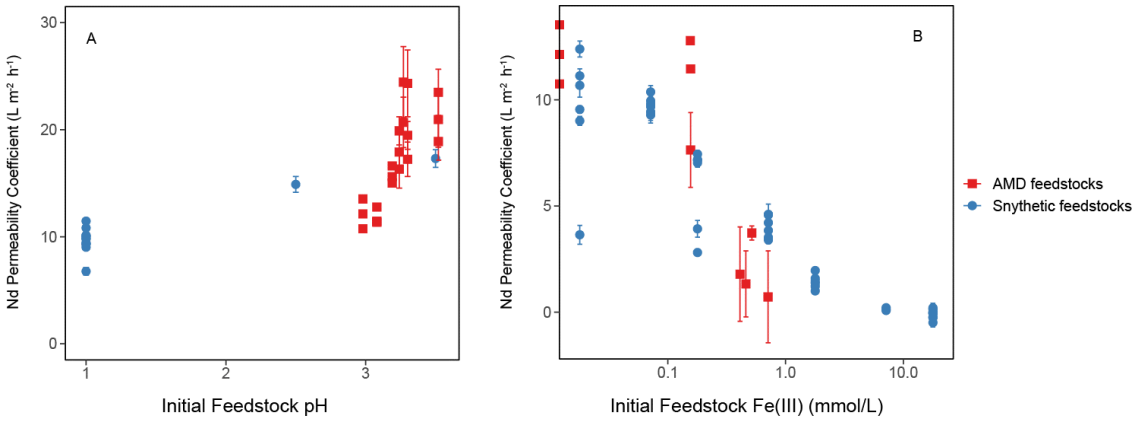

Figure 19: Comparison of Nd mass transfer when using synthetic feedstocks and real AMD feedstocks. (A) Nd *P* coefficients as a function of the initial feedstock pH; (B) Nd *P* coefficients as a function of the initial feedstock Fe(III) concentration.

Overall, this work helped identify factors that can drive and limit REE recovery during acid leaching and separation using SLMs for feedstocks of real waste materials and synthetic feedstocks. We were also able to show how simplified systems can be used to predict recovery of REEs when using real waste materials, which have much more complex aqueous chemistries. Ultimately, this work can be used to help design more efficient REE recovery processes when using low-grade feedstocks.

5.2 Future Research Needs

5.2.1. Reduction of Acid Usage in Leaching Processes

One of the major issues associated with traditional leaching of REEs from solid waste materials is the high acid consumption. Using large amounts of acid to solubilize REEs is cost intensive and presents environmental and occupational risks. Future work should therefore be focused on finding methods to reduce acid consumption during leaching. In this work, we were able to show that pulp density is a tunable parameter that can be used to increase REE purity and reduce acid consumption. We further showed that at high pulp densities, REEs were adsorbed and co-precipitated with Fe-(hydr)oxide and alumino-silicate minerals. One limitation to this work is that we were not able to show which specific mineral phases REEs were most associated with when they were precipitated. Future work should investigate the specific REE associations with oversaturated minerals formed during leaching. This information can be used to design leaching methods that avoid formation of the minerals that are most likely to scavenge aqueous REEs in acid leachates of CCR and potentially allow for leaching at higher pulp densities. Additionally, further work should focus on using alternative leaching processes (e.g., bioleaching and electroleaching) that require little to no acid inputs to recovery REEs.

5.2.2. Increased Focus on Low-Quality Feedstocks for REE Recovery

In this work, we were able to demonstrate that SLMs can be used to selectively separate REEs from low-grade feedstocks. We also showed that simple synthetic feeds can be good predictors of more complex systems; however, the variables tested were far

from extensive. Future work in the field of SLMs should continue to use synthetic feedstocks to explore the ways in which aqueous chemistry affects REE recovery in feeds mimicking low-grade feedstocks. These results should then be extended to SLMs configurations that are more industrially relevant, such as continuous processes using hollow-fiber membranes. Future work could also apply mass transfer models to further understand the mechanisms driving mass transfer. Most importantly, future work should focus on using SLMs to recover REEs from more types of low-quality feedstocks to determine the ways in which synthetic feedstocks can be used to make predictions about real feedstocks.

Appendix A. Chapter 2 Supporting Information

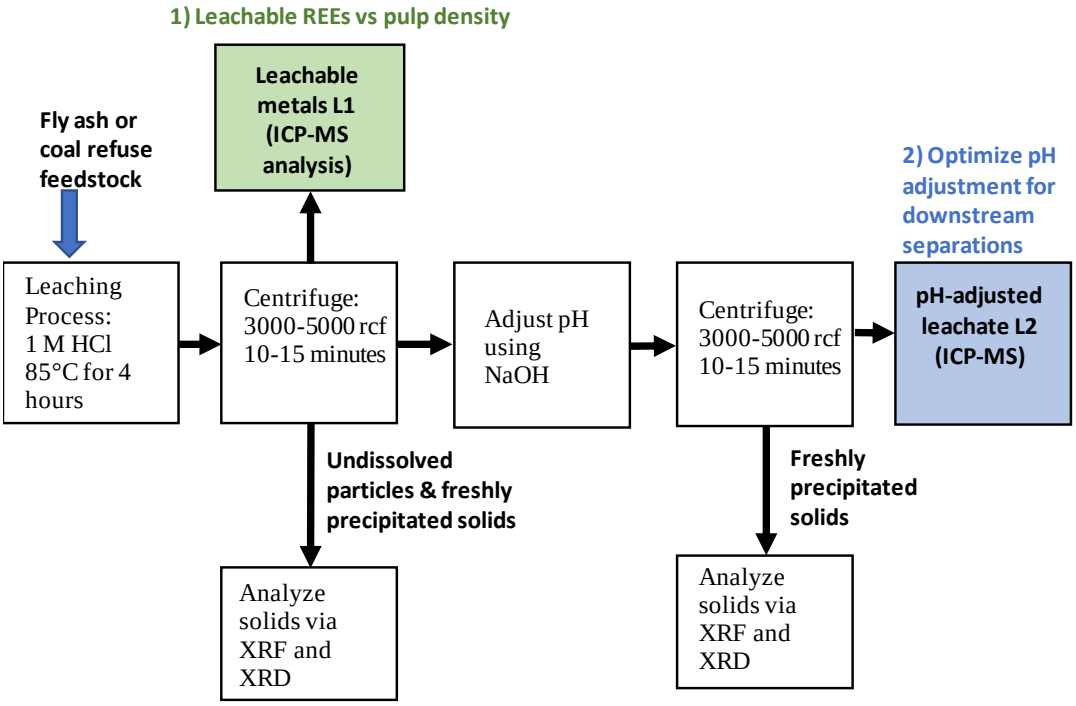

Figure A1: Process diagram for leaching method.

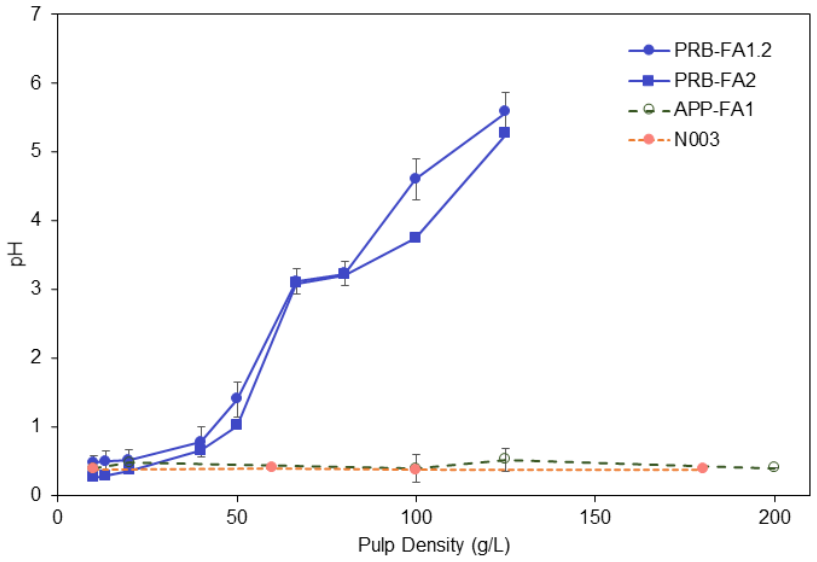

Figure A2: **Leachate pH as a function of pulp density for two PRB fly ashes (blue), one APP fly ash (green), and a Navajo coal refuse (orange).**

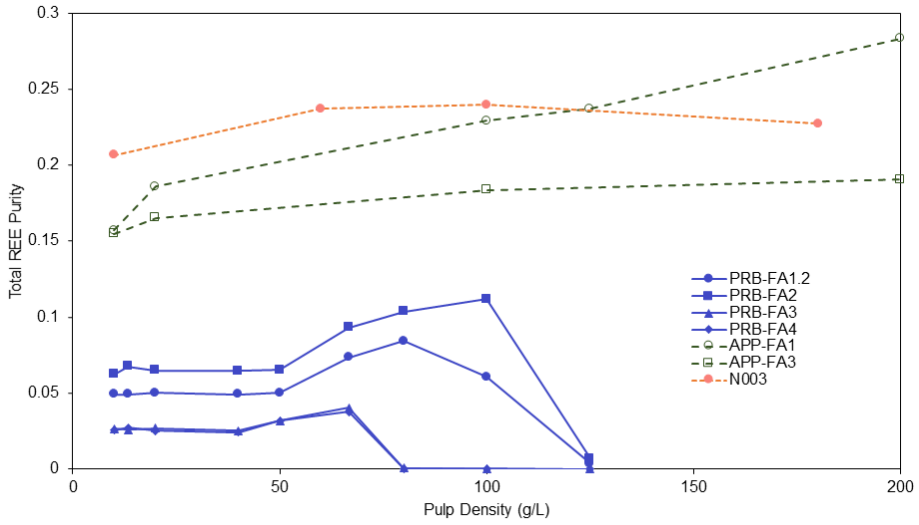

Figure A3: **Leachate purity for two PRB fly ashes (blue), one APP fly ash (green), and a Navajo coal refuse (orange) for total REEs as a function of pulp density. Purity was calculated as a %wt on a dry mass basis from the measured major metal ion concentrations in leachates and assuming that all metals precipitate as chloride salts after dehydration of the leachate.**

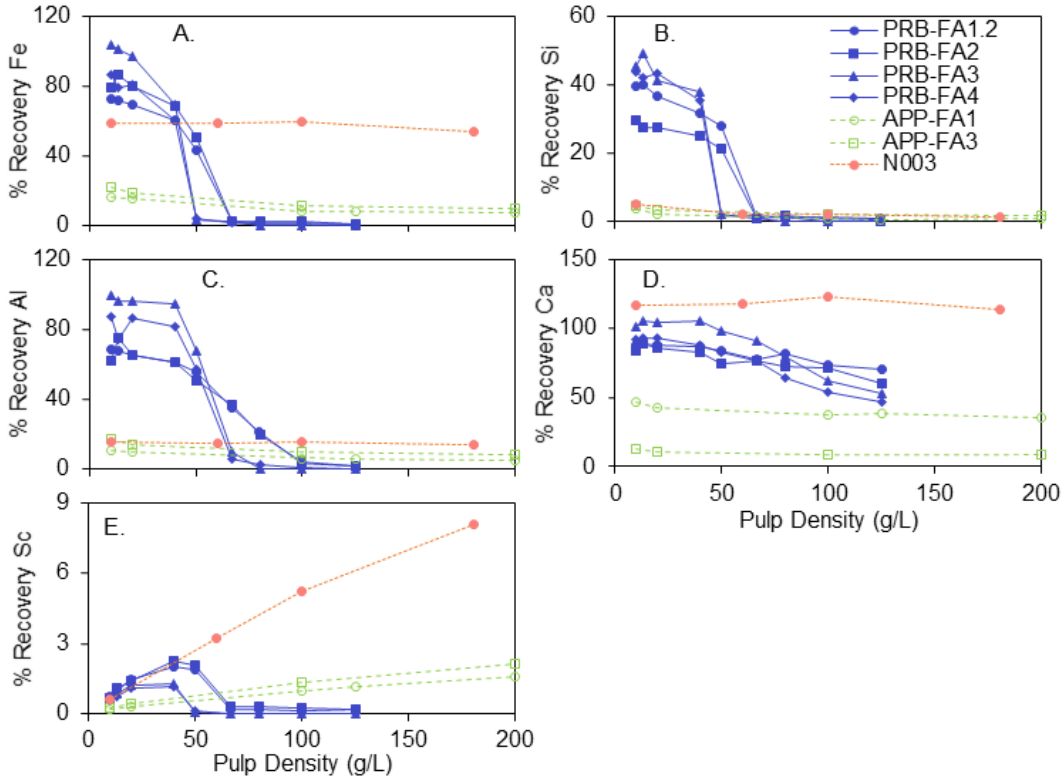

Figure A4: Percent recoveries for (A) Fe, (B) Si, (C) Al, (D) Ca, and (E) Sc for four PRB ashes (blue), two APP ashes (green), and a Navajo coal (orange) after leaching at various pulp densities.

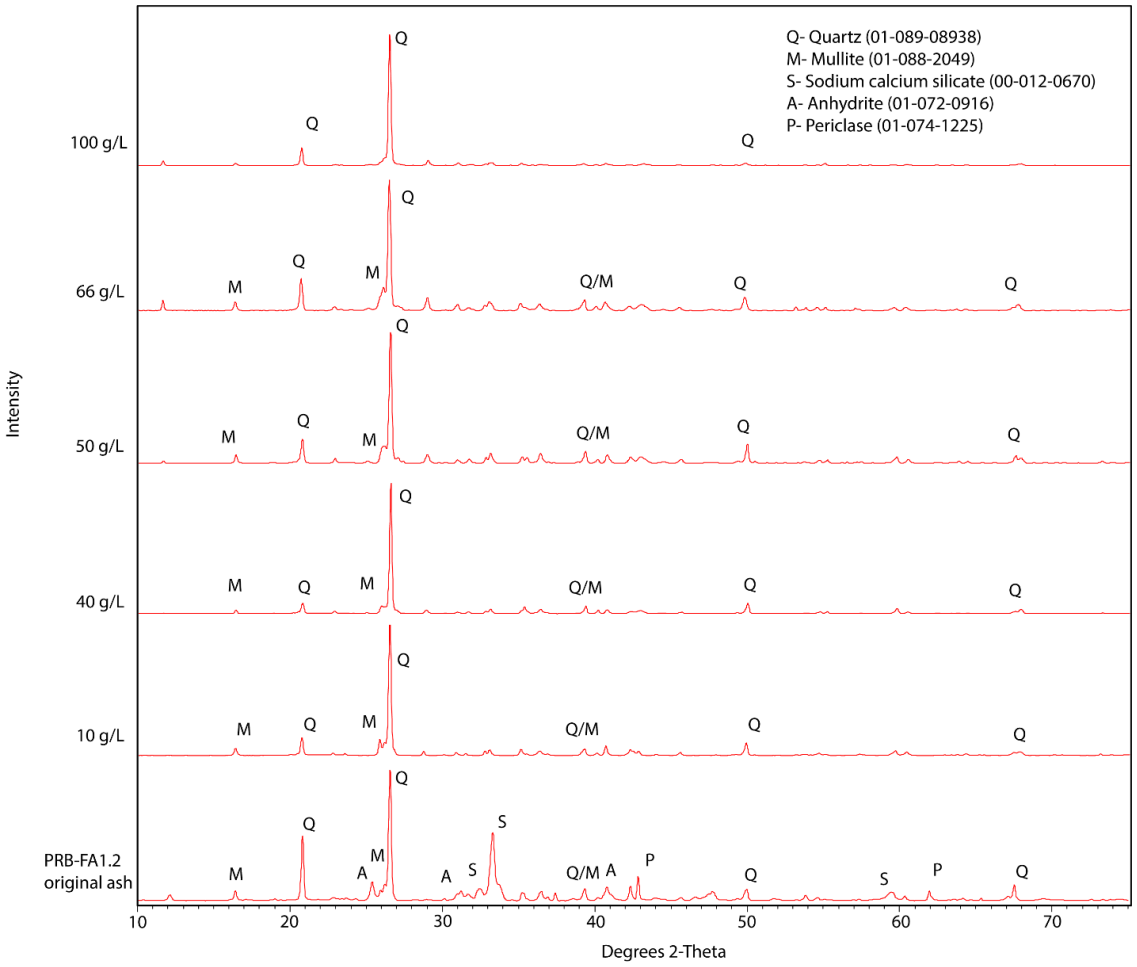

Figure A5: XRD patterns for PRB-FA1.2 and the solid phase residuals remaining after heated leaching in 1 mol/L HCl at various pulp densities.

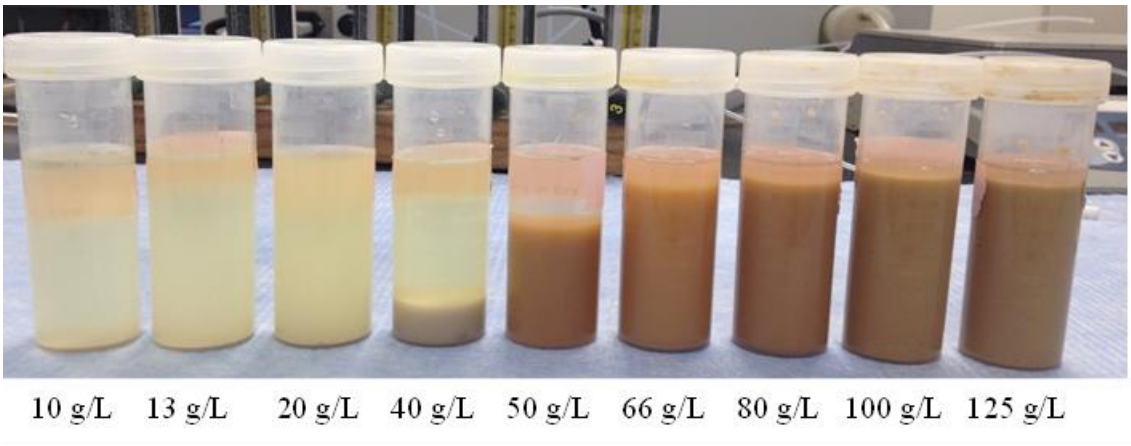

Figure A6: Photograph of slurry mixtures after leaching PRB-FA1.2 at various pulp densities prior to final centrifuge.

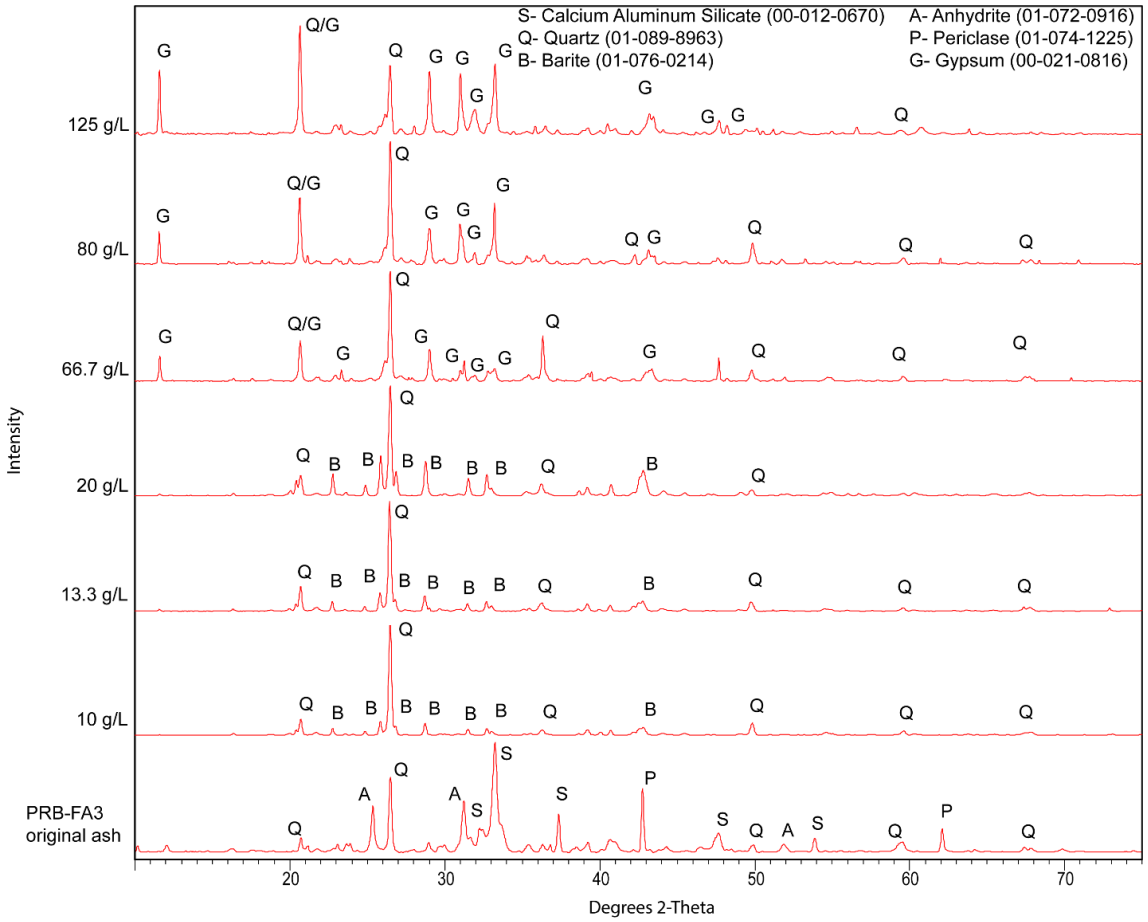

Figure A7: XRD patterns for PRB-FA3 and the solid phase residuals after heated leaching in 1 mol/L HCl at various pulp densities. Samples were not immediately freeze-dried prior to analysis.

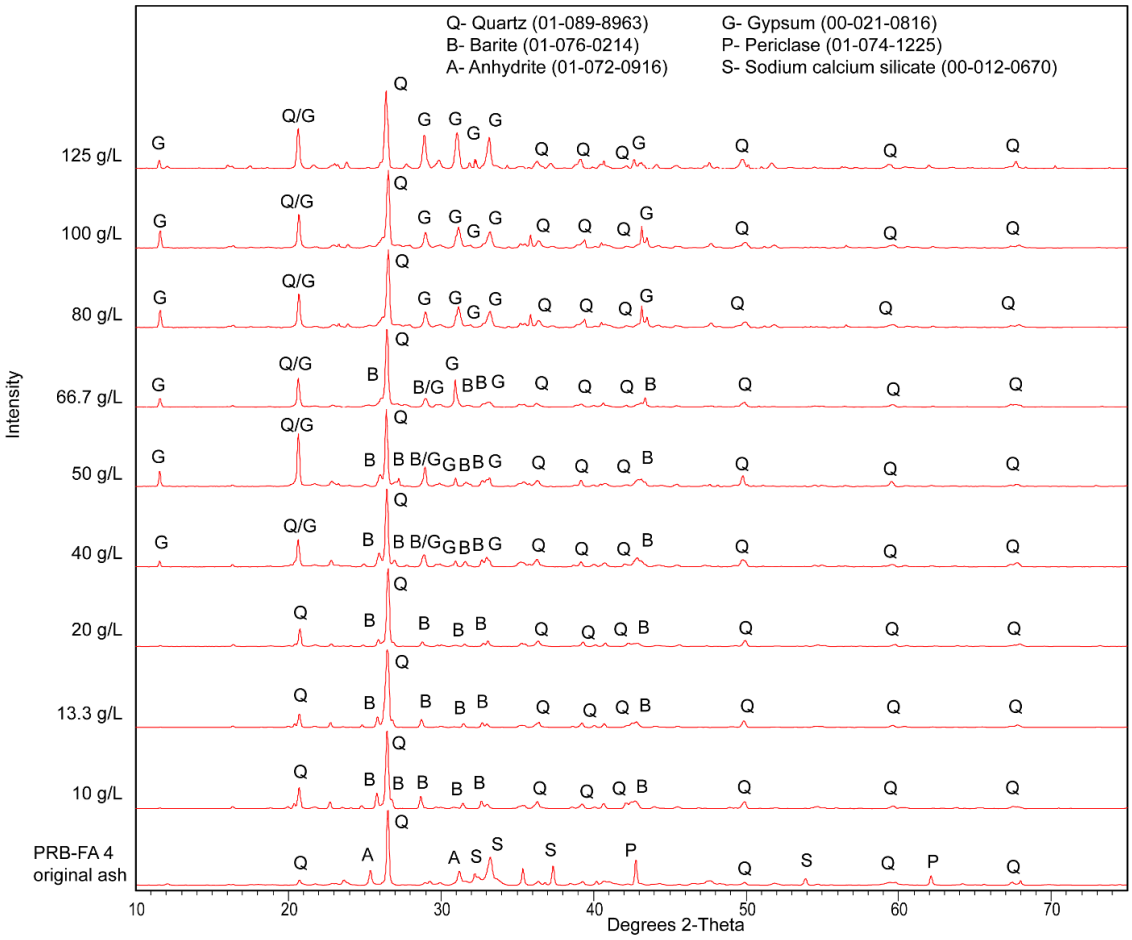

Figure A8: XRD patterns for PRB-FA4 and the solid phase residuals after heated leaching in 1 mol/L HCl at various pulp densities. Samples were not immediately freeze-dried prior to analysis.

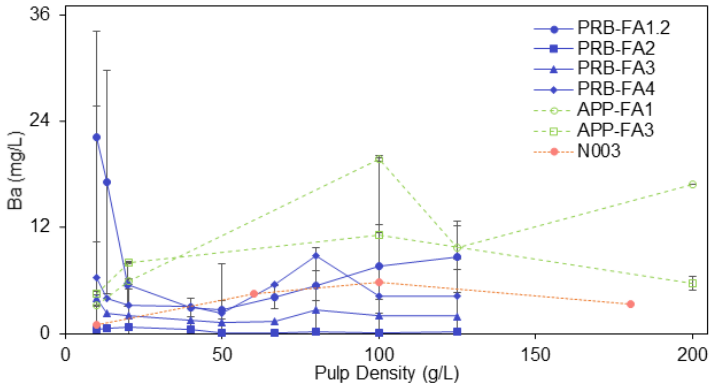

Figure A9: Effect of leaching pulp density on aqueous concentrations of Ba for four PRB ashes (blue), two APP ashes (green), and a Navajo coal (orange). Data points and error bars represent the average and standard deviation of replicate leachates for PRB-FA1.2 (n=3), PRB-FA2 (n=2), and APP-FA1 (n=2-9), APP-FA3 (n=2). Data points for all other samples represent single leachates.

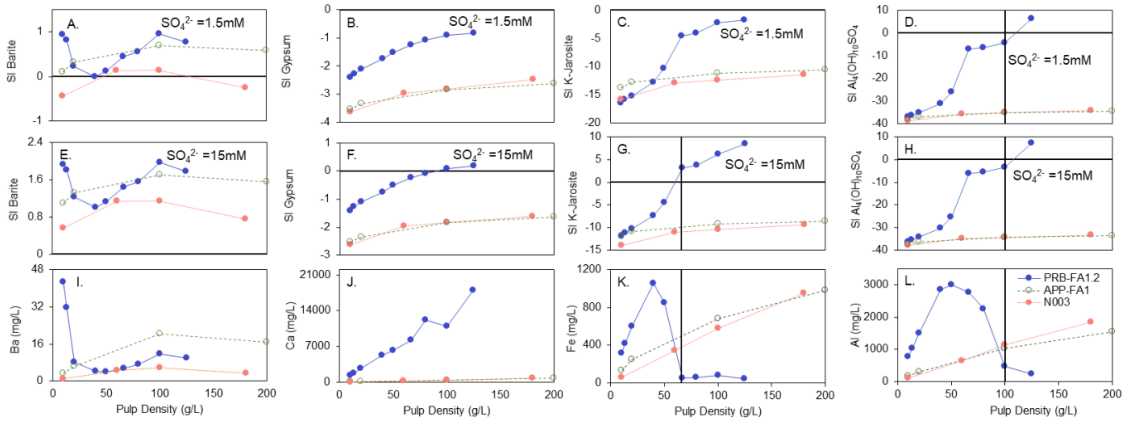

Figure A10: Saturation index (*SI*) values for (A, E) barite, (B, F) gypsum, (C, G) K-Jarosite, and (D, H) $Al_4(OH)_{10}SO_4$, determined with an assumed sulfate concentration of 1.5 mM (A-D) or a sulfate concentration of 15 mM (E-H). Positive *SI* values indicate that the mineral phase is thermodynamically oversaturated and could be expected to precipitate. Calculations were performed using the measured pH and the aqueous concentrations of major ions including (I) Ba, (J) Ca, (K) Fe, and (L) Al for leachates of PRB-FA1.2 (blue), APP-FA1 (green), and N003 (orange).

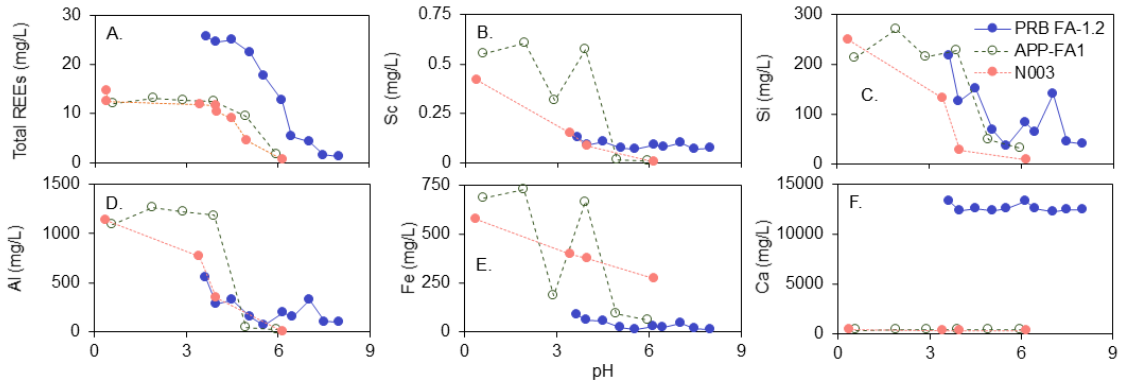

Figure A11: Aqueous concentrations of (A) total REEs, (B) Sc, (C) Si, (D) Al, (E) Fe, and (F) Si after adjusting the pH of leachates generated from three PRB ashes (blue), one APP ash (green), and a Navajo coal refuse (orange) after leaching at a pulp density of 100 g/L.

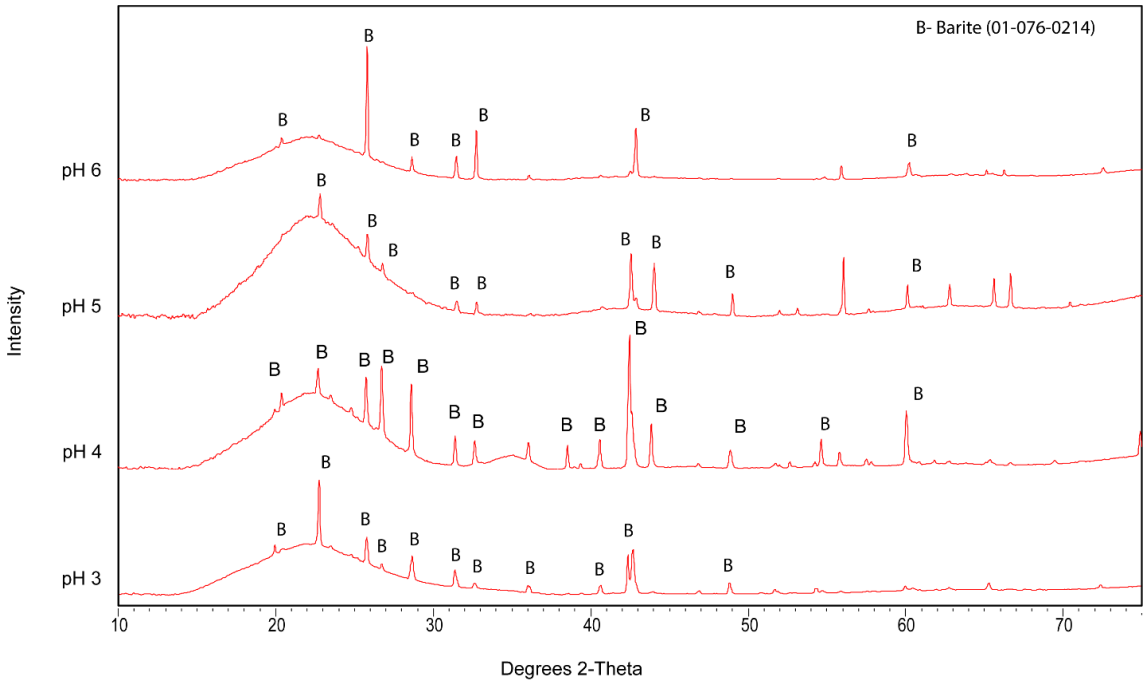

Figure A12: XRD patterns for solids formed after pH adjustment of leachates derived from PRB-FA1.2. Lechate were generated at a pulp density of 10 g/L.

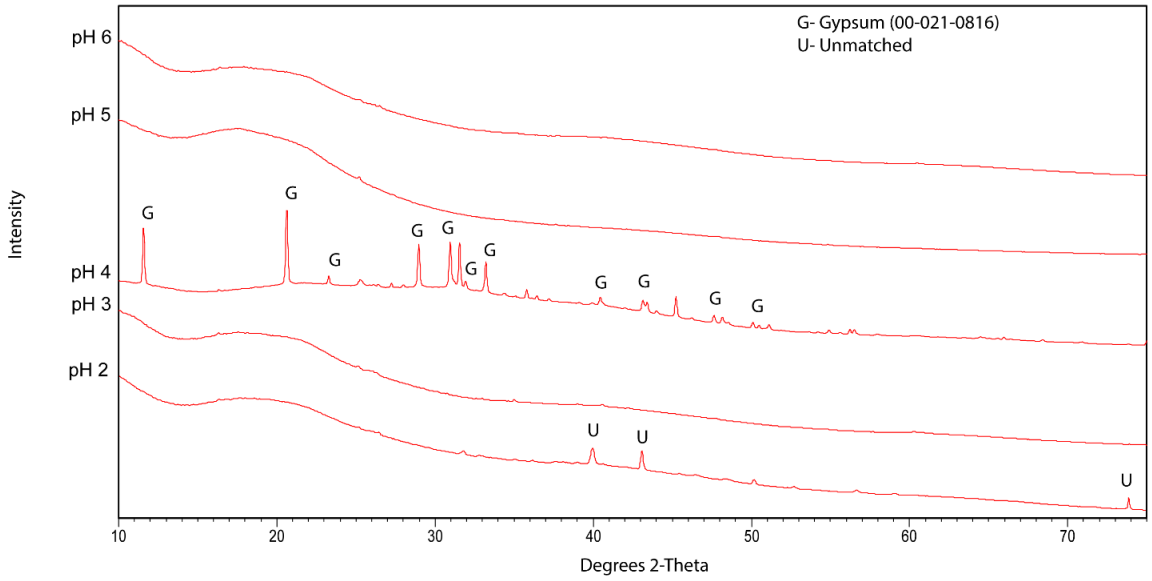

Figure A13: XRD patterns for solids formed after pH adjustment of leachates from PRB-FA1.2. Leachates were generated at a pulp density of 100 g/L. As shown the patterns are not background subtracted. Where applicable, peak matching was done using the background subtracted pattern.

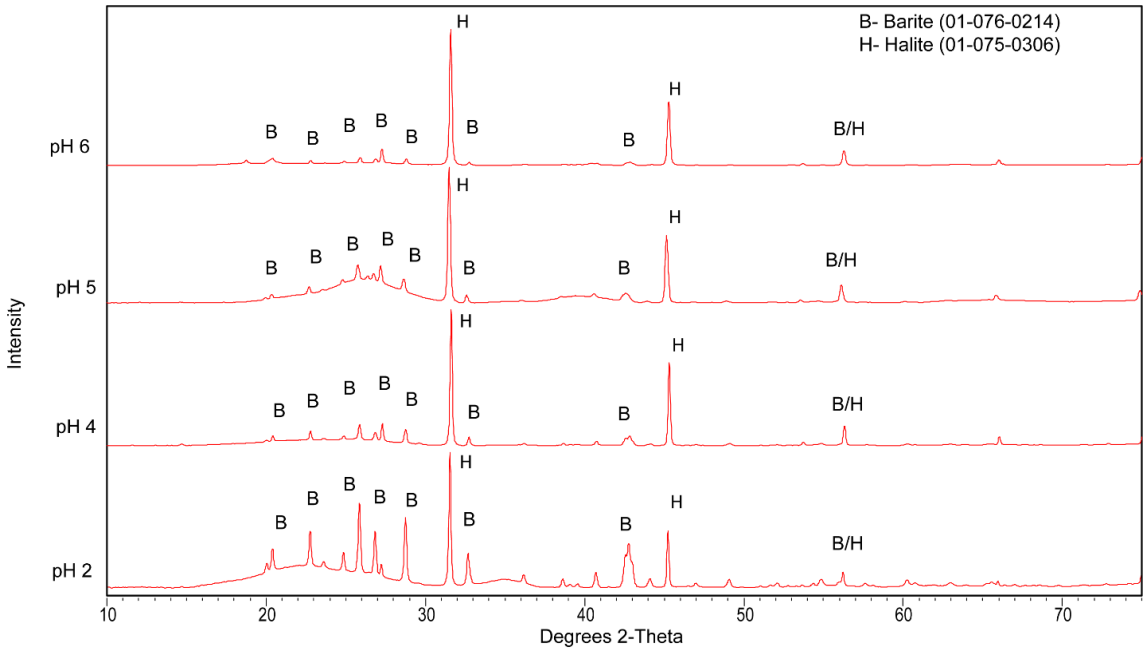

Figure A14: XRD patterns for solids formed after pH adjustment of leachates from PRB-FA2. Leachates were generated at a pulp density of 10 g/L.

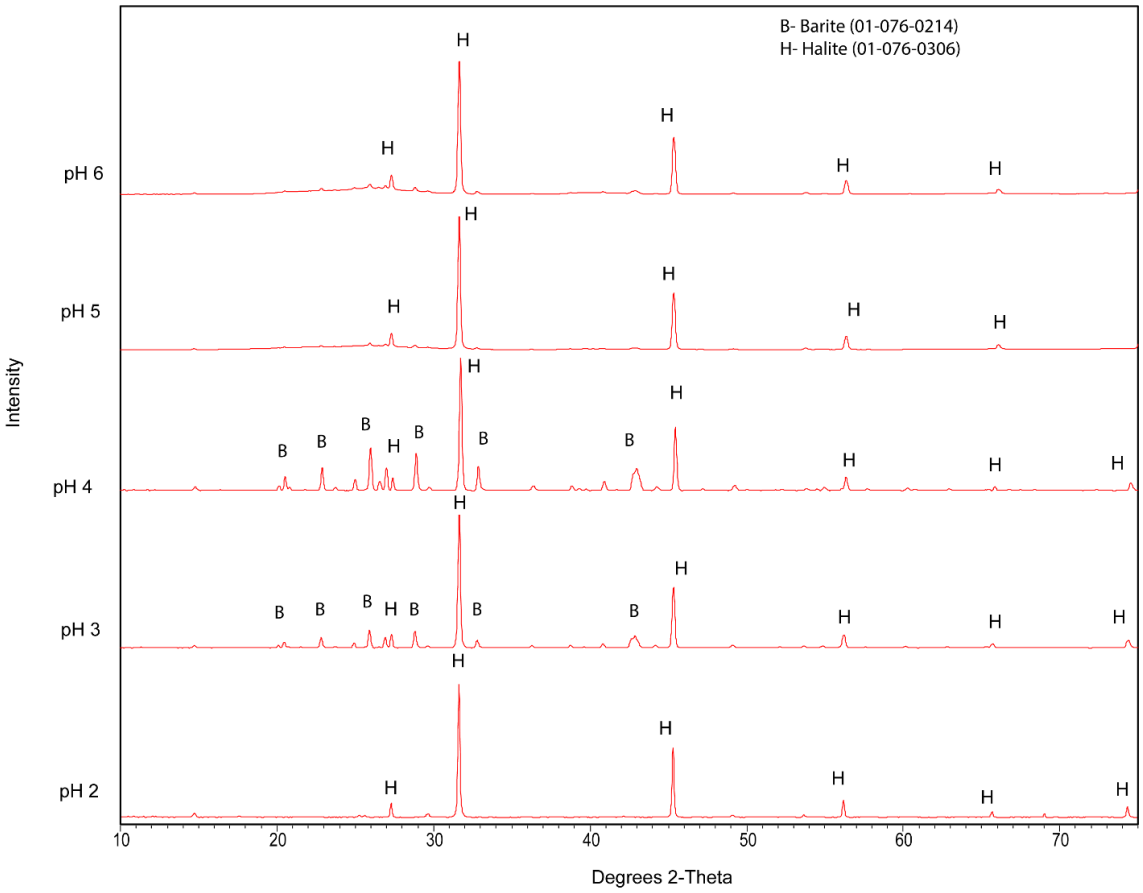

Figure A15: XRD patterns for solids formed after pH adjustment of leachates from PRB-FA3. Leachates were generated at a pulp density of 10 g/L.

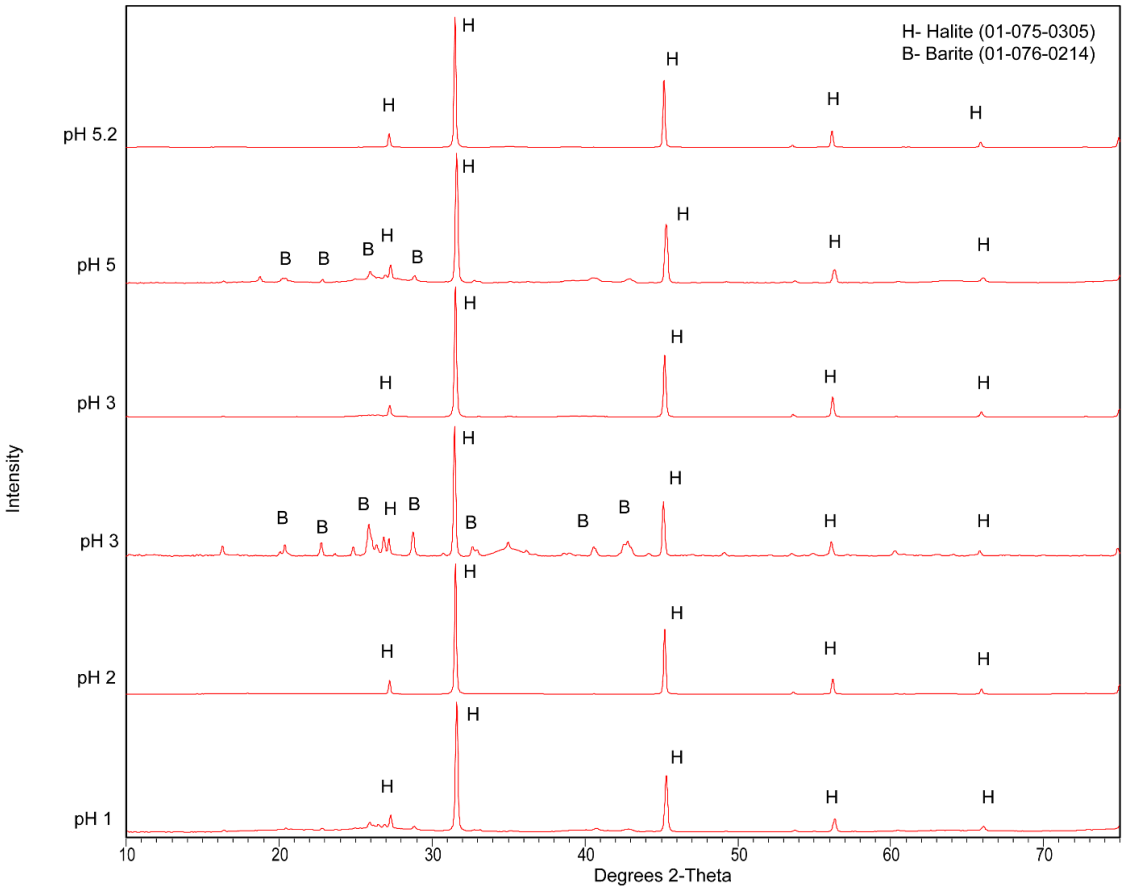

Figure A16: XRD patterns for solids formed after pH adjustment of leachates from APP-FA1. Leachates were generated at a pulp density of 10 g/L.

Appendix B. Chapter 3 Supporting Information

Table B1: Summary of SLM experiments performed. The first column provides the metals used in each set of experiments. The following columns show the approximate initial metals concentrations and pH in the feed.

Feed Components	Nd (μmol/L)	Er (μmol/L)	Fe(III) (mmol/L)	Fe(II) mmol/L	Al (mmol/L)	pH
Nd	0.01-100	-	-	-	-	1-3.5
Er	-	0.01-10	-	-	-	
Nd/Fe(III)	0.01-10	-	0.017-17	-	-	1-3.39
Er/Fe(III)	-	0.01-10	0.017-17.8	-	-	
Nd/Fe(II)	0.01-10	-	-	0.17-178	-	
Nd/Al	0.01	-	-	-	0.018-35	1-3.5

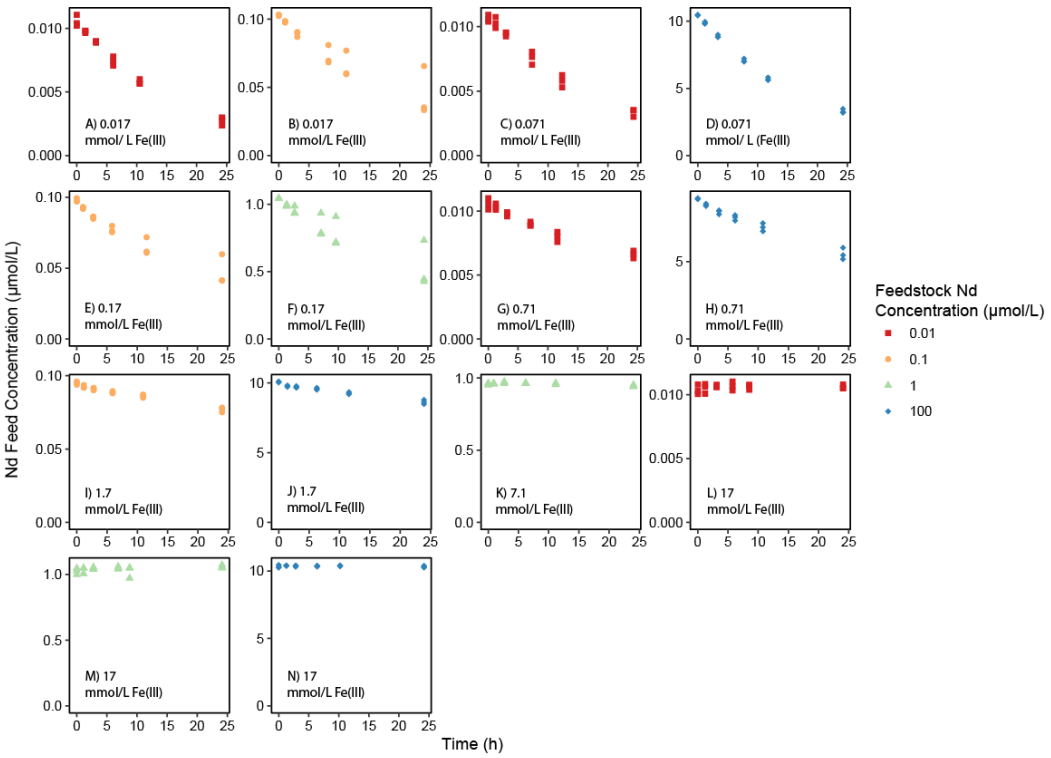

Figure B1: Concentration of Nd in the feed over the lifetime of the reactor for the set of Nd/Fe(III) experiments at pH 1. This set of experiments was chosen because it represents the range of separations that were observed across all experiments.

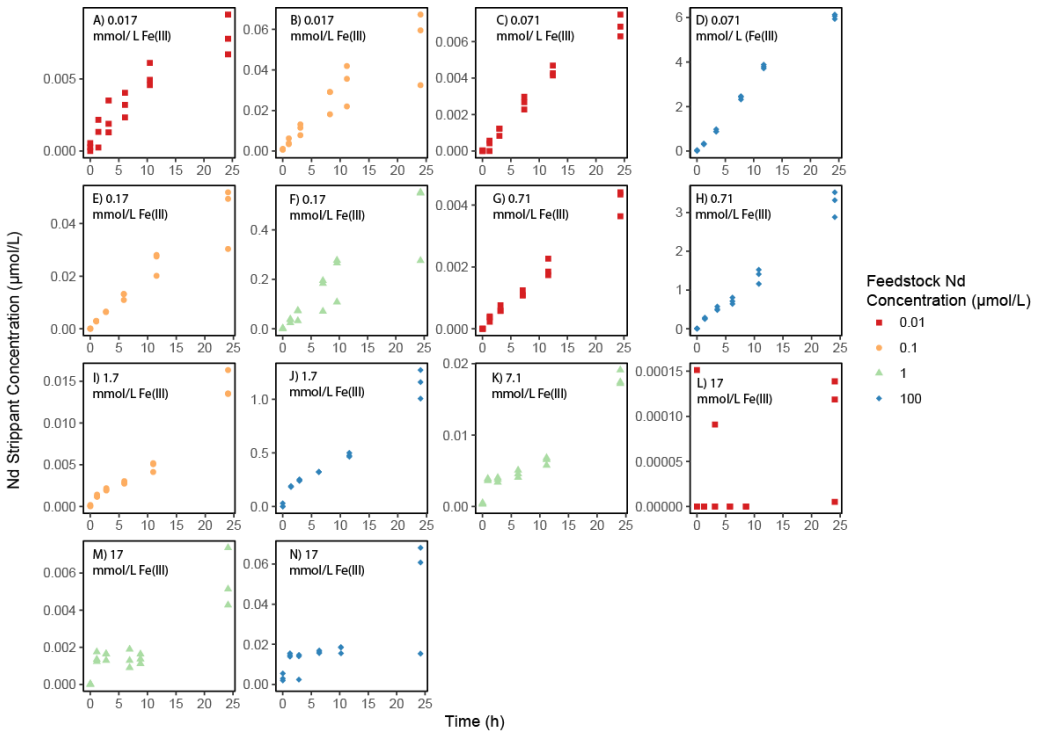

Figure B2: Concentration of Nd in the strippant over the lifetime of the reactor for the set of Nd/Fe(III) experiments at pH 1. This set of experiments was chosen because it represents the range of separations that were observed across all experiments.

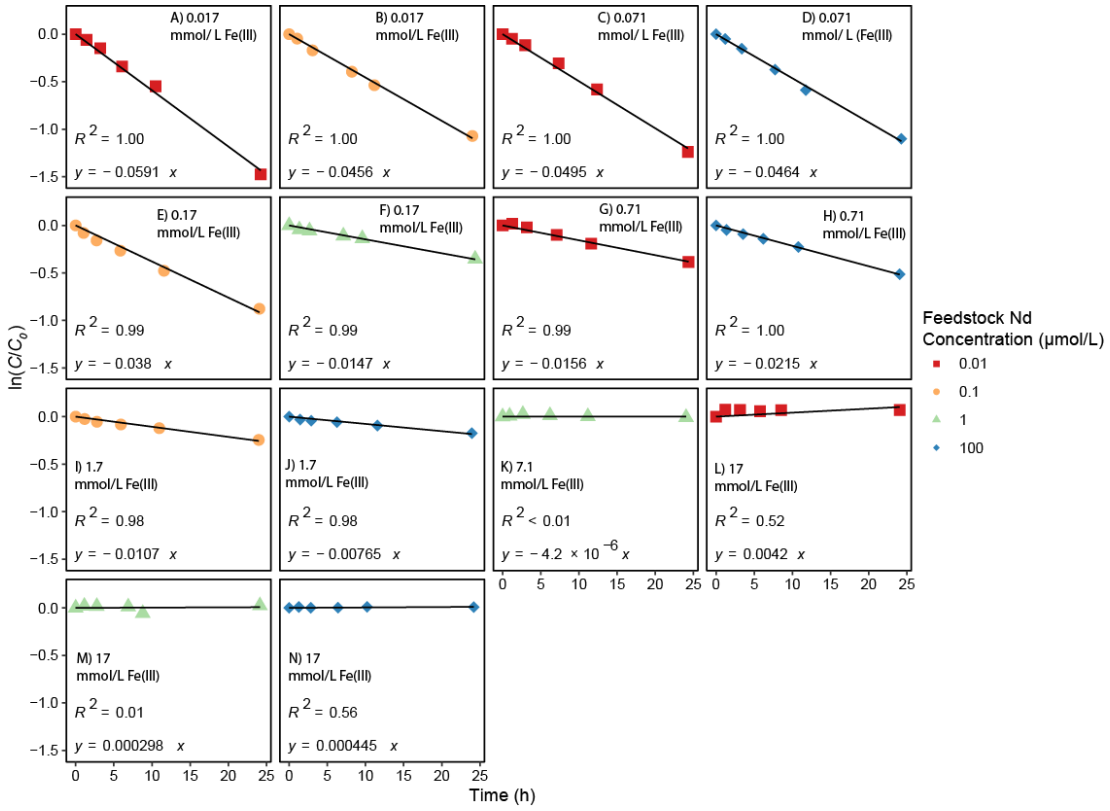

Figure B3: Linear regression of ln(C/C_0) versus time for Nd in the feed over the lifetime of the reactor for the set of Nd/Fe(III) experiments at pH 1. This set of experiments was chosen because it represents the range of separations that were observed across all experiments. The linear regressions and associated R^2 values are provided.

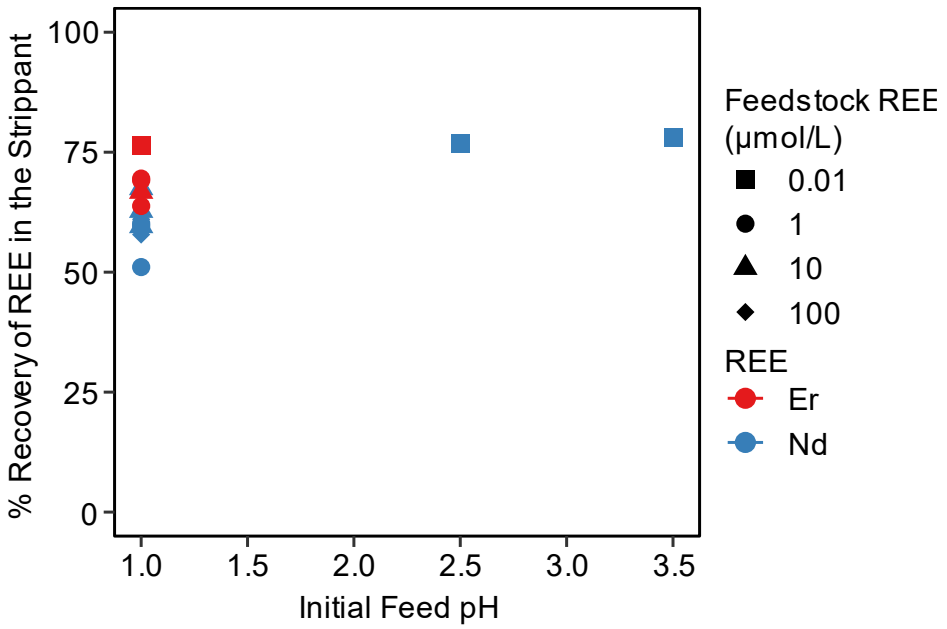

Figure B4: Percent recovery of Nd and Er in strippant after 24 hours for feeds of REEs only. Initial feed REE concentrations ranged from 0.01-10 µmol/L. Each shape represents and different REE concentration and the color indicates the specific REE.

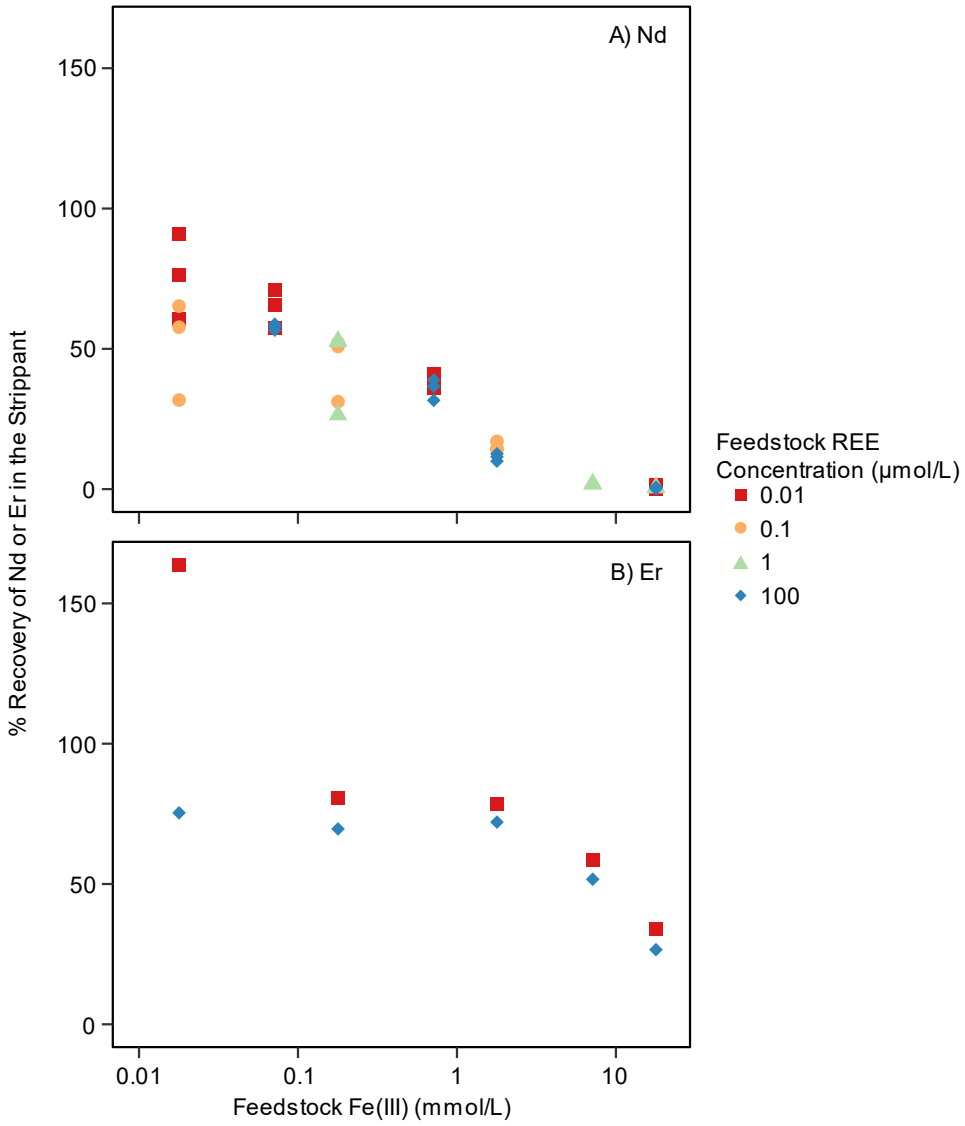

Figure B5: Percent recovery of (A) Nd and (B) Er in the acid strippant after a 24-hour separation of two-component mixtures of (A) Nd/Fe(III) and (B) Er/Fe(III) feedstocks at initial pH 1. Initial feed concentrations of REE and Fe(III) range from 0.01-10 µmol/L and 0.017-17 mmol/L, respectively. Each symbol shape represents a different Nd or Er concentration.

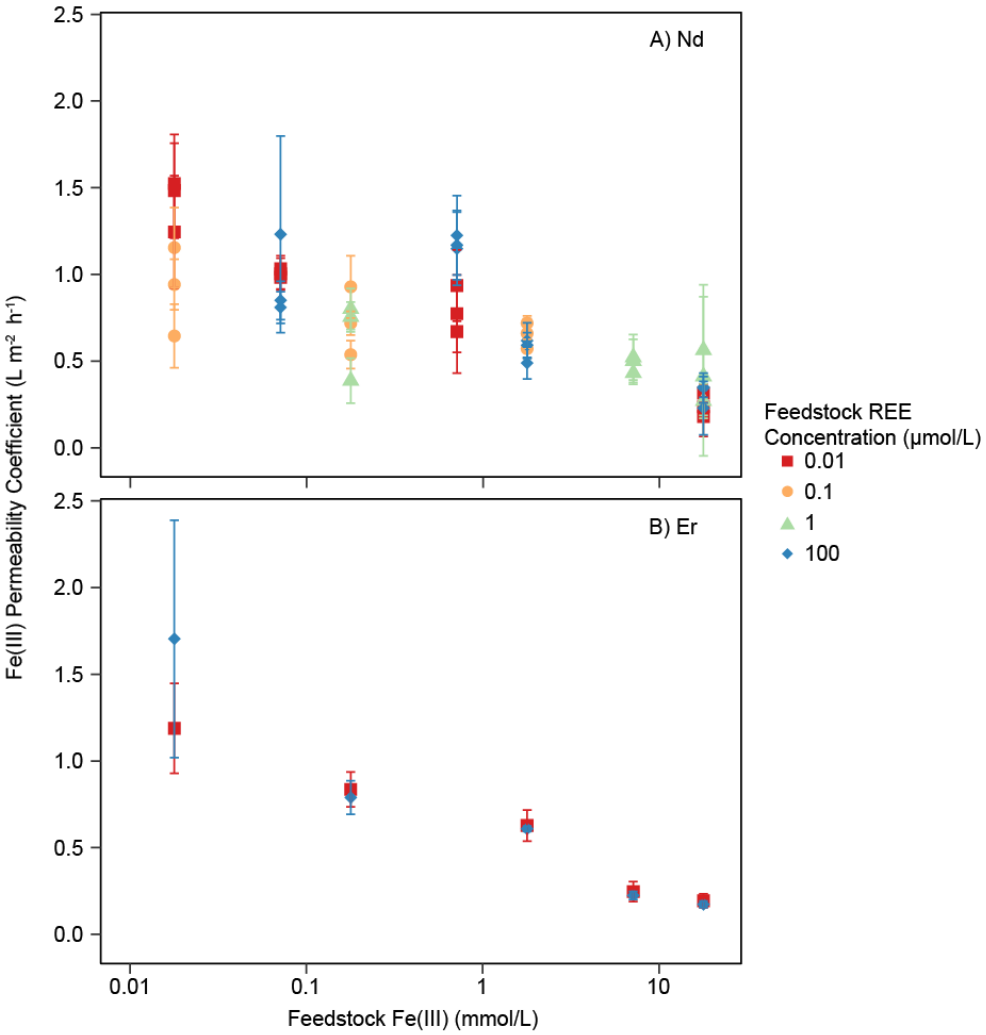

Figure B6: *P* coefficients for Fe(III) as a function of initial feed Fe(III) concentration of two-component mixtures of (A) Nd/Fe(III) and (B) Er/Fe(III) feedstocks at initial pH 1. Initial feed concentrations of Nd and Fe(III) range from 0.01-10 µmol/L and 0.018-18 mmol/L, respectively. Each color represents a different initial feed Nd concentration. The error bars represent the standard error of the regression slope.

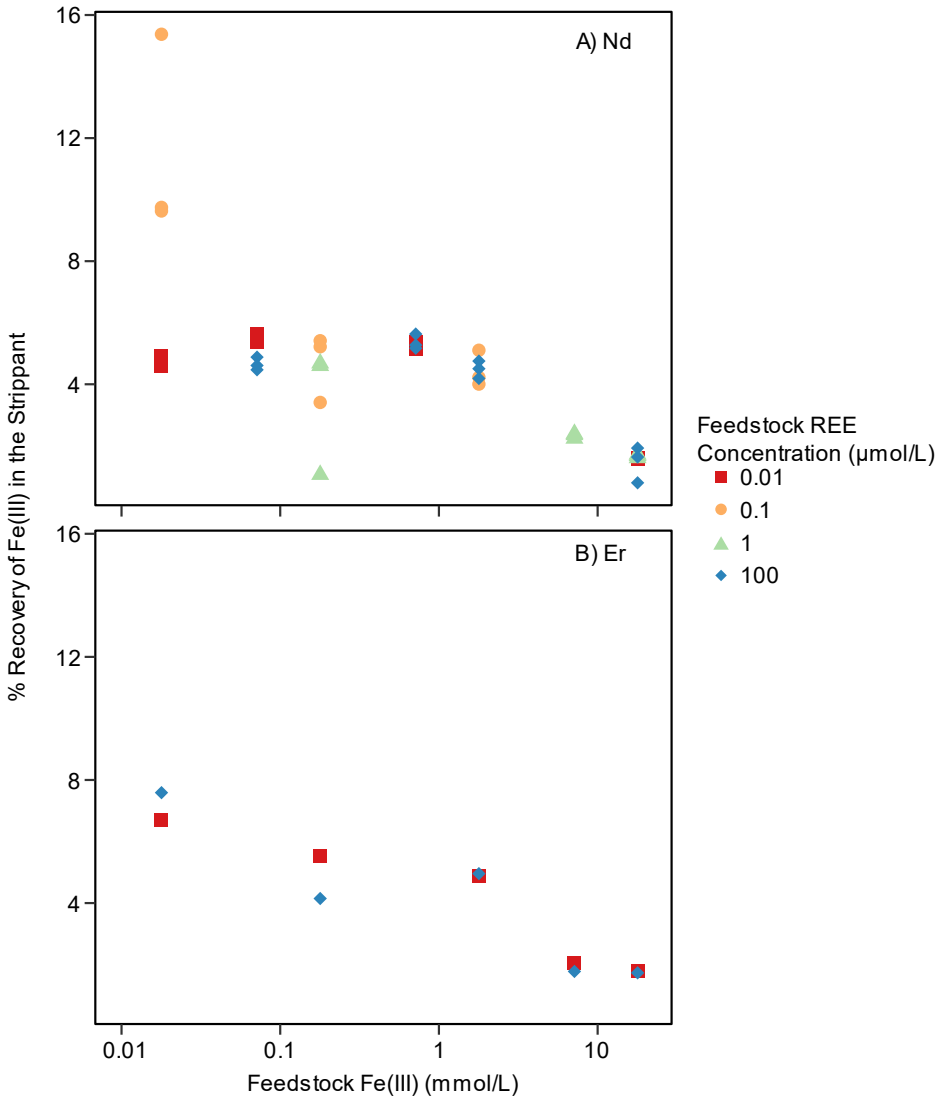

Figure B7: Percent recovery of Fe(III) in the strippant after a 24-hour separation of two-component mixtures of (A) Nd/Fe(III) and (B) Er/Fe(III) feedstocks at initial pH 1. Initial feed concentrations of Nd and Fe(III) range from 0.01-10 µmol/L and 0.018-18 mmol/L, respectively. Each shape and color represent a different initial feed Nd concentration.

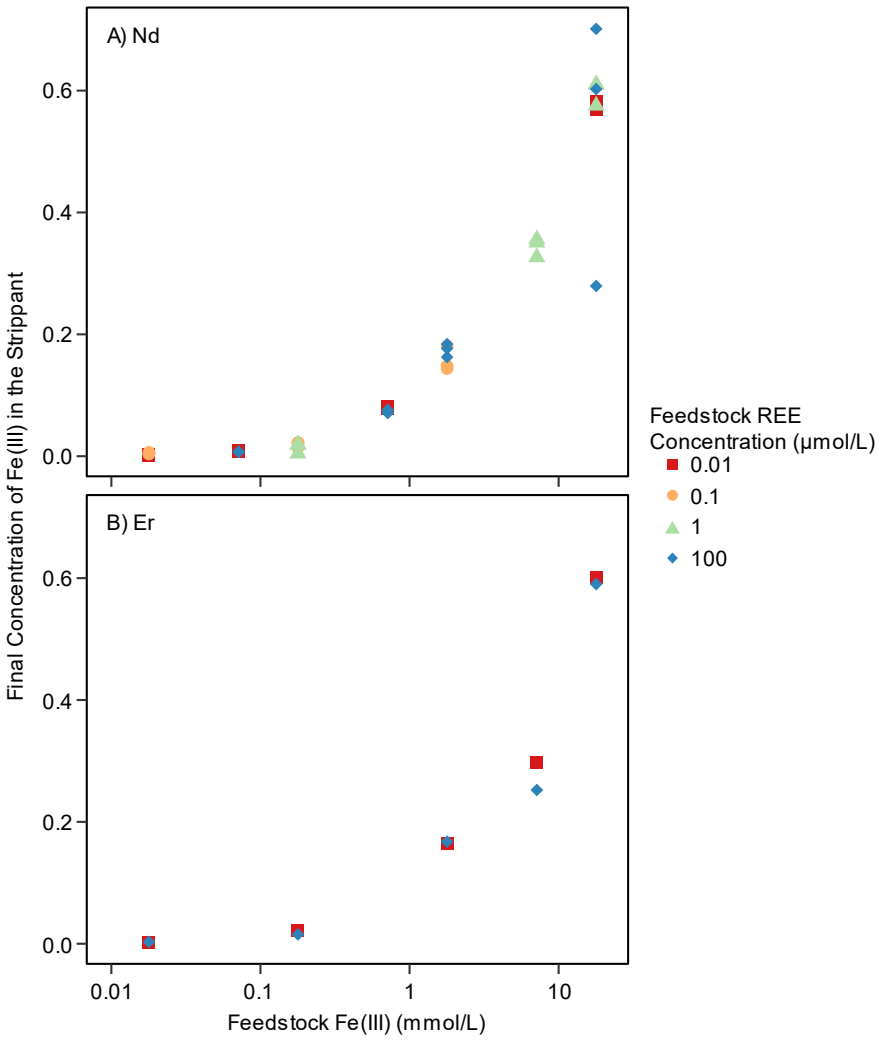

Figure B8: Fe(III) concentration in the strippant after a 24-hour separation of two-component mixtures of (A) Nd/Fe(III) and (B) Er/Fe(III) feedstocks at initial pH 1. Initial feed concentrations of Nd and Fe(III) range from 0.01-10 µmol/L and 0.018-18 mmol/L, respectively. Each shape and color represent a different initial feed Nd concentration.

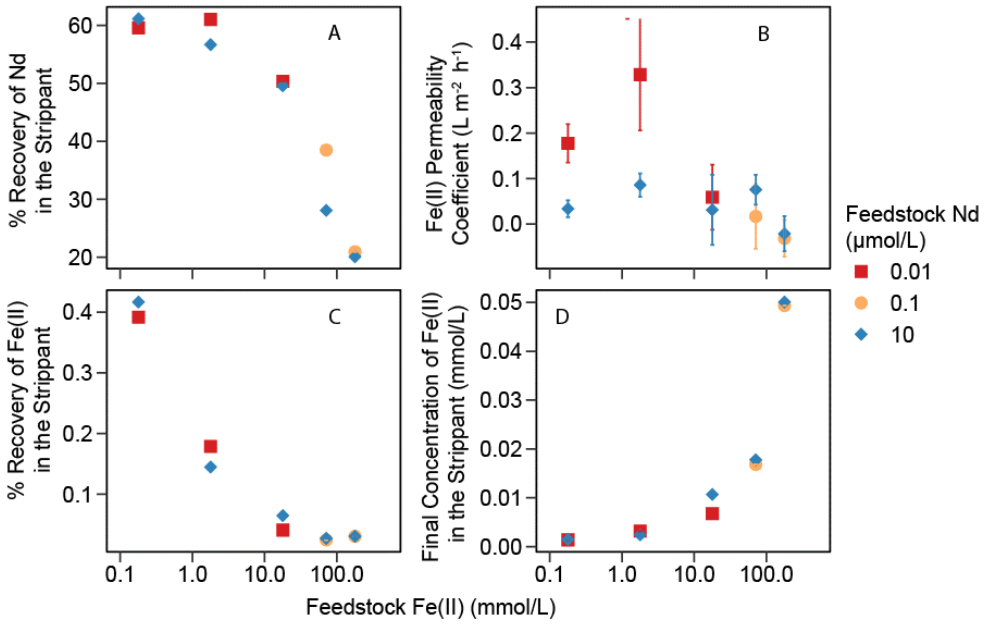

Figure B9: SLM separation of a two-component Nd/Fe(II) feed solutions prepared with a range of Nd and Fe(II) concentrations at pH 1. (A) Percent recovery of Nd in the acid strippant; (B) Fe(II) permeability coefficient *P*; (C) Percent recovery of Fe(II) in the strippant; (D) Fe(II) concentration in the strippant after a 24-hour separation.

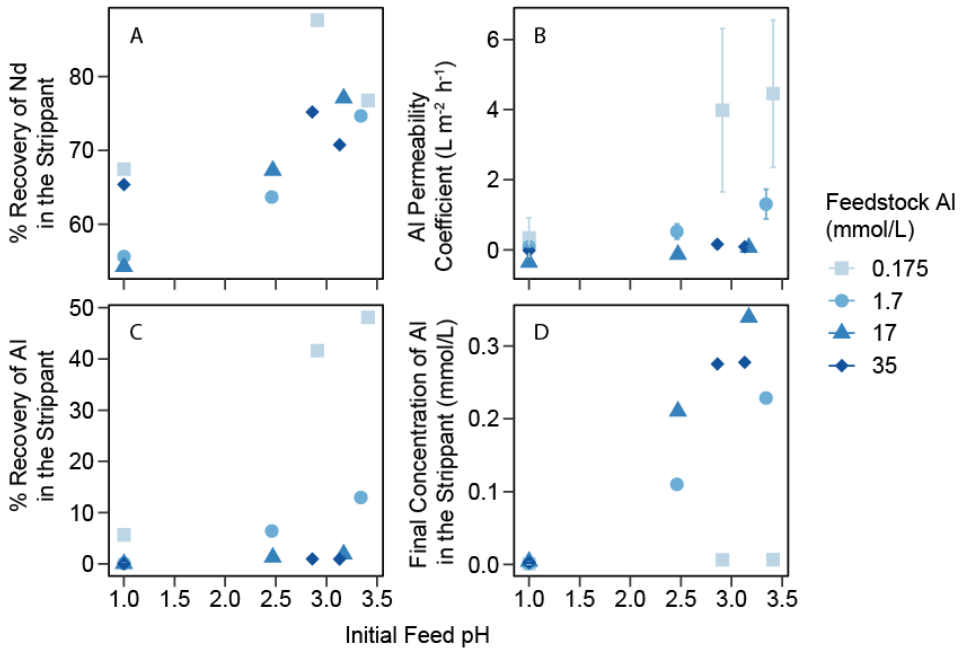

Figure B10: SLM separation of a two-component Nd/Al(III) feed solutions prepared with 0.01 µmol/L Nd and a range of Al concentrations at pH 1. (A) Percent recovery of Nd in the acid strippant; (B) Al permeability coefficient *P*; (C) Percent recovery of Al in the strippant; (D) Al concentration in the strippant after a 24-hour separation.

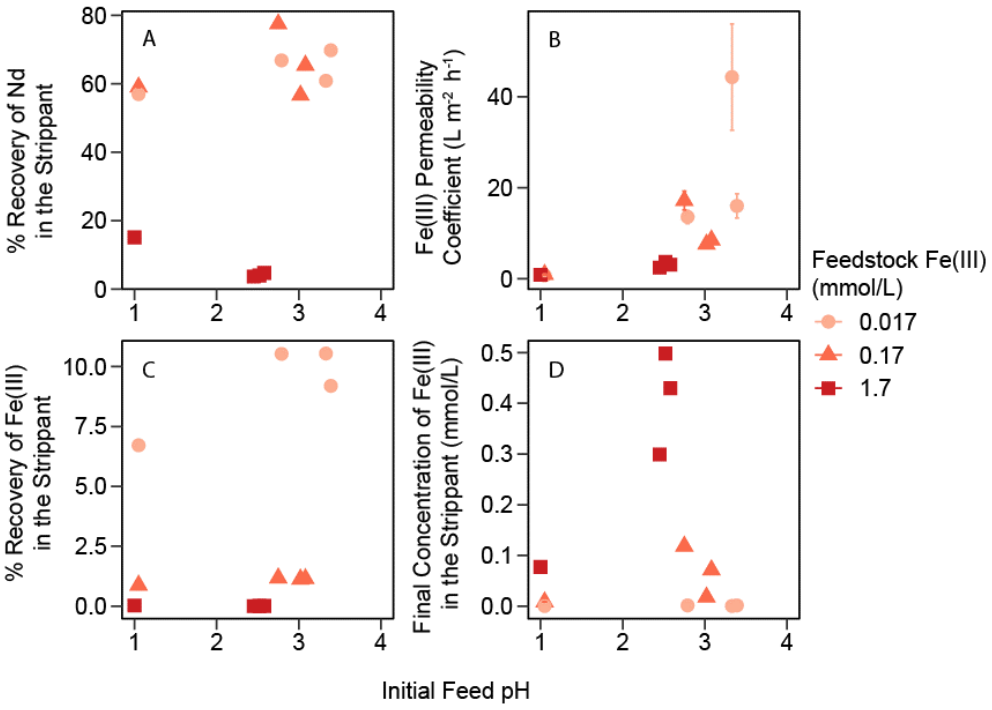

Figure B11: SLM separation of two-component Nd/Fe(III) feed solutions prepared with 1 µmol/L Nd and a range of Fe(III) concentrations at pH 1. (A) Percent recovery of Nd in the acid strippant; (B) Fe(III) permeability coefficient *P*; (C) Percent recovery of Fe in the strippant; (D) Fe concentration in the strippant after a 24-hour separation.

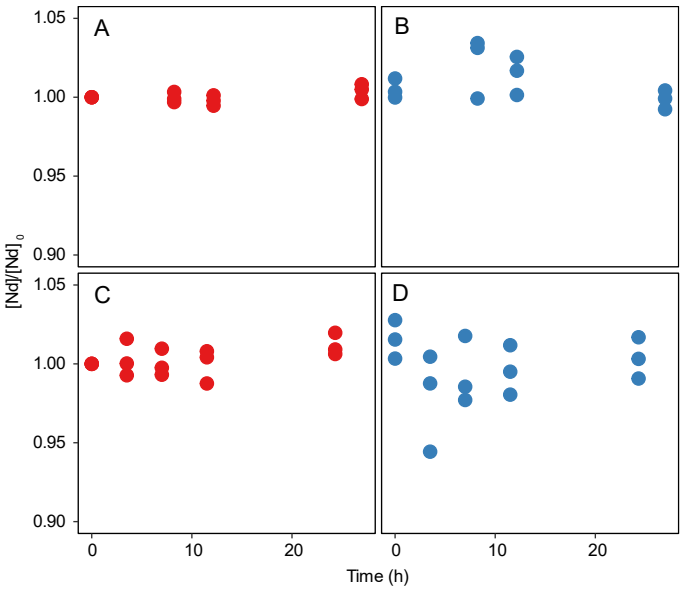

Figure B12: [Nd]/[Nd]$_0$ for unreacted feed controls with (A) 0 mmol/L Fe(III) before centrifugation and filtration; (B) 0 mmol/L Fe(III) after centrifugation and filtration; (C) 17 mmol/L Fe(III) before centrifugation and filtration; and (D) 17 mmol/L Fe(III) after centrifugation and filtration. All feeds were made with 0.01 µmol/L Nd at pH 1.

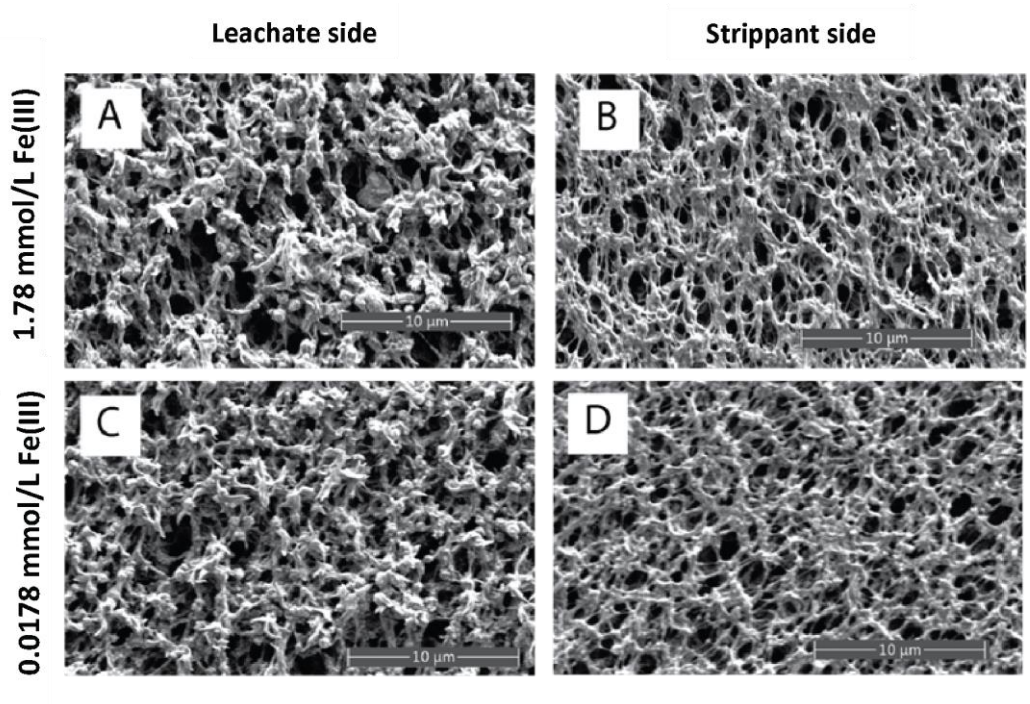

Figure B13: SEM images of spent membranes after 24 hour separation of Nd/Fe(III) feed solutions with: (A, B) 1.7 mmol/L Fe(III); (C, D) 0.017 mmol/L Fe(III). All feed solutions contained 1 µmol/L Nd and initial pH 1. The SEM images show the leachate side (A, C) and the strippant side (B, D) of the membrane. No new particles were observed in the spent membranes compared to the unused membrane.

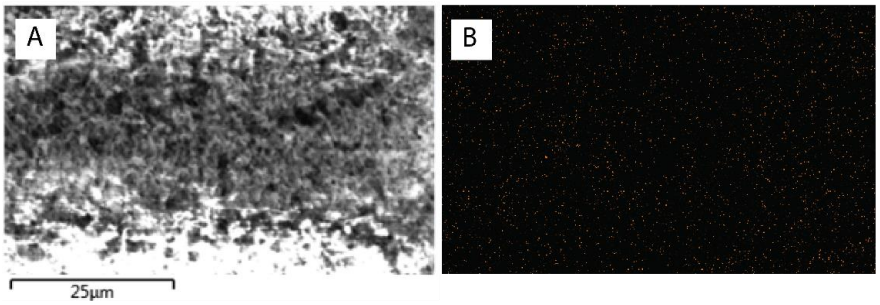

Element	Weight %
C	59.87
F	38.8
P	1.1
Fe	0.23

Figure B14:. (A) SEM image and (B) EDS map for Fe of the leachate side of a spent membrane used for a Nd/Fe(III) separation experiment. The elemental composition as obtained by EDS is also provided. The experimental feed solution contained 1 µmol/L Nd, 1.7 mmol/L Fe(III), initial pH 1.

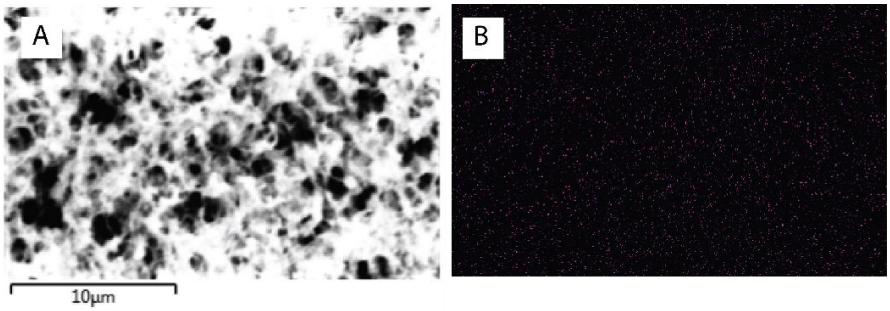

Element	Weight %
C	54.01
F	44.73
P	0.99
Fe	0.19

Figure B15: (A) SEM image and (B) EDS map for Fe of the strippant side of a spent membrane used for a Nd/Fe(III) separation experiment. The elemental composition as obtained by EDS is also provided. The experimental feed solution contained 1 µmol/L Nd, 1.7 mmol/L Fe(III), initial pH 1.

Appendix C. Chapter 4 Supporting Information

Table C1: Individual REE concentrations (mg/L) for each AMD site. Concentrations are from the field acidified samples.

	Sc	Y	La	Ce	Pr	Nd	Sm	Eu	Gd	Tb	Dy	Ho	Er	Tm	Yb	Lu
	mg/L	mg/L	mg/L	mg/L	mg/L	mg/L	mg/L	mg/L	mg/L	mg/L	mg/L	mg/L	mg/L	mg/L	mg/L	mg/L
McIntire	0.52	29.49	6.93	20.66	2.93	15.03	4.52	1.17	6.67	0.97	5.13	1.05	2.66	0.30	1.73	0.25
DeSale	0.21	28.68	7.70	21.39	3.07	15.57	4.49	1.16	6.94	0.95	4.76	0.93	2.31	0.25	1.37	0.19
Sterrett	0.69	26.37	8.31	21.42	3.12	15.71	4.69	1.25	7.05	0.95	4.79	0.95	2.47	0.29	1.68	0.25
Racic	0.65	20.32	11.17	28.12	3.64	16.49	4.08	0.96	5.53	0.74	3.61	0.74	2.02	0.24	1.48	0.22
US 91	0.98	19.85	10.75	26.87	3.69	16.91	4.17	1.00	5.60	0.77	4.03	0.83	2.25	0.28	1.76	0.25
Milk Run	1.87	22.58	5.92	22.86	3.80	19.59	5.32	1.27	6.79	0.88	4.34	0.88	2.15	0.23	1.32	0.20
Kentucky Hollow	1.40	20.82	7.12	24.81	3.84	19.07	5.34	1.25	6.63	0.88	4.21	0.84	2.03	0.22	1.34	0.20

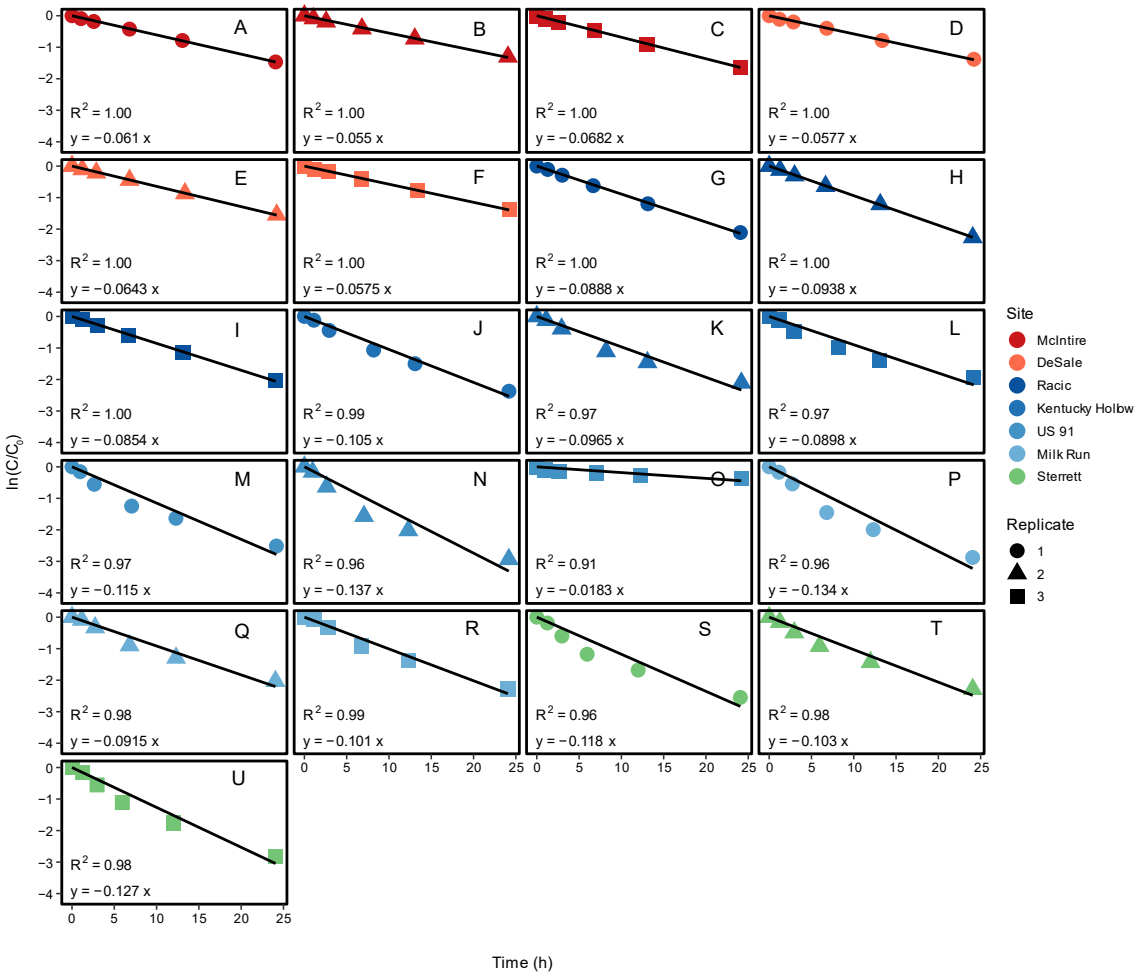

Figure C1: Linear regression of ln(C/C_0) for Nd in the feed versus time over the lifetime of the reactor for fresh unfiltered feeds for each of the seven sites ((A-C) McIntire, (D-F) DeSale, (G-I) Racic, (J-L) Kentucky Hollow, (M-O) US 91, (P-R) Milk Run, and (S-U) Sterrett). Sites in groups 1, 2, and 3 are shown in red, blue, and green, respectively. The equations for the linear regressions and the associated R^2 values are provided. This set of ln(C/C_0) versus time data is shown because it is representative subset of experiments.

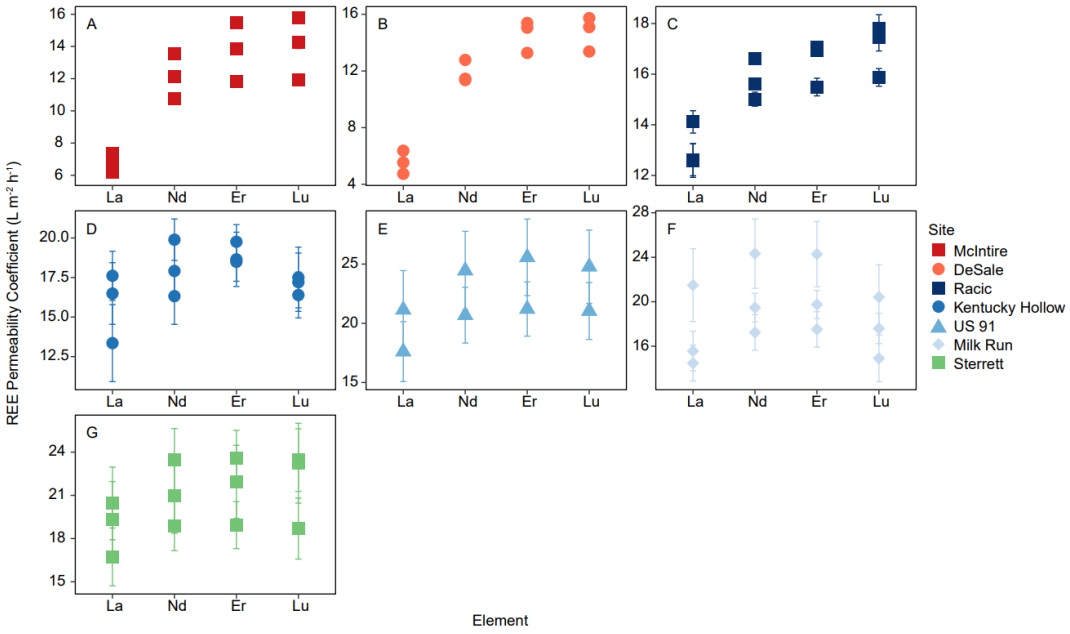

Figure C2: *P* coefficients for La, Nd, Er, and Lu using fresh unfiltered feeds from the (A) McIntire, (B) DeSale, (C) Racic, (D) Kentucky Hollow, (E) US 91, (F) Milk Run, and (G) Sterrett sites. The error bars represent the standard error associated with the slope of the linear regression of the ln(C/C_0) versus time data used to calculate the *P* coefficient.

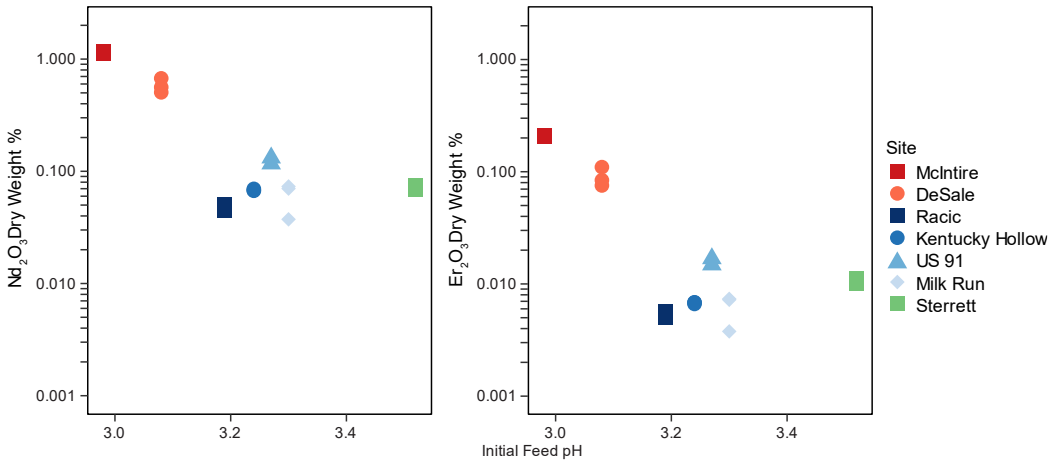

Figure C3: Dry weight % of (A) Nd_2O_3 and (B) Er_2O_3 in the product as a function of the initial feed pH for each site using fresh unfiltered feeds.

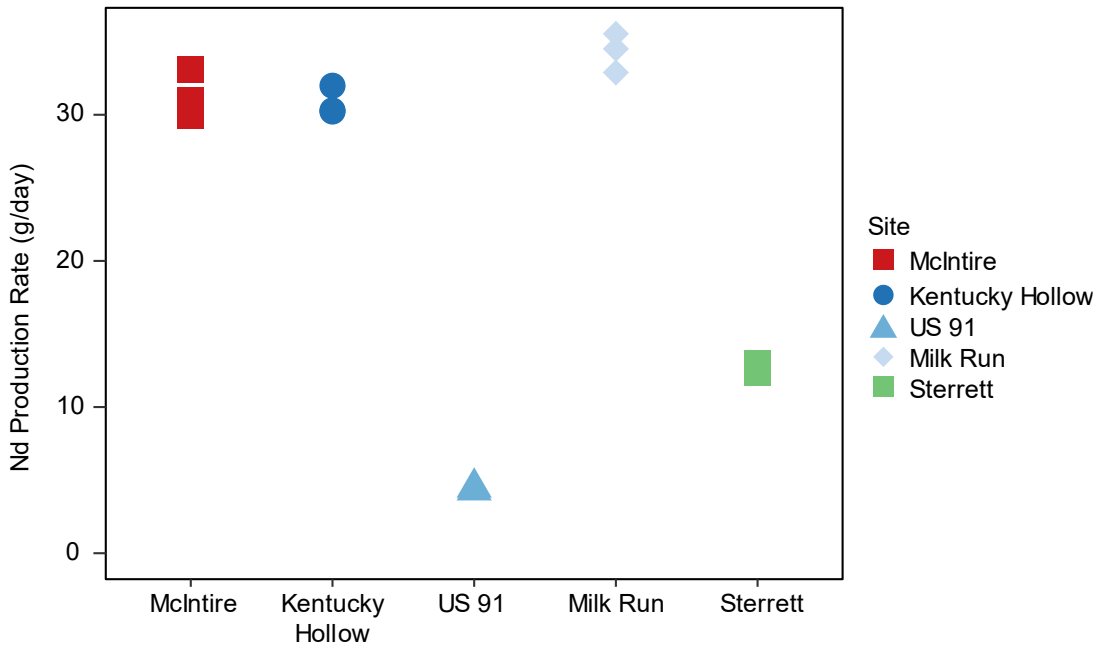

Figure C4: Production rate (g/day) of Nd for each of the sites where flowrate data was collected.

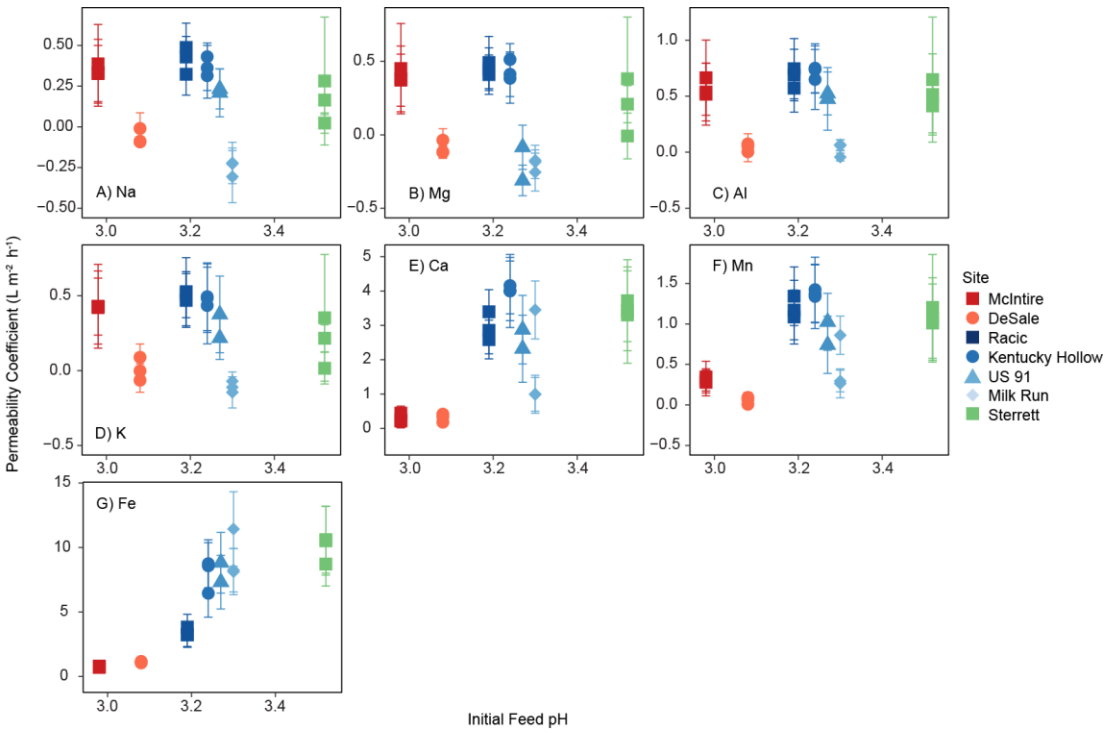

Figure C5: *P* coefficients for (A) Na, (B) Mg, (C) Al, (D) K, (E) Ca, (F) Mn, and (G) Fe for each site as functions of the initial feed pH using unfiltered fresh feeds. The error bars represent the standard error associated with the slope of the linear regression of the ln(C/C_0) versus time data used to calculate the *P* coefficient.

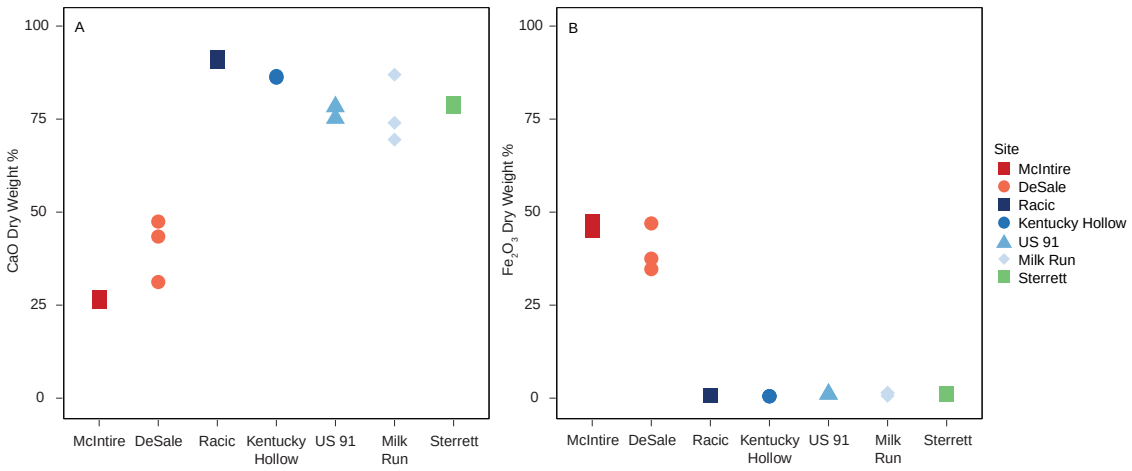

Figure C6: Dry weight % of (A) CaO and (B) Fe_2O_3 in the product for each site using unfiltered fresh feeds.

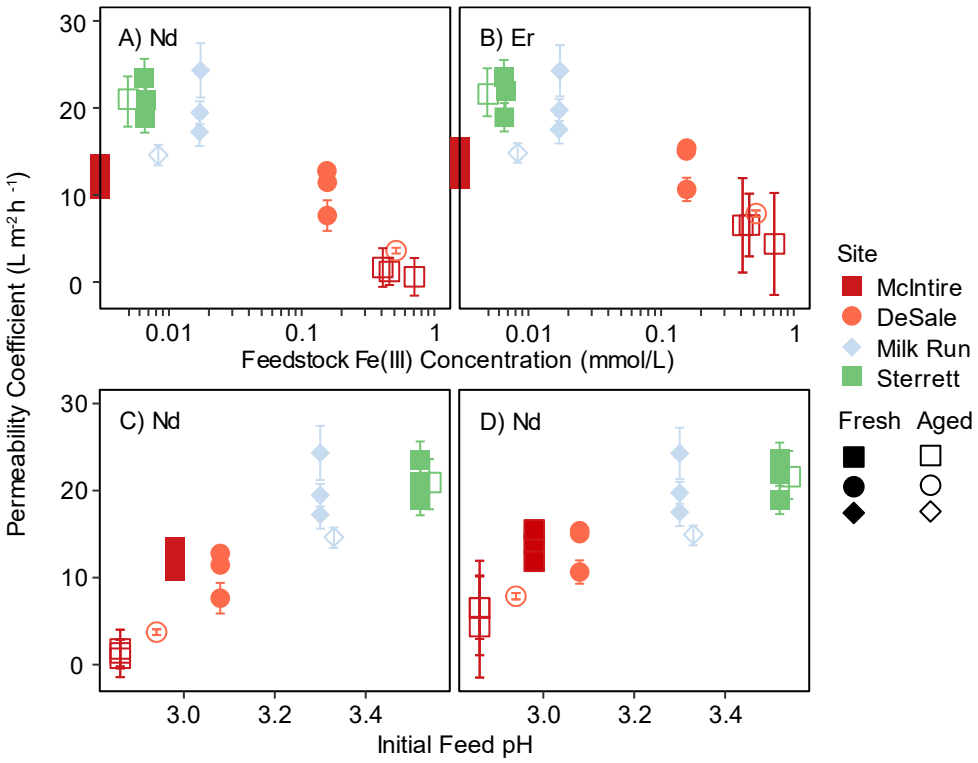

Figure C7: (A-B) *P* coefficients for (A) Nd and (B) Er as a function of the initial Fe(III) feedstock concentration (mmol/L) for four fresh and aged feeds. (C-D) *P* coefficients (C) Nd and (D) Er as a function of the initial feed pH for four fresh and aged feeds. The error bars represent the standard error associated with the slope of the linear regression of the ln(C/C_0) versus time data used to calculate the *P* coefficient.

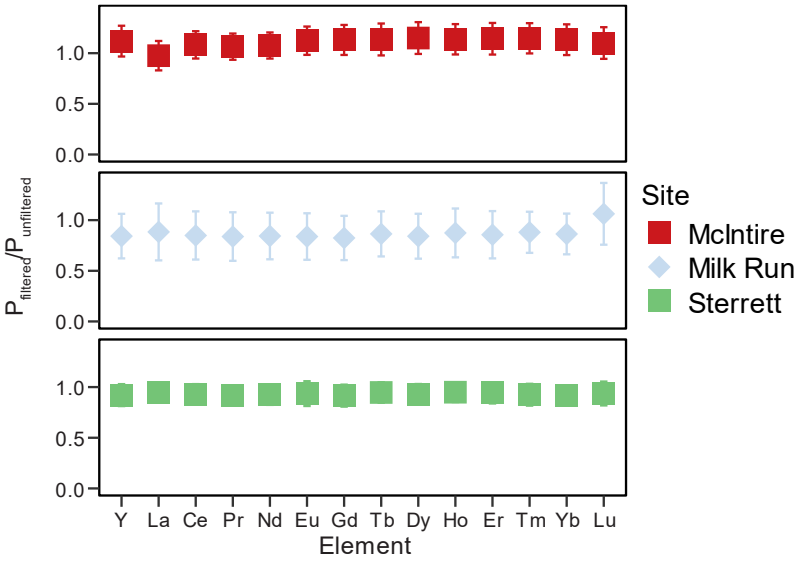

Figure C8: Ratios of individual REE *P* coefficients for fresh feeds divided by *P* coefficients for filtered feeds. The ratios were calculated using the average *P* coefficients from each of the three replicates for treatment. The standard deviation for each set of replicates was also calculated. The standard deviation was then propagated through the calculation of the ratio and this propagated error is represented by the error bars.

References

(1) Ding, Y.; Harvey, D.; Wang, N.-H. L. Two-zone ligand-assisted displacement chromatography for producing high-purity praseodymium, neodymium, and dysprosium with high yield and high productivity from crude mixtures derived from waste magnets. *Green Chemistry* **2020**, *22* (12), 3769-3783, 10.1039/D0GC00495B. DOI: 10.1039/D0GC00495B.

(2) Alonso, E.; Sherman, A. M.; Wallington, T. J.; Everson, M. P.; Field, F. R.; Roth, R.; Kirchain, R. E. Evaluating Rare Earth Element Availability: A Case with Revolutionary Demand from Clean Technologies. *Environ. Sci. Technol.* **2012**, *46* (6), 3406-3414. DOI: 10.1021/es203518d.

(3) Survey, U. S. G. *Mineral Commodity Summaries 2022*; Reston, VA, 2022. http://pubs.er.usgs.gov/publication/mcs2022DOI: 10.3133/mcs2022.

(4) Taggart, R. K.; Hower, J. C.; Dwyer, G. S.; Hsu-Kim, H. Trends in the Rare Earth Element Content of U.S.-Based Coal Combustion Fly Ashes. *Environ. Sci. Technol.* **2016**, *50* (11), 5919-5926.

(5) Hower, J. C.; Dai, S.; Seredin, V. V.; Zhao, L.; Kostova, I. J.; Silva, L. F.; Mardon, S.; Gurdal, G. A note on the occurrence of yttrium and rare earth elements in coal combustion products. *Coal Combustion and Gasification Products* **2013**, *5*, 39-47.

(6) Cravotta III, C. A. Dissolved metals and associated constituents in abandoned coal-mine discharges, Pennsylvania, USA. Part 1: Constituent quantities and correlations. *Applied Geochemistry* **2008**, *23* (2), 166-202.

(7) Stewart, B. W.; Capo, R. C.; Hedin, B. C.; Hedin, R. S. Rare earth element resources in coal mine drainage and treatment precipitates in the Appalachian Basin, USA. *International Journal of Coal Geology* **2017**, *169*, 28-39.

(8) Parker, R. L., and Fleisher, Michael. *Data of Geochemistry Sixth Edition- Chapter D. Composition of the Earth's Crust.* . 1967. (accessed.

(9) Seredin, V. V. A new method for primary evaluation of the outlook for rare earth element ores. *Geology of Ore Deposits* **2010**, *52* (5), 428-433. DOI: 10.1134/S1075701510050077.

(10) Wu, S.; Wang, L.; Zhao, L.; Zhang, P.; El-Shall, H.; Moudgil, B.; Huang, X.; Zhang, L. Recovery of rare earth elements from phosphate rock by hydrometallurgical processes – A critical review. *Chem. Eng. J.* **2018**, *335*, 774-800. DOI: https://doi.org/10.1016/j.cej.2017.10.143.

(11) Drew, L. J.; Qingrun, M.; Weijun, S. The Bayan Obo iron-rare-earth-niobium deposits, Inner Mongolia, China. *Lithos* **1990**, *26* (1), 43-65. DOI: https://doi.org/10.1016/0024-4937(90)90040-8.

(12) Qifan, W. *Overview of Legacy/NORM Sites in Bayan Obo and Baotou, Inner Mongolia, China*. 2011. (accessed 20191 April 17).

(13) Wang, L.; Liang, T.; Zhang, Q.; Li, K. Rare earth element components in atmospheric particulates in the Bayan Obo mine region. *Environ. Res.* **2014**, *131*, 64-70. DOI: https://doi.org/10.1016/j.envres.2014.02.006.

(14) Li, B.; Wang, N.; Wan, J.; Xiong, S.; Liu, H.; Li, S.; Zhao, R. In-situ gamma-ray survey of rare-earth tailings dams – A case study in Baotou and Bayan Obo Districts, China. *Journal of Environmental Radioactivity* **2016**, *151*, 304-310. DOI: https://doi.org/10.1016/j.jenvrad.2015.10.027.

(15) Pan, Y.; Li, H. Investigating heavy metal pollution in mining brownfield and its policy implications: a case study of the Bayan Obo rare earth mine, Inner Mongolia, China. *Environmental management* **2016**, *57* (4), 879-893.

(16) Guo, W.; Zhao, R.-X.; Zhang, J.; Bao, Y.-Y.; Wang, H.; Yang, M.; Sun, X.-L.; Jin, F. [Distribution characteristic and assessment of soil heavy metal pollution in the iron mining of Baotou in Inner Mongolia]. *Huan Jing Ke Xue* **2011**, *32* (10), 3099-3105. PubMed.

(17) Wang, Z.; Luo, Y.; Zheng, C.; An, C.; Mi, Z. Spatial distribution, source identification, and risk assessment of heavy metals in the soils from a mining region: a case study of Bayan Obo in northwestern China. *Human and Ecological Risk Assessment: An International Journal* **2020**, 1-20. DOI: 10.1080/10807039.2020.1821350.

(18) Li, K.; Liang, T.; Wang, L.; Yang, Z. Contamination and health risk assessment of heavy metals in road dust in Bayan Obo Mining Region in Inner Mongolia, North China. *Journal of Geographical Sciences* **2015**, *25* (12), 1439-1451. DOI: 10.1007/s11442-015-1244-1.

(19) Tamer, M. N.; Köroğlu, B. K.; Arslan, Ç.; Akdoğan, M.; Köroğlu, M.; Çam, H.; Yildiz, M. Osteosclerosis due to endemic fluorosis. *Science of the total environment* **2007**, *373* (1), 43-48.

(20) Klinger, J. M. The Environment-Security Nexus in Contemporary Rare Earth Politics. In *The Political Economy of Rare Earth Elements: Rising Powers and Technological Change*, Kiggins, R. D. Ed.; Palgrave Macmillan UK, 2015; pp 133-155.

(21) Estrade, G.; Marquis, E.; Smith, M.; Goodenough, K.; Nason, P. REE concentration processes in ion adsorption deposits: Evidence from the Ambohimirahavavy alkaline complex in Madagascar. *Ore Geology Reviews* **2019**, *112*, 103027. DOI: https://doi.org/10.1016/j.oregeorev.2019.103027.

(22) Moldoveanu, G. A.; Papangelakis, V. G. Recovery of rare earth elements adsorbed on clay minerals: II. Leaching with ammonium sulfate. *Hydrometallurgy* **2013**, *131-132*, 158-166. DOI: https://doi.org/10.1016/j.hydromet.2012.10.011.

(23) Deng, H.; Kendall, A. Life cycle assessment with primary data on heavy rare earth oxides from ion-adsorption clays. *The International Journal of Life Cycle Assessment* **2019**, *24* (9), 1643-1652. DOI: 10.1007/s11367-019-01582-1.

(24) Yang, X. J.; Lin, A.; Li, X.-L.; Wu, Y.; Zhou, W.; Chen, Z. China's ion-adsorption rare earth resources, mining consequences and preservation. *Environmental Development* **2013**, *8*, 131-136. DOI: https://doi.org/10.1016/j.envdev.2013.03.006.

(25) Vahidi, E.; Navarro, J.; Zhao, F. An initial life cycle assessment of rare earth oxides production from ion-adsorption clays. *Resources, Conservation and Recycling* **2016**, *113*, 1-11. DOI: https://doi.org/10.1016/j.resconrec.2016.05.006.

(26) Randall, D. J.; Tsui, T. K. N. Ammonia toxicity in fish. *Marine Pollution Bulletin* **2002**, *45* (1), 17-23. DOI: https://doi.org/10.1016/S0025-326X(02)00227-8.

(27) Sprecher, B.; Daigo, I.; Spekkink, W.; Vos, M.; Kleijn, R.; Murakami, S.; Kramer, G. J. Novel Indicators for the Quantification of Resilience in Critical Material Supply Chains, with a 2010 Rare Earth Crisis Case Study. *Environ. Sci. Technol.* **2017**, *51* (7), 3860-3870. DOI: 10.1021/acs.est.6b05751.

(28) Hower, J. C.; Ruppert, L. F.; Eble, C. F. Lanthanide, yttrium, and zirconium anomalies in the Fire Clay coal bed, Eastern Kentucky. *International Journal of Coal Geology* **1999**, *39* (1), 141-153. DOI: https://doi.org/10.1016/S0166-5162(98)00043-3.

(29) Mardon, S. M.; Hower, J. C. Impact of coal properties on coal combustion by-product quality: examples from a Kentucky power plant. *International Journal of Coal Geology* **2004**, *59* (3), 153-169. DOI: https://doi.org/10.1016/j.coal.2004.01.004.

(30) Hower, J. C.; Groppo, J. G.; Henke, K. R.; Hood, M. M.; Eble, C. F.; Honaker, R. Q.; Zhang, W.; Qian, D. Notes on the Potential for the Concentration of Rare Earth Elements and Yttrium in Coal Combustion Fly Ash. *Minerals* **2015**, *5* (2), 356-366.

(31) *2018 Coal Combustion Product (CCP) Production & Use Survey Report*; Association, A. C. A., 2019.

(32) Hedin, B. C.; Hedin, R. S.; Capo, R. C.; Stewart, B. W. Critical metal recovery potential of Appalachian acid mine drainage treatment solids. *International Journal of Coal Geology* **2020**, *231*, 103610. DOI: https://doi.org/10.1016/j.coal.2020.103610.

(33) Vass, C. R.; Noble, A.; Ziemkiewicz, P. F. The occurrence and concentration of rare earth elements in acid mine drainage and treatment by-products: Part 1—Initial survey of the Northern Appalachian Coal Basin. *Mining, Metallurgy & Exploration* **2019**, *36* (5), 903-916.

(34) Zaimes, G. G.; Hubler, B. J.; Wang, S.; Khanna, V. Environmental Life Cycle Perspective on Rare Earth Oxide Production. *ACS Sustainable Chemistry & Engineering* **2015**, *3* (2), 237-244. DOI: 10.1021/sc500573b.

(35) Sadri, F.; Nazari, A. M.; Ghahreman, A. A review on the cracking, baking and leaching processes of rare earth element concentrates. *Journal of Rare Earths* **2017**, *35* (8), 739-752. DOI: https://doi.org/10.1016/S1002-0721(17)60971-2.

(36) Taggart, R. K.; Hower, J. C.; Hsu-Kim, H. Effects of roasting additives and leaching parameters on the extraction of rare earth elements from coal fly ash. *International Journal of coal geology* **2018**, *196*, 106-114.

(37) King, J. F.; Taggart, R. K.; Smith, R. C.; Hower, J. C.; Hsu-Kim, H. Aqueous acid and alkaline extraction of rare earth elements from coal combustion ash. *International Journal of Coal Geology* **2018**, *195*, 75-83. DOI: https://doi.org/10.1016/j.coal.2018.05.009.

(38) Laudal, D. A.; Benson, S. A.; Addleman, R. S.; Palo, D. Leaching behavior of rare earth elements in Fort Union lignite coals of North America. *International Journal of Coal Geology* **2018**, *191*, 112-124. DOI: https://doi.org/10.1016/j.coal.2018.03.010.

(39) Zhang, W.; Honaker, R. Q. Rare earth elements recovery using staged precipitation from a leachate generated from coarse coal refuse. *International Journal of Coal Geology* **2018**, *195*, 189-199. DOI: https://doi.org/10.1016/j.coal.2018.06.008.

(40) Taggart, R. K.; Rivera, N. A.; Levard, C.; Ambrosi, J.-P.; Borschneck, D.; Hower, J. C.; Hsu-Kim, H. Differences in bulk and microscale yttrium speciation in coal combustion fly ash. *Environmental Science: Processes & Impacts* **2018**, *20* (10), 1390-1403, 10.1039/C8EM00264A. DOI: 10.1039/C8EM00264A.

(41) Liu, P.; Huang, R.; Tang, Y. Comprehensive Understandings of Rare Earth Element (REE) Speciation in Coal Fly Ashes and Implication for REE Extractability. *Environ. Sci. Technol.* **2019**, *53* (9), 5369-5377.

(42) Park, D. M.; Reed, D. W.; Yung, M. C.; Eslamimanesh, A.; Lencka, M. M.; Anderko, A.; Fujita, Y.; Riman, R. E.; Navrotsky, A.; Jiao, Y. Bioadsorption of Rare

Earth Elements through Cell Surface Display of Lanthanide Binding Tags. *Environ. Sci. Technol.* **2016**, *50* (5), 2735-2742. DOI: 10.1021/acs.est.5b06129.

(43) Kose Mutlu, B.; Cantoni, B.; Turolla, A.; Antonelli, M.; Hsu-Kim, H.; Wiesner, M. R. Application of nanofiltration for Rare Earth Elements recovery from coal fly ash leachate: Performance and cost evaluation. *Chem. Eng. J.* **2018**, *349*, 309-317. DOI: https://doi.org/10.1016/j.cej.2018.05.080.

(44) Dittrich, C.; Yagmurlu, B.; Friedrich, B. Effect of Aqueous Media on the Recovery of Scandium by Selective Precipitation. *Metals (2075-4701)* **2018**, *8* (5).

(45) Bertuol, D. A.; Bernardes, A. M.; Tenório, J. A. S. Spent NiMH batteries—The role of selective precipitation in the recovery of valuable metals. *Journal of Power Sources* **2009**, *193* (2), 914-923.

(46) Bradbury, M.; Baeyens, B. Sorption of Eu on Na-and Ca-montmorillonites: experimental investigations and modelling with cation exchange and surface complexation. *Geochimica et Cosmochimica Acta* **2002**, *66* (13), 2325-2334.

(47) Bozau, E.; Göttlicher, J.; Stärk, H.-J. Rare earth element fractionation during the precipitation and crystallisation of hydrous ferric oxides from anoxic lake water. *Applied Geochemistry* **2008**, *23* (12), 3473-3486. DOI: https://doi.org/10.1016/j.apgeochem.2008.08.007.

(48) Verplanck, P. L.; Nordstrom, D. K.; Taylor, H. E.; Kimball, B. A. Rare earth element partitioning between hydrous ferric oxides and acid mine water during iron oxidation. *Applied Geochemistry* **2004**, *19* (8), 1339-1354. DOI: https://doi.org/10.1016/j.apgeochem.2004.01.016.

(49) Quinn, K. A.; Byrne, R. H.; Schijf, J. Sorption of yttrium and rare earth elements by amorphous ferric hydroxide: Influence of pH and ionic strength. *Marine Chemistry* **2006**, *99* (1), 128-150. DOI: https://doi.org/10.1016/j.marchem.2005.05.011.

(50) Quinn, K. A.; Byrne, R. H.; Schijf, J. Sorption of yttrium and rare earth elements by amorphous ferric hydroxide: Influence of solution complexation with carbonate. *Geochimica et Cosmochimica Acta* **2006**, *70* (16), 4151-4165. DOI: https://doi.org/10.1016/j.gca.2006.06.014.

(51) Bau, M. Scavenging of dissolved yttrium and rare earths by precipitating iron oxyhydroxide: experimental evidence for Ce oxidation, Y-Ho fractionation, and lanthanide tetrad effect. *Geochimica et Cosmochimica Acta* **1999**, *63* (1), 67-77.

(52) Noack, C. W.; Dzombak, D. A.; Karamalidis, A. K. Rare earth element distributions and trends in natural waters with a focus on groundwater. *Environ. Sci. Technol.* **2014**, *48* (8), 4317-4326.

(53) Ayora, C.; Macías, F.; Torres, E.; Lozano, A.; Carrero, S.; Nieto, J.-M.; Pérez-López, R.; Fernández-Martínez, A.; Castillo-Michel, H. Recovery of Rare Earth Elements and Yttrium from Passive-Remediation Systems of Acid Mine Drainage. *Environ. Sci. Technol.* **2016**, *50* (15), 8255-8262.

(54) Danesi, P. R. Separation of Metal Species by Supported Liquid Membranes. *Separation Science and Technology* **1984**, *19* (11-12), 857-894. DOI: 10.1080/01496398408068598.

(55) Danesi, P. R.; Reichley-Yinger, L.; Rickert, P. G. Lifetime of supported liquid membranes: the influence of interfacial properties, chemical composition and water transport on the long-term stability of the membranes. *Journal of Membrane Science* **1987**, *31* (2), 117-145. DOI: https://doi.org/10.1016/S0376-7388(00)82223-1.

(56) Danesi, P. R.; Chiarizia, R.; Coleman, C. F. The Kinetics of Metal Solvent Extraction. *C R C Critical Reviews in Analytical Chemistry* **1980**, *10* (1), 1-126. DOI: 10.1080/10408348008542724.

(57) Smith, R. C.; Taggart, R. K.; Hower, J. C.; Wiesner, M. R.; Hsu-Kim, H. Selective Recovery of Rare Earth Elements from Coal Fly Ash Leachates Using Liquid Membrane Processes. *Environ. Sci. Technol.* **2019**, *53* (8), 4490-4499.

(58) Deshmane, V. G.; Islam, S. Z.; Bhave, R. R. Selective Recovery of Rare Earth Elements from a Wide Range of E-Waste and Process Scalability of Membrane Solvent Extraction. *Environ. Sci. Technol.* **2020**, *54* (1), 550-558. DOI: 10.1021/acs.est.9b05695.

(59) Hedin, B. C.; Capo, R. C.; Stewart, B. W.; Hedin, R. S.; Lopano, C. L.; Stuckman, M. Y. The evaluation of critical rare earth element (REE) enriched treatment solids from coal mine drainage passive treatment systems. *International Journal of Coal Geology* **2019**, *208*, 54-64.

(60) de Gyves, J.; de San Miguel, E. R. Metal ion separations by supported liquid membranes. *Industrial & Engineering Chemistry Research* **1999**, *38* (6), 2182-2202, Review. DOI: 10.1021/ie980374p.

(61) Kim, D.; Powell, L. E.; Delmau, L. H.; Peterson, E. S.; Herchenroeder, J.; Bhave, R. R. Selective Extraction of Rare Earth Elements from Permanent Magnet Scraps with Membrane Solvent Extraction. *Environ Sci Technol* **2015**, *49* (16), 9452-9459. DOI: 10.1021/acs.est.5b01306.

(62) Kim, D.; Powell, L.; Delmau, L. H.; Peterson, E. S.; Herchenroeder, J.; Bhave, R. R. A supported liquid membrane system for the selective recovery of rare earth elements from neodymium-based permanent magnets. *Separation Science and Technology* **2016**, *51* (10), 1716-1726. DOI: 10.1080/01496395.2016.1171782.

(63) Danesi, P. R.; Horwitz, E. P.; Rickert, P. Transport of Eu3+ through a Bis(2-ethylhexyl)-phosphoric Acid, n-Dodecane Solid Supported Liquid Membrane. *Separation Science and Technology* **1982**, *17* (9), 1183-1192. DOI: 10.1080/01496398208060282.

(64) Danesi, P.; Horwitz, E.; Rickert, P. Rate and mechanism of facilitated americium (III) transport through a supported liquid membrane containing a bifunctional organophosphorous mobile carrier. *The Journal of Physical Chemistry* **1983**, *87* (23), 4708-4715.

(65) Lim, T. M. Kinetic studies of solvent extraction of rare earths into di-2-ethylhexyl phosphoric acid (DEHPA). **1998**.

(66) Tsuyoshi, A.; Ito, H.; Hoshi, H.; Akiba, K.; Nakamura, S. Separation of yttrium(III) from iron(III) through liquid membrane impregnated with di(2-ethylhexyl)phosphoric acid. *Journal of Radioanalytical and Nuclear Chemistry* **1999**, *242* (2), 451-456. DOI: 10.1007/BF02345577.

(67) Doležal, J.; Moreno, C.; Hrdlička, A.; Valiente, M. Selective transport of lanthanides through supported liquid membranes containing non-selective extractant, di-(2-ethylhexyl)phosphoric acid, as a carrier. *Journal of Membrane Science* **2000**, *168* (1), 175-181. DOI: https://doi.org/10.1016/S0376-7388(99)00311-7.

(68) Hrdlička, A.; Fialová, I.; Dolezalová, J. Dialkylphosphoric acids as carriers in separation of lanthanides and thorium on supported liquid membranes. *Talanta* **1996**, *43* (4), 649-657. DOI: https://doi.org/10.1016/0039-9140(95)01803-4.

(69) Kolařík, Z.; Pankova, H. Acidic organophosphorus extractants—I Extraction of lanthanides by means of dialkyl phosphoric acids—effect of structure and size of alkyl group. *Journal of Inorganic and Nuclear Chemistry* **1966**, *28* (10), 2325-2333.

(70) Peppard, D.; Mason, G.; Maier, J.; Driscoll, W. Fractional extraction of the lanthanides as their di-alkyl orthophosphates. *Journal of Inorganic and Nuclear Chemistry* **1957**, *4* (5-6), 334-343.

(71) Tsurubou, S.; Mizutani, M.; Kadota, Y.; Yamamoto, T.; Umetani, S.; Sasaki, T.; Le, Q. T.; Matsui, M. Solvent extraction of alkaline earths and lanthanides using crown ethers as ion size selective masking reagents: A macrocycle application. *Analytical Chemistry* **1995**, *67* (8), 1465-1469.

(72) Martínez, J.; Rodríguez Varela, R.; Forsberg, K.; Rasmuson, Å. Factors influencing separation selectivity of rare earth elements in flat sheet supported liquid membranes. *Chemical Engineering Science* **2018**, *191*, 134-155. DOI: https://doi.org/10.1016/j.ces.2018.06.018.

(73) Sato, T.; Nakamura, T.; Ikeno, M. The extraction of iron(III) from aqueous acid solutions by di(2-ethylhexyl)phosphoric acid. *Hydrometallurgy* **1985**, *15* (2), 209-217. DOI: https://doi.org/10.1016/0304-386X(85)90055-6.

(74) Sato, T.; Yoshino, T.; Nakamura, T.; Kudo, T. The kinetics of aluminium(III) extraction from sulphuric acid solutions by Di-(2-ethylhexyl)-phosphoric acid. *Journal of Inorganic and Nuclear Chemistry* **1978**, *40* (8), 1571-1574. DOI: https://doi.org/10.1016/0022-1902(78)80470-9.

(75) Sato, T.; Yoshino, T.; Nakamura, T.; Kudo, T. The kinetics of aluminium(III) extraction from hydrochloric and nitric acid solutions by di-(2-ethylhexyl)-phosphoric acid. *Journal of Inorganic and Nuclear Chemistry* **1979**, *41* (5), 731-734. DOI: https://doi.org/10.1016/0022-1902(79)80363-2.

(76) Gaonkar, A. G.; Neuman, R. D. Interfacial activity, extractant selectivity, and reversed micellization in hydrometallurgical liquid/liquid extraction systems. *Journal of Colloid and Interface Science* **1987**, *119* (1), 251-261. DOI: https://doi.org/10.1016/0021-9797(87)90264-5.

(77) Vandegrift, G.; Horwitz, E. The mechanism of interfacial mass transfer of calcium in the system: Di (2-ethylhexyl) phosphoric acid in dodecane-dilute nitric acid. *Journal of Inorganic and Nuclear Chemistry* **1977**, *39* (8), 1425-1432.

(78) Naik, M. T.; Dhadke, P. M. Extraction of Iron(III) with Bis(2-ethylhexyl)phosphinic Acid and Bis(2-ethylhexyl)phosphoric Acid: Experimental Equilibrium Study. *Journal of Chemical & Engineering Data* **1999**, *44* (5), 1037-1040. DOI: 10.1021/je980280m.

(79) Akiba, K.; Ito, M.; Nakamura, S. Selective transport of yttrium(III) in the presence of iron(III) through liquid-membrane impregnating acidic organophosphonate mobile carrier. *Journal of Membrane Science* **1997**, *129* (1), 9-17. DOI: https://doi.org/10.1016/S0376-7388(96)00314-6.

(80) Baba, Y.; Kubota, F.; Kamiya, N.; Goto, M. Selective Recovery of Dysprosium and Neodymium Ions by a Supported Liquid Membrane Based on Ionic Liquids. *Solvent Extraction Research and Development, Japan* **2011**, *18*, 193-198. DOI: 10.15261/serdj.18.193.

(81) Loiacono, O.; Drioli, E.; Molinari, R. Metal ion separation and concentration with supported liquid membranes. *Journal of Membrane Science* **1986**, *28* (2), 123-138. DOI: https://doi.org/10.1016/S0376-7388(00)82205-X.

(82) Hajarabeevi, N.; Mohammed Bilal, I.; Easwaramoorthy, D.; Palanivelu, K. Facilitated transport of cationic dyes through a supported liquid membrane with D2EHPA as carrier. *Desalination* **2009**, *245* (1), 19-27. DOI: https://doi.org/10.1016/j.desal.2008.06.009.

(83) Chiarizia, R.; Danesi, P. R. A Double Liquid Membrane System for the Removal of Actinides and Lanthanides from Acidic Nuclear Wastes. *Separation Science and Technology* **1987**, *22* (2-3), 641-659. DOI: 10.1080/01496398708068972.

(84) Ni'am, A. C.; Wang, Y.-F.; Chen, S.-W.; Chang, G.-M.; You, S.-J. Simultaneous recovery of rare earth elements from waste permanent magnets (WPMs) leach liquor by solvent extraction and hollow fiber supported liquid membrane. *Chemical Engineering and Processing - Process Intensification* **2020**, *148*, 107831. DOI: https://doi.org/10.1016/j.cep.2020.107831.

(85) Elshkaki, A.; Graedel, T. E. Dysprosium, the balance problem, and wind power technology. **2014**, *136*, 548-559.

(86) Du, X.; Graedel, T. E. Uncovering the end uses of the rare earth elements. *Science of The Total Environment* **2013**, *461-462*, 781-784. DOI: https://doi.org/10.1016/j.scitotenv.2013.02.099.

(87) Long, K. R.; Van Gosen, B. S.; Foley, N. K.; Cordier, D. The Principal Rare Earth Elements Deposits of the United States: A Summary of Domestic Deposits and a Global Perspective. In *Non-Renewable Resource Issues: Geoscientific and Societal Challenges*, Sinding-Larsen, R., Wellmer, F.-W. Eds.; Springer Netherlands, 2012; pp 131-155.

(88) Gulley, A. L.; Nassar, N. T.; Xun, S. China, the United States, and competition for resources that enable emerging technologies. *Proceedings of the National Academy of Sciences* **2018**, *115* (16), 4111. DOI: 10.1073/pnas.1717152115.

(89) Mancheri, N. A.; Sprecher, B.; Bailey, G.; Ge, J.; Tukker, A. Effect of Chinese policies on rare earth supply chain resilience. *Resources, Conservation and Recycling* **2019**, *142*, 101-112. DOI: https://doi.org/10.1016/j.resconrec.2018.11.017.

(90) Sandalow, D.; Bauer, D.; Diamond, D.; Li, J.; McKittrick, M.; Telleen, P. Critical materials strategy. *US Department of Energy, USA* **2010**.

(91) Lichte, F. E.; Meier, A. L.; Crock, J. G. Determination of the rare-earth elements in geological materials by inductively coupled plasma mass spectrometry. *Analytical Chemistry* **1987**, *59* (8), 1150-1157.

(92) Meier, A.; Slowik, T.; Taggart, J. Rare earth elements by inductively coupled plasma–mass spectrometry. *Analytical methods manual for the Mineral Resource Surveys Program US Geological Survey* **2002**, 166.

(93) Meier, A. L.; Lichte, F. E.; Briggs, P. H.; Bullock Jr, J. H. Coal ash by inductively coupled plasma-atomic emission spectrometry and inductively coupled plasma-mass spectrometry. *Analytical methods manual for the Mineral Resource Surveys Program US Geological Survey* **1996**, 109.

(94) Ilavsky, J. Nika: software for two-dimensional data reduction. *Journal of Applied Crystallography* **2012**, *45* (2), 324-328.

(95) Degen, T.; Sadki, M.; Bron, E.; König, U.; Nénert, G. The HighScore suite. *Powder Diffraction* **2014**, *29* (S2), S13-S18. DOI: 10.1017/S0885715614000840 From Cambridge University Press Cambridge Core.

(96) Gustafsson, J. P. *Visual MINTEQ, version 3.1*. https://vminteq.lwr.kth.se/ (accessed 2020 25 February 2020).

(97) Reardon, E. J.; Czank, C. A.; Warren, C. J.; Dayal, R.; Johnston, H. M. Determining Controls On Element Concentrations in Fly Ash Leachate. *Waste Management & Research* **1995**, *13* (5), 435-450. DOI: 10.1177/0734242x9501300504.

(98) Schwartz, G. E.; Redfern, L. K.; Ikuma, K.; Gunsch, C. K.; Ruhl, L. S.; Vengosh, A.; Hsu-Kim, H. Impacts of coal ash on methylmercury production and the methylating microbial community in anaerobic sediment slurries. *Environmental Science: Processes & Impacts* **2016**, *18* (11), 1427-1439, 10.1039/C6EM00458J. DOI: 10.1039/C6EM00458J.

(99) Brewer, A.; Chang, E.; Park, D. M.; Kou, T.; Li, Y.; Lammers, L. N.; Jiao, Y. Recovery of Rare Earth Elements from Geothermal Fluids through Bacterial Cell Surface Adsorption. *Environ. Sci. Technol.* **2019**, *53* (13), 7714-7723. DOI: 10.1021/acs.est.9b00301.

(100) Kolker, A.; Scott, C.; Hower, J. C.; Vazquez, J. A.; Lopano, C. L.; Dai, S. Distribution of rare earth elements in coal combustion fly ash, determined by SHRIMP-RG ion microprobe. *International Journal of Coal Geology* **2017**, *184*, 1-10. DOI: https://doi.org/10.1016/j.coal.2017.10.002.

(101) Hower, J. C.; Groppo, J. G.; Joshi, P.; Dai, S.; Moecher, D. P.; Johnston, M. Location of cerium in coal-combustion fly ashes: implications for recovery of lanthanides. *Coal Combustion and Gasification Products* **2013**, *5*, 73-78.

(102) Moeller, T.; Kremers, H. E. The Basicity Characteristics of Scandium, Yttrium, and the Rare Earth Elements. *Chemical Reviews* **1945**, *37* (1), 97-159.

(103) Chassé, M.; Griffin, W. L.; O'Reilly, S. Y.; Calas, G. Scandium Speciation in a World-Class Lateritic Deposit. *Geochemical Perspectives Letters* **2016**, *3* (2), 105-114. DOI: 10.7185/geochemlet.1711.

(104) Vind, J.; Malfliet, A.; Bonomi, C.; Paiste, P.; Sajó, I. E.; Blanpain, B.; Tkaczyk, A. H.; Vassiliadou, V.; Panias, D. Modes of occurrences of scandium in Greek bauxite and bauxite residue. *Minerals Engineering* **2018**, *123*, 35-48. DOI: https://doi.org/10.1016/j.mineng.2018.04.025.

(105) Levard, C.; Borschneck, D.; Grauby, O.; Rose, J.; Ambrosi, J.-P. Goethite, a tailor-made host for the critical metal scandium: The FexSc(1-x)OOH solid solution. *Geochemical Perspectives Letters* **2018**, *9*, 16-20. DOI: 10.7185/geochemlet.1832.

(106) Das, S.; Gaustad, G.; Sekar, A.; Williams, E. Techno-economic analysis of supercritical extraction of rare earth elements from coal ash. *Journal of Cleaner Production* **2018**, *189*, 539-551. DOI: https://doi.org/10.1016/j.jclepro.2018.03.252.

(107) U.S. Geologic Survey. *Rare Earths Data Sheet- Mineral Commodity Summaries 2020*. 2020. https://www.usgs.gov/centers/nmic/rare-earths-statistics-and-information (accessed 12/10/2020).

(108) Ochsenkühn-Petropulu, M.; Lyberopulu, T.; Parissakis, G. Direct determination of landthanides, yttrium and scandium in bauxites and red mud from alumina production. *Analytica Chimica Acta* **1994**, *296* (3), 305-313. DOI: https://doi.org/10.1016/0003-2670(94)80250-5.

(109) Abdel-Aal, E. A.; Mahmoud, M. H. H.; Sanad, M. M. S.; Criscuoli, A.; Figoli, A.; Drioli, E. Membrane contactor as a novel technique for separation of iron ions from ilmenite leachant. *International Journal of Mineral Processing* **2010**, *96* (1), 62-69. DOI: https://doi.org/10.1016/j.minpro.2010.05.002.

(110) Danesi, P. R.; Horwitz, E. P.; Vandegrift, G. F.; Chiarizia, R. Mass Transfer Rate through Liquid Membranes: Interfacial Chemical Reactions and Diffusion as Simultaneous Permeability Controlling Factors. *Separation Science and Technology* **1981**, *16* (2), 201-211. DOI: 10.1080/01496398108058114.

(111) Singer, P. C.; Stumm, W. Acidic Mine Drainage: The Rate-Determining Step. *Science* **1970**, *167* (3921), 1121-1123. (acccessed 2022/08/25/).JSTOR.

(112) Millero, F. J.; Sotolongo, S.; Izaguirre, M. The oxidation kinetics of Fe(II) in seawater. *Geochimica et Cosmochimica Acta* **1987**, *51* (4), 793-801. DOI: https://doi.org/10.1016/0016-7037(87)90093-7.

(113) Duhamet, J.; Möhwald, H.; Pleines, M.; Zemb, T. Self-Regulated Ion Permeation through Extraction Membranes. *Langmuir* **2017**, *33* (38), 9873-9879. DOI: 10.1021/acs.langmuir.7b02256.

(114) Black, C. A. *Methods of soil analysis*; Madison, Wis., American Society of Agronomy, 1965., 1965.

(115) Eaton, A. D.; Franson, M. A. H.; American Public Health, A.; American Water Works, A.; Water Environment, F. *Standard methods for the examination of water & wastewater*; Washington, DC : American Public Health Association, c2005., 2005.

(116) Watzlaf, G. R.; Schroeder, K. T.; Kleinmann, R. L.; Kairies, C. L.; Nairn, R. W. The passive treatment of coal mine drainage. *United States Department of Energy National Energy Technology Laboratory Internal Publication* **2004**, 1-72.

Biography

Andrew Middleton graduated from the University of Oklahoma (Norman, OK) with a B.S. in Chemical Engineering in 2014. After completing his undergraduate education, he worked for three years at the Oklahoma Department of Environmental Quality as a wastewater engineer. He then started his Ph.D. work at Duke University (Durham, NC) in 2017. He obtained his M.S. in Civil and Environmental Engineering from Duke University in 2018.